PRO-ATHEROGENIC MACROPHAGES INDUCE UPREGULATION OF MLKL AND CELL DEATH IN VASCULAR SMOOTH MUSCLE CELLS DURING ATHEROGENIC STIMULATION

By

RAMA SARAKBI

Thesis submitted to the University of Ottawa in partial fulfillment of the requirements for the Master's degree in Biochemistry

Department of Biochemistry, Microbiology, and Immunology
Faculty of Medicine
University of Ottawa

ABSTRACT

Background: A hallmark of advanced, rupture-prone atherosclerotic lesions is the presence of a necrotic core – a dense mass of pro-inflammatory and cellular debris. Traditionally, it has been thought that most of the foam cells within this core are derived from macrophages. However, recent advances in single cell technologies have revealed that vascular smooth muscle cells have the capacity to transdifferentiate into "macrophage-like foam cells", accounting for almost half of the cell content in advanced plaques. Our lab and others have discovered that a primary cause of the necrotic core is necroptotic cell death, where the mixed lineage kinase domain like pseudokinase MLKL is a key executioner of this process. While the contribution of necroptosis in macrophages and macrophage-derived foam cells to plaque growth and instability has been fairly-well studied, the role of necroptosis in vascular smooth muscle cells in this process remains unclear.

Objective: This work explores the role of MLKL in regulating necroptosis of macrophages and vascular smooth muscle cells when challenged with pro-inflammatory and pro-atherogenic stimuli.

Hypothesis: MLKL regulates cell death differently in macrophages and vascular smooth muscle cells when challenged with pro-inflammatory or pro-atherogenic stimuli.

Methods and Results: Bone marrow-derived macrophages (BMDMs) and aortic vascular smooth muscle cells (VSMCs) were isolated from wildtype and $MLKL^{-/-}$ mice and treated with pro-atherogenic stimuli in the presence or absence of apoptosis and necroptosis inhibitors, zVAD and Necrostatin-1 (Nec1). BMDMs underwent cell death in response to treatment within 3-6 hours (as measured by LDH release and SYTOX assays), while VSMCs survive up to 18-24 hours. However, when treated with BMDM conditioned media, VSMCs

begin to show higher rates of relative cell death compared to controls, particularly in response to treatment with oxLDL. Confocal microscopy and Western blots revealed that VSMCs treated with oxLDL in addition to BMDM conditioned media show an increase in relative expression of total and phosphorylated-MLKL – a key hallmark of necroptosis – compared to VSMCs without conditioned media. Moreover, these experiments implicate STAT1 and IRF1 as possible transcriptional regulators of MLKL expression in VSMCs treated in BMDM conditioned media. Preliminary staining of atherosclerotic lesions in mice may suggest that MLKL expression is more abundant within macrophages, and upregulation of MLKL expression in VSMCs may be associated with phenotypic switching.

Conclusion: Overall, this work suggests VSMCs are inherently resistant to necroptosis, unless treated with conditioned media from BMDMs, which may suggest that macrophages have the capacity to prime necroptosis in VSMCs, likely through secreted factors.

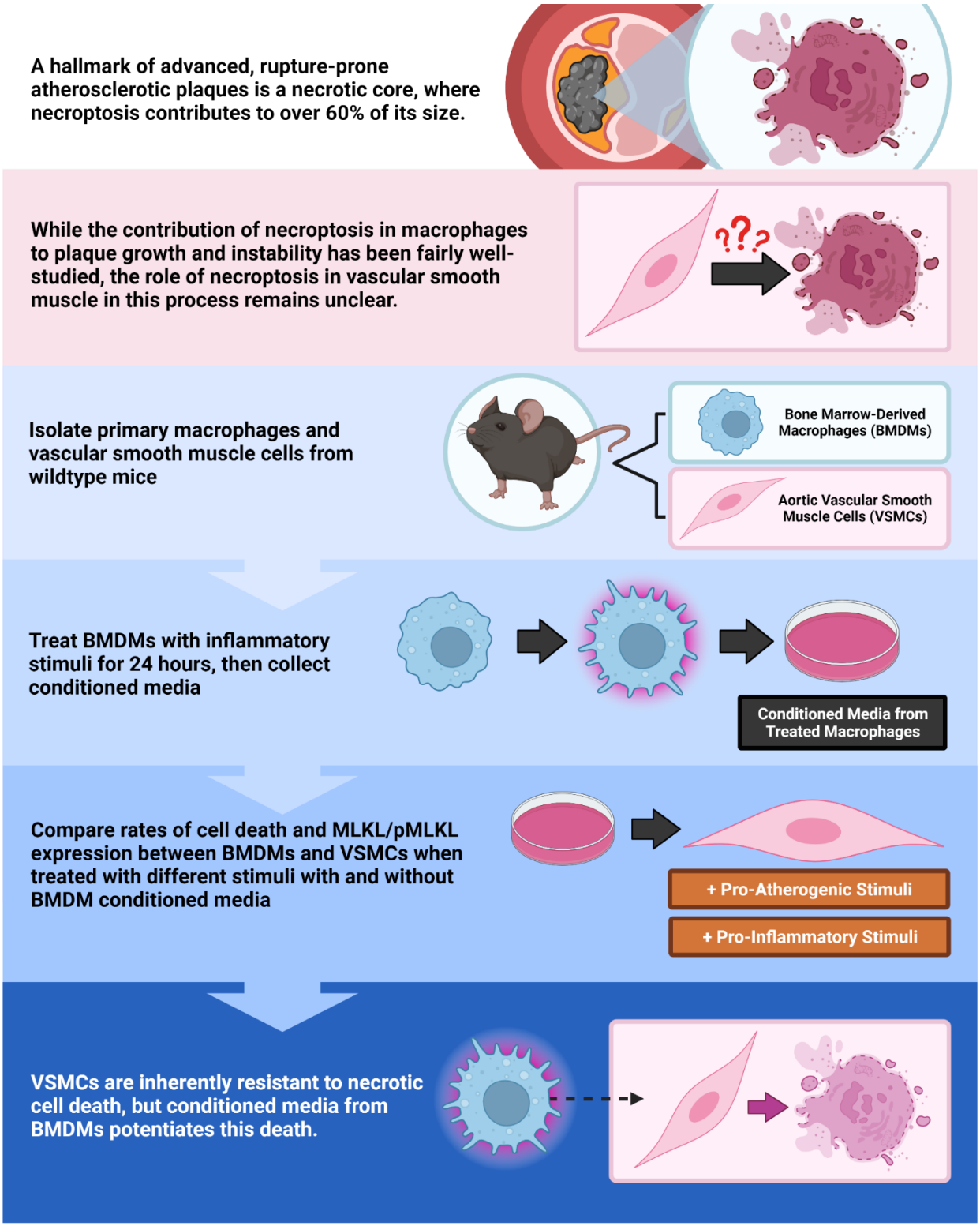

Figure 1. BMDM conditioned media potentiates cell death in VSMCs.

ACKNOWLEDGEMENTS

First and foremost, I would like to thank Dr. Katey Rayner for being an incredible supervisor and role model. From culturing my first smooth muscle cells to presenting my first Thesis Advisory Committee (TAC) meeting, Katey's enthusiasm and encouragement have been a constant source of reassurance throughout all the bumps and doubts of graduate school. Her guidance and expertise have been essential to helping the project develop into where it stands today. I am incredibly grateful for Katey's kindness and all that she has taught me.

Equally, I would like to thank my TAC members, Dr. Jim Sun and Dr. Shawn Beug, for their direction and support throughout this project. Jim and Shawn always knew how to pull us through new and exciting areas of exploration. I am thankful for the interest and compassion they brought to each meeting and their feedback throughout this process.

I would also like to thank our phenomenal lab members, past and present, at the Ottawa Heart Institute – Michèle Geoffrion, Nancy Simon, Dr. My-Anh Nguyen, Dr. David Smyth, Dr. Adil Rasheed, Dr. Jonathan Salazar Leon, Dr. Victoria Lorant, Dr. Chanèle Polenz, Dr. Leah Susser, Cameron Stotts, Abagael Hudak, Deniz Ekin Camcı, Stijn Van Linden, Maria Ivanova, Michelle Gandelman, Anastasia Fahlman, Serena Solari, Claire Padley, Haley Dal Farra, Grace Fader, and Gabrielle MacEwen. For absolutely everything – from helping hands to sanity checks, donuts, poutine, and coffee – thank you.

I would also like to thank our Director of Research Services, Vivian Franklin, and our fourth-floor neighbours from the Ouimet, Lagace, and McPherson labs – especially Christina Emerton, Valérie Rochon, Dr. Thomas Laval, Arlette Aluma Kasongo, Nathan Joyce, Mishita Dharia, Paulina Lau, Dr. Anh-Thu Dang, Tanja Kosenko, and Alana Renon. For being a sounding

board when nothing would go right and saving an experiment (or two) from annihilation, thank you.

From the University of Ottawa CBIA Core, I would like to thank Dr. Chloë Van Oostende-Triplet and Dr. Liyuan Wang for all their guidance with anything and everything microscopy and FIJI-related.

From the University of Ottawa GEM Core, I would like to thank Dr. Maxime Rousseaux, Dr. James Taylor, and Steve Callaghan for their guidance with designing the TurboID project. In particular, I would like to thank Dr. Taylor for helping us design our TurboID constructs, and for preparing the plasmids and lentivirus we used. I would also like to thank Dr. Sanna Abbasi from Western University for her help navigating all things BioID and related to studying protein-protein interactions.

To my parents, Samar Al Kutb and Bassam Al Sarakbi, and my siblings, Kamar, Diana, Rami, and Reem – I would not have grown into the person I am today without your gentle encouragement and patience. To my nephew, Adam, thank you for your endless curiosity. To my friends, thank you for reminding me to find joy outside of a biosafety cabinet. From the bottom of my heart to each and every one of you – thank you.

TABLE OF CONTENTS

ABBREVIATIONS

ABCA1/G1	ATP-binding cassette transporter A1/G1
ANOVA	Analysis of variance
BCA	Bicinchoninic acid
BCM	BMDM-conditioned media
BMDM	Bone marrow-derived macrophage
BME	ß-mercaptoethanol
BSA	Bovine serum albumin
CSA	Cyclosporin A
CVD	Cardiovascular disease
DAMP	Damage-associated molecular pattern
DMEM	Dulbecco's modified eagle medium
ECM	Extracellular matrix
ELISA	Enzyme-linked immunosorbent assay
ER	Endoplasmic reticulum
FBS	Fetal bovine serum
GAPDH	Glyceraldehyde 30phosphate dehydrogenase
GSDMD	Gasdermin D
HBSS	Hank's balanced salt solution
ICAM-1	Intercellular adhesion molecule-1
IRF1	Interferon regulatory factor 1
KO	Knockout
LDL	Low-density lipoprotein

LIF	Leukemia inhibitor factor
MCS-F	Macrophage colony-stimulating factor
MFI	Mean fluorescence intensity
MLKL-/-	Homozygous knockout of MLKL
MOI	Multiplicity of infection
NADH	β-Nicotinamide adenine dinucleotide
Nec1	Necrostatin-1
NT	No treatment
oxLDL	Oxidized low-density lipoprotein
PBS	Phosphate-buffered saline
PCD	Programmed cell death
PFA	Paraformaldehyde
PhIC	Phosphatase inhibitor cocktail
PIC	Protease inhibitor cocktail
RIPA	Radioimmunoprecipitation assay
RIPK1	Receptor-interacting serine/threonine-protein kinase 1
RIPK3	Receptor-interacting serine/threonine-protein kinase 3
ROS	Reactive oxygen species
RT	Room temperature
SD	Standard deviation
SDS	Sodium dodecyl sulfate
SEM	Standard error mean
SMC	Smooth muscle cell

ST	Staurosporine
STAT1	Signal transducer and activator of transcription 1
STAT3	Signal transducer and activator of transcription 3
TBS	Tris-buffered saline
TLR4	Toll-like receptor 4
TNFR1	Tumour necrosis factor receptor 1
TNFα	Tumour necrosis factor alpha
TUNEL	Terminal deoxynucleotidyl transferase dUTP nick-end labelling
VCAM-1	Vascular cell adhesion molecule 1
VSMC	Vascular smooth muscle cell
WD	Western diet
WT	Wildtype
zVAD	Benzyloxycarbonyl-Val-Ala-Asp-fluoromethylketone

LIST OF FIGURES

1.0 Introduction

Atherosclerosis is a chronic, progressive inflammatory disease whereby modified low-density lipoproteins (LDL) accumulate along with immune cells within the intimal layer of the artery wall to form a plaque[1–5]. The rupture or breakage of advanced, vulnerable plaque releases collagen, lipids, inflammatory molecules, and cellular debris into the bloodstream, activating platelets and initiating the coagulation cascade to form a clot, or thrombus[6–8]. Depending on the location of the ruptured lesion, thrombosis can result in heart attack or stroke and cause potentially irreversible and life-threatening injury[9]. A hallmark of advanced, rupture-prone atherosclerotic lesions is the presence of a necrotic core – a dense mass of pro-inflammatory and cellular debris[10,11].

1.1 Atherogenesis

1.1.1 Early Lesion

Atherogenesis is thought to begin with damage or a loss of integrity in the endothelial wall of the artery, which is often associated with certain major risk factors of cardiovascular disease, including hypertension, hyperlipidemia, diabetes, and aging[12–14]. In the early lesion, pro-atherogenic factors, including LDL particles, oxidative stress, and disturbed or complex flow have been shown to induce endothelial cell death[15–17]. This weakening of the endothelium provides an opportunity for circulating LDL particles to breach the arterial wall and begin to accumulate within the vessel. Alternatively, emerging evidence describes active, intracellular transport of LDL particles into the vessel wall through transcytosis by activated endothelial cells, expressing scavenger receptor class B type 1 (SR-B1)[18–21].

As LDL particles accumulate within the intimal layer of the artery wall, bound to proteoglycans of the extracellular matrix (ECM), they become more susceptible to oxidation and

aggregation[22–26]. The accumulation of these modified LDL particles, rich with fats and cholesterol, within the vessel wall activates nearby endothelial cells and tissue-resident macrophages to begin secreting pro-inflammatory cytokines and chemokines, activating both an innate and adaptive immune response[5,27].

Circulating monocytes are recruited by these signals and enter the vessel wall at sites of inflammation, where they differentiate into macrophages to begin clearing LDL particles through scavenger receptor (SR)-mediated phagocytosis[28,29]. However, as macrophages become overwhelmed with an excess of modified LDL particles, including oxidized LDL (oxLDL) and aggregated LDL (agLDL), they struggle to effectively regulate uptake and metabolism of their lipid load[30]. As these cells become densely packed with excess lipids, their cytoplasm begins to take on a lipid droplet-rich, "foam"-like appearance[29,31].

Under normal physiological conditions, excess intracellular free cholesterol promotes downregulation of cell surface LDL receptors (LDLRs) through inhibition of sterol regulatory element binding protein (SREBP) cleavage to slow intake of additional exogeneous lipids[32–37]. However, atherogenic LDL particles disrupt this process by up-regulating uptake of modified LDL particles[38]. In particular, oxLDL has been shown to downregulate cholesterol efflux transporters including ATP binding cassettes A1/G1 (ABCA1/G1) and scavenger receptor class B type I (SR-B1)[39,40]. This loss of efflux acceptors coupled with impaired metabolism of lipid droplets induces ER stress and triggers programed cell death[41,42]. In an early atherosclerotic plaque, apoptosis and efferocytosis work in tandem to limit the inflammatory burden of accumulating cellular debris from dying foam cells overwhelmed by lipid uptake[43–46].

1.1.2 Growing and Late Lesion

When apoptosis is coupled with effective efferocytosis, phagocytes are able to find and clear apoptotic bodies, thereby minimizing stress on surrounding cells and tissues[43]. However, as the disease progresses, apoptosis and efferocytosis become overwhelmed or inhibited.

Recognition of apoptotic bodies is mediated by macrophage erythroblast receptor tyrosine kinase (MERTK) of phagocytes[46]. MERTK binds to exposed phosphatidylserine (PtdSer) along the surface of apoptotic bodies using growth arrest 6 (GAS6) or protein S adaptor proteins[46]. While the exact mechanism behind impaired efferocytosis within the atherosclerotic lesion remains unclear, some evidence suggests that reactive oxygen species (ROS) may drive A disintegrin and metalloprotease 17 (ADAM17)-mediated cleavage of MERTK in phagocytes[47–49]. Without efferocytosis, lingering apoptotic bodies undergo a form of cell death called secondary necrosis, where cleaved caspase-3 has been shown to activate gasdermin-E (GSDME)-mediated cell lysis[11,50–52].

As the lesion continues to advance, apoptosis itself can become inhibited through inactivation of caspase-8[11]. It is theorized that oxidation or iNOS-driven S-nitrosylation may drive inactivation of this proteolytic enzyme, blocking apoptosis[11]. In the absence of apoptosis, foam cells may opt to undergo necroptosis, a more inflammatory form of programmed cell death, where the plasma membrane swells and ruptures, releasing its intracellular contents as damage-associated molecular patterns (DAMPs) to trigger an acute inflammatory immune response[53,54]. At this stage of plaque progression, an “early” necrotic core begins to form through the accumulation of apoptotic bodies and necrotic cellular debris along with cholesterol crystals[10]. As the necrotic core expands, the artery wall begins to thicken and harden with migrating

vascular smooth muscle cells (VSMCs), forming a strong fibrous cap, reinforced with collagen and extracellular matrix[55].

1.1.3 Rupture-Prone

A rupture-prone atherosclerotic lesion is an increasingly hostile, inflammatory environment that feeds an expanding necrotic core, growing to account for over 10-25% of total lesion area[10]. The fibrous cap grows unstable as invading monocytes and macrophages accumulate along with dying vascular smooth muscle cells that release matrix metalloproteinases (MPPs) and micro-calcifications [10]. Pro-inflammatory cytokines including IFNγ are associated with loss of collagen production, while IL-1ß, TNFα, and CD40 ligand have been implicated in the higher rates of MMP expression by VSMCs *in vitro*[13,56–58], contributing to a loss of integrity of the fibrous cap. This thinning subendothelial fibrous cap is all that stands between the tensile pressure of blood flow through the lumen and a pro-thrombotic core.

1.1.4 Plaque Rupture

Upon plaque rupture, the contents of the lesion and necrotic core spill into the lumen, interacting with platelets and coagulation factors to seal the injured artery wall[7]. The coagulation cascade is triggered by the exposure of tissue factor from the ruptured plaque[59,60]. Tissue factor interacts with components from blood plasma to convert coagulation factor II ("pro-thrombin") into thrombin – a serine protease necessary for generating fibrin from its blood-soluble precursor protein, fibrinogen[59]. Unlike its counterpart, fibrin is characteristically insoluble in blood, and precipitates to form long strands of polymerized fibers that bind to platelets and harden to seal the injured artery wall[61,62]. This assembly of fibrin polymers and platelets form a thrombus, or blood clot, which can block blood flow at the rupture site or, if dislodged, further along the narrowed vessel[63].

1.1.5 Plaque Erosion

Contrary to plaque rupture, erosion describes a gradual tearing, "or lifting" of endothelial cells away from the vessel wall[64]. This process exposes the underlying plaque to blood flowing through the lumen, and triggers formation of a thrombus[64]. Erosion is initiated by pro-inflammatory cytokines and stimuli, including oxLDL and sheer stress, which induce expression of endothelial MMPs that degrade collagen fibers and the extracellular matrix of the basement membrane[64,65]. This loss of basement membrane integrity leads to endothelial "tearing", or lifting, from the vessel wall. Signaling through toll-like receptor 2 (TLR2) in particular is known to contribute to endothelial activation and erosion[66,67]. Upregulation of TLR2 in endothelial cells is associated with regions of disturbed blood flow, leading to increased expression of leukocyte adhesion receptors, ICAM1 and E-selectin, and increased secretion of IL-8[64,66–69]. Erosion is believed to contribute to both the onset of plaque development and in promoting thrombosis of more advanced lesions[64].

1.2 The Vessel Wall

1.2.1 Endothelial Cells

The endothelium is made up of a tight monolayer of endothelial cells that acts as a dynamic barrier between the intimal layer of the artery wall and the flow of blood and nutrients through the lumen[70]. The endothelium serves two major functions: (a) to produce vasoactive substances (e.g. nitric oxide, NO) to constrict or dilate the vessel wall in response to extracellular cues from its environment, and (b) to control the passage of substances, including cells, between the lumen and the inner layer of the artery wall to the surrounding tissue[71].

Activated endothelial cells secrete inflammatory cytokines and present adhesive cell surface receptors (e.g. VCAM-1 and ICAM-1) to pull in circulating leukocytes from the blood to

respond to sources of stress and injury in the artery wall[72,73]. Under normal physiological conditions, this activation is essential to direct tissue repair and clear sources of infection and inflammation[71,73]. However, chronic activation of endothelial cells is associated with endothelial dysfunction (ED), senescence, and erosion, leading to a breakdown in the integrity of the endothelium, which lays a foundation for the development of atherosclerosis[70].

1.2.2 Macrophages

Populations of macrophages within atherosclerotic lesions have historically been characterized by three major phenotypes: quiescent "M0", pro-inflammatory "M1", and pro-resolving "M2"[74,75]. Generally, M1 macrophages tend to rely more heavily on glycolytic metabolism, express high levels of inducible nitric oxide synthase (iNOS), and secrete reactive oxygen species and highly inflammatory cytokines and chemokines, including TNFα, IL-1ß, and IL-6[76]. These pro-inflammatory macrophages are typically associated with plaque growth and active inflammation. Alternatively, M2 macrophages tend to be considered reparative for their reliance on oxidative metabolism and release of pro-resolving factors (e.g. IL-10, TGFß) to promote angiogenesis, tissue repair, and regulate immune response[76]. These anti-inflammatory macrophages are associated with regressive and generally stable plaques.

While it can be helpful to use these categories to broadly predict and describe the response or role of a subset of macrophages, it is important to consider that these classifications describe transient states – a given M1 macrophage may adopt a more M2 phenotype depending on a combination of environmental and intrinsic cues[77,78]. Furthermore, recent work using single cell technologies has described multiple populations of macrophages that exist beyond the characterization of M0, M1, and M2 phenotypes within a developing lesion, each with their own distinct function[79,80].

1.2.3 Vascular Smooth Muscle Cells

Within an atherosclerotic lesion, vascular smooth muscle cells are generally known for their role in fibrous cap formation, where they contribute to plaque stability by producing and depositing collagen and extracellular matrix[81–83]. The loss of these VSMCs through cell death is associated with a thinning fibrous cap, increased plaque calcification, and an expanding necrotic core – characteristic features of advanced, rupture-prone atherosclerotic lesions[84].

VSMCs are generally characterized as having either a contractile or synthetic phenotype. Contractile VSMCs are typically associated with regulating vascular tone and express characteristically contractile genes, including α-SMA and myosin-11 (Myh11)[81]. Alternatively, synthetic VSMCs tend to be associated with tissue repair and vascular remodeling (or angiogenesis) and express higher levels of ECM-related proteins, including collagen and MMPs[85]. The switch between these two states is regulated by Krüppel-like factor 4 (KLF4) and platelet-derived growth factor BB (PDGF-BB) signaling, which drive changes in gene expression and cellular behaviour in response to vascular injury and disease[85–87].

However, the phenotypic diversity of VSMCs within the atherosclerotic lesion is far richer and more complex than originally thought, as VSMCs have been shown to adopt "adipocyte-", "myofibroblast-", "endothelial-", and "macrophage-like" phenotypes[88–90]. Typically, the identification of plaque VSMCs depended on expression of key contractile genes including smooth muscle alpha-2 actin (α-SMA)[90]. However, lineage tracing models have revealed that almost 80% of plaque VSMCs in mouse atherosclerotic lesions are negative for α-SMA[87,90]. The rise of single cell technologies has provided a more robust understanding of VSMC plasticity and heterogeneity within atherosclerotic lesions, and their corresponding contributions to both plaque stability and vulnerability[91,92].

In particular, VSMCs and macrophage-like VSMCs have been shown to account for over half the foam cell content within atherosclerotic lesions[93,94]. However, while these cells may adopt certain characteristics of macrophages, they are not true macrophages. Macrophage-like VSMCs exhibit about a quarter of the phagocytic and efferocytic capacity of monocyte-derived or tissue resident macrophages[37,95,96]. Moreover, vascular smooth muscle cells characteristically express lower levels of lysosomal acid lipase (LAL) compared to macrophages and tend to store excess cholesterol within lysosomes rather than in the cytoplasm[96]. It has been reported that vascular smooth muscle cells are comparatively deficient in expression of ABCA1, which may contribute to their poor capacity for cholesterol efflux[96].

1.3 Mechanisms of Programmed Cell Death

Programmed cell death (PCD) is a tightly regulated process. Different forms of PCD often share certain molecular machinery or converge at particular points in their signaling cascade, with different switches and keys that drive the cell toward one form of cell death over another.

1.3.1 Apoptosis

During apoptosis, the plasma membrane remains largely intact as the dying cell fragments into apoptotic bodies expressing phosphatidylserine (PtdSer, a potent "eat-me" signal)[44]. When apoptosis is coupled with effective efferocytosis, phagocytes are able to clear apoptotic cells, thereby minimizing the stress they can incur on surrounding cells and tissue [43,97]. In the context of atherosclerosis, apoptosis is associated with resolution or plaque stability in the earlier stages of the disease[76].

Mechanistically, apoptosis is often broken into two main forms: *intrinsic* and *extrinsic* apoptosis. Intrinsic apoptosis is activated in response to internal sources of cellular stress,

including DNA damage, hypoxia, and ER stress[98,99]. Within an atherosclerotic lesion, these intracellular stressors often include DNA damage and ER stress from an abundance of reactive oxygen species and impaired rates of cholesterol efflux or metabolism. Conversely, extrinsic apoptosis is activated in response to extracellular sources of stress, particularly signaling associated with chemokines and cytokines, along with damage associated molecular patterns (DAMPs)[98,99]. In particularly advanced, unstable lesions, these pro-apoptotic signals can come from distress signals secreted by nearby cells and the remains of cells having undergone lytic forms of programmed (e.g. necroptosis, pyroptosis) or spontaneous cell death (e.g. necrosis)[11,100].

While intrinsic and extrinsic apoptosis may be initiated through different mechanisms, their signaling cascades converge to activate pro-apoptotic proteins BAX and BAK, which form pores in the mitochondria, triggering release of cytochrome c into the cytoplasm[101]. Cytochrome c binds and activates apoptotic protease activating factor-1 (Apaf-1), allowing it to oligomerize into a heptameric ring, where each unit of Apaf-1 recruits and cleave procaspase-9[102,103]. Together, this assembly forms the apoptosome. Once activated, caspase-9 cleaves procaspases-3 and 7 into their active, executioner forms, where they coordinate the controlled destruction of the cell[104].

As the cell dies, the plasma membrane begins to bleb and fragment into apoptotic bodies presenting phosphatidylserine (PtdSer), ICAM3, CRT, and DD1α, potent “eat me” signals, while secreting “find-me” signals to nearby phagocytes in the form of nucleotides along with cytokines and chemokines lysophosphatidylcholine (LPC), sphinosine-1-phosphate (S1P), and fractalkine (FKN)[99].

Because the cell membrane remains largely intact, apoptosis is generally considered an immunologically “silent” or “pro-resolving” form of cell death in terms of inflammatory

burden[105], particularly when compared to characteristically lytic forms of cell death, including pyroptosis and necroptosis[106].

1.3.2 Pyroptosis

Pyroptosis is a form of programmed cell death, traditionally mediated through inflammasome and caspase-1-dependent activation of gasdermins that form pores in the cell membrane, leading to cell lysis[107]. Pyroptosis has been described in late, vulnerable atherosclerotic lesions, and as an early effector for endothelial cell death and erosion triggered by shear stress[108,109].

Pyroptosis is initiated through recognition of intracellular distress signals including cytosolic DNA, ROS, and DAMPs by certain pattern recognition receptors (PRRs, e.g. AIM2, NLRP3)[110,111]. Upon activation, these sensors recruit apoptosis associated speck-like protein containing a CARD (ASC) adaptor proteins through recognition of matching pyrin-domains (PYD)[107]. As they form, these dimers assemble themselves into a multimeric ring structure called the inflammasome, which functions as a scaffold for caspase-1 activation[107,112].

Procaspase-1 is recruited to the CARD domain of the inflammasome, where it cleaves itself into distinct 20 kDa and 10 kDa subunits[112]. These subunits assemble to form an active tetramer, capable of cleaving the executioner of pyroptosis, gasdermin-D (GSDMD) along with precursor forms of pro-inflammatory cytokines, pro-IL-1ß and pro-IL-18[113–115]. The N-terminal fragment of cleaved GSDMD (N-GSDMD) is recruited to the plasma membrane where it oligomerizes to form pores that begin to trigger the lytic stage of pyroptosis[116].

At this stage, with N-GSDMD bound to the plasma membrane, an influx of extracellular Ca^{2+} can be sensed by membrane repair machinery, endosomal sorting complex required for

transport, ESCRT-0/I/II/III, to protect the cell against lysis[117]. Interestingly, ESCRT-III and associated membrane repair machinery have also been implicated in regulation of necroptosis, downstream of MLKL phosphorylation[118].

This ESCRT-mediated protection can be achieved through either: (a) secretion of the damaged portion of the cell membrane into ectosomes, or (b) endocytosis of the membrane-bound pores[119]. However, when pro-pyroptotic signaling is unrelenting and pore formation across the plasma membrane is extensive, the function of ESCRT machinery can become overwhelmed[120]. In these instances, pyroptosis succeeds against pro-survival mechanisms and the cell bursts, releasing IL-1ß, IL-18, along with other pro-inflammatory cytokines and chemokines, and DAMPs into the surrounding environment[108]. Interestingly, there have been reports showing activated caspase-3 and -7 are able to cleave GSDMD at Asp87, disabling its pore-forming activity[116,121,122].

Pyroptosis was first described in macrophages as a novel caspase-1 mediated form of necrotic programmed cell death in response to bacterial and viral infection[123–128]. In the years that followed, several non-canonical forms of pyroptosis were characterized[107]. In particular, caspase-8 has been shown to directly cleave GSDMD to activate pyroptosis[129]. Caspase-3 has also been reported to cleave GSDME, leading to pyroptosis through GSDME-mediated pore formation[130]. Alternatively, GSDME has been shown to function as a PRR to trigger inflammasome formation[131].

1.3.3 Necroptosis

Necroptosis is mediated primarily through a receptor-interacting serine/threonine-protein kinase 1 and 3 (RIPK1/RIPK3) axis, where the mixed lineage kinase domain like pseudokinase (MLKL) acts as the final executioner of cell death[132]. This process is activated through many of

the same cell death signaling receptors as apoptosis, including TNFR1, FAS, and TLR4 via binding of TNFα, FasL, and LPS respectively[133,134].

However, necroptosis is negatively regulated by caspase-8 mediated proteolytic cleavage of RIPK1 and RIPK3, targeting them for subsequent proteasomal or lysosomal degradation[135–138]. In this sense, in order for necroptosis to proceed, it relies on a key caspase-8 dependent switch to drive the cell toward necroptosis over apoptosis. In the atherosclerotic plaque, inactivation of caspase-8 is achieved organically[48], however, *in vitro* these conditions can be artificially simulated using a pharmacological pan-caspase inhibitor, zVAD[139].

When committed to necroptosis, the goal of the cell is to activate RIPK3-mediated phosphorylation of MLKL, which can be achieved through a RIPK1-dependent or independent mechanism[140]. When phosphorylated, RIPK1 and RIPK3 interactions are strengthened through their RIP homotypic interaction motif (RHIM), and recruit and phosphorylate two additional RIPK3 kinases to form the necrosome and phosphorylate MLKL[54].

Phosphorylation of MLKL promotes oligomerization of the pseudokinase, leading to a conformational change where the N-terminal 4-helix bundle (4HB) domain is exposed, which is necessary to mediate lytic activity of the complex[141]. Upon translocation of pMLKL to the plasma membrane through interactions with phosphoinositides (PIPs; including, $PI(4,5)P2_2$, PI5P, and PIP3) and phosphatidylserines (PtdSer), the oligomer uses its N-terminal 4HB domain to pierce the plasma membrane[141,142], forming a pore that ultimately lyses the cell to release its contents as DAMPs along with inflammatory cytokines and chemokines, recruiting additional monocyte-derived macrophages to the atherosclerotic lesion while feeding an acutely inflammatory, highly unstable plaque microenvironment[134,143].

1.4 Cell Death in Atherosclerosis

1.4.1 Necrotic Core

Early electron microscopy studies showed that advanced human lesions were characterized by the presence of a lipid-rich, acellular core, containing crystalline cholesterol clefts, and calcium deposits amid a "graveyard" of fragments of plasma membrane, organelles, and free DNA from dying cells[144–149]. Initial observations attributed cell death within the lesion to a combination of apoptosis, identified using terminal deoxynucleotidyl transferase-mediated dUTP nick-end labelling (TUNEL) assay, and spontaneous necrosis, whereby cells were punctured by cholesterol crystals or other debris within the lesion[145]. However, with the discovery of lytic forms of programmed cell death, our understanding of cell death within the atherosclerotic plaque evolved[106,150].

While early necrotic core formation is defined by defective phagocytosis coupled with an abundance of apoptotic cell death, advanced lesions are marked by a shift toward necroptosis, leading to increased inflammation, cellular debris, and overall destabilization of the plaque[8,37,55,93,151]. Our lab and others have demonstrated that necroptosis is a key driving force of necrotic core formation and expansion, where necroptosis accounts for over 60% of its size[11,152–156].

In advanced atherosclerotic lesions the necrotic core grows to account for over 10% of total lesion area[4]. Higher levels of RIPK1 and RIPK3 are associated with vulnerable lesions, as their activation leads to increased inflammatory signaling[155,157]. Moreover, inhibition of necroptosis through either RIPK1, RIPK3, or MLKL has been found to dramatically reduce necrotic core size[152,156,158].

Nonetheless, while apoptosis does remain a feature of both early and late atherosclerotic lesions[44,145], necroptosis appears to be a more prominent form of programmed cell death within late atherosclerotic lesions, contributing to an expanding necrotic core and overall, more pro-inflammatory, vulnerable plaque microenvironment[133,134,159,160].

1.4.2 The Bi-Directional Relationship Between Inflammation and Cell Death

Inflammation within atherosclerotic lesions can be attributed to a few key sources: distress, deprivation, and death. Disturbed or complex patterns of blood flow, along with accumulation of modified cholesterol particles, promote secretion of pro-inflammatory cytokines and chemokines within a lesion[68,161,162]. Moreover, the overwhelming increase in cell burden and activity strains the availability of resources within the vessel wall, leading to regions within a plaque that are nutrient-poor and hypoxic, where cells more readily activate inflammatory signaling pathways[163–165]. The addition of necrotic cell death within the artery wall and from responding immune cells only serves to aggravate an already prone environment through increased release of pro-inflammatory signaling molecules and cellular debris[10,11].

In early lesions where the immune system is able to overpower this cycle of cell death and inflammation, a gradual state of resolution can be restored[28,48]. However, in lesions where the degree of cell death and inflammation is too extreme, the lesion progresses to a more advanced, or vulnerable state[10,11,143]. Plaque progression is reinforced by this feedback between persistent inflammation leading to cell death, and cell death that releases acutely inflammatory signals to in turn trigger more cell death. This cycle of death and inflammation drives instability in an atherosclerotic plaque[10,11,143].

2.0 Rationale, Hypothesis, Objectives

2.1 Rationale

A key hallmark of advanced, rupture-prone atherosclerotic lesions is the presence of a necrotic core – a dense mass of pro-inflammatory and cellular debris. Moreover, technological advances have revealed that vascular smooth muscle cells have the capacity to transdifferentiate into "macrophage-like foam cells", which account for almost half of the cell content in advanced plaques. Our lab and others have discovered that a primary cause of the necrotic core is necroptosis – a lytic and acutely inflammatory form of cell death, where the mixed lineage kinase domain like pseudokinase MLKL is a key executioner of this process. While the contribution of necroptosis in macrophages to plaque growth and instability has been fairly well-studied, the role of necroptosis in vascular smooth muscle cells in this process remains unclear.

2.2 Hypothesis

MLKL regulates cell death differently in macrophages and vascular smooth muscle cells when challenged with pro-inflammatory or pro-atherogenic stimuli.

2.3 Objective and Aims

This work explores the role of MLKL in regulating necroptosis of macrophages and vascular smooth muscle cells when challenged with pro-inflammatory and pro-atherogenic stimuli.

Aim 1: Compare how macrophages and vascular smooth muscle cells undergo cell death in response to treatment with pro-inflammatory and pro-atherogenic stimuli.

Aim 2: Compare the expression and localization of MLKL in macrophages and vascular smooth muscle cells.

3.0 Materials and Methods

3.1 Isolation of Primary Cells and Cell Culture

3.1.1 Bone Marrow-Derived Macrophages (BMDMs)

Bone marrow was isolated from C57BL/6 wildtype (WT) or homozygous MLKL knockout ($MLKL^{-/-}$) mice and cultured in 20% L929 fibroblast conditioned media with 10% FBS (Gibco, 12483-020) and 1% antibiotic/antimycotic (Gibco, 15240-062) in high-glucose DMEM (Gibco, 11965-092). This conditioned media is prepared in-house from L929 fibroblasts cultured in 20% FBS (Gibco, 12483-020) and 1% penicillin-streptomycin (Gibco, 15140-122) in high glucose DMEM (Gibco, 11965-092). Bone marrow isolates are cultured at 37°C, 5% CO_2 for 7 days to allow time for differentiation of progenitor cells into macrophages, and these differentiated cells were used between 7-14 days post-isolation.

3.1.2 Aortic Vascular Smooth Muscle Cells (VSMCs)

The aorta was isolated from C57BL/6 wildtype (WT) or homozygous MLKL knockout ($MLKL^{-/-}$) mice and digested in an enzyme solution of Liberase TM (2 units/mL; Roche, 05401127001) and elastase (2 units/mL; Worthington Biochemical, LS002274) in HBSS (Gibco, 14175-095). The digested aorta was then filtered through a sterile 70 µm filter (Fisher, 22-363-548) before being cultured in high-glucose DMEM containing sodium pyruvate (Gibco, 11995-073) and supplemented with 20% FBS, fresh 20 mM L-glutamine (Gibco, 25030-081), 10 ng/mL murine leukemia inhibitor factor (LIF; Peprotech, 250-02), and 1 µM ß-mercaptoethanol (BME; MP Biomedicals LLC, 194705) in plates coated with 0.1% gelatin (Millipore, ES-006-B). Cells were used between passages 2 and 5.

3.2 Cell Treatments

3.2.1 BMDM-Conditioned Media (BCM)

BMDMs were treated under serum-reduced conditions (10% L929 in DMEM) with either 100 ng/mL LPS (Sigma, L4391-1MG), 50 ng/mL of TNFα (Peprotech, 315-01A-20UG) or 100 µg/mL oxLDL (prepared in-house) for a period of 24 hours. The resulting media was then collected and centrifuged at 300 g for 5 minutes. The supernatant was used to prepare treatments for VSMCs as indicated below.

3.2.2 Treatments

BMDMs and VSMCs were treated under serum-reduced conditions (10% L929 or 2% FBS in DMEM) with either 50 ng/mL TNFα, 100 ng/mL LPS, or 100 µg/mL oxLDL +/- 50 µM zVAD (APExBIO, A1902) and Nec1 (Sigma, N9037) for up to 72 hours. Treatments for VSMCs were prepared using either 2% FBS/DMEM, 10% L929/DMEM or BMDM conditioned media (BCM).

3.2.3 TNFR1 Inhibition

For experiments using TNFR1 inhibitor (R&D Systems, MAB430), BMDMs and VSMCs were pre-treated for 1 hour in their appropriate growth media supplemented with either 12- or 18-µg/mL of inhibitor. Cells were then treated under serum-reduced conditions (10% L929 or 2% FBS) with 100 µg/mL oxLDL +/- 50 µM zVAD and Nec1 or 50 ng/mL of TNFα for up to 72 hours, along with either 12- or 18-µg/mL of TNFR1 inhibitor.

3.3 Cytotoxicity Assays

3.3.1 Lactate Dehydrogenase (LDH) Assay

Samples were plated in technical triplicate in 24-well plates. BMDMs were plated at a density of approximately 0.5 million cells per well, while VSMCs were plated at a density of

approximately 0.2 million cells per well (or one tenth of cell suspension from a confluent 10-cm dish). Cells were treated according to the descriptions above in a volume of 250 µL per well.

To perform this assay, 10 µL of media is sampled from the treatment vessel and plated in duplicate in a clear 96-well plate (Evergreen, 290-8115-01F). To each well, 200 µL of reaction buffer (0.015% NADH (BioShop, NAD002.1), 0.0275% sodium pyruvate (Fisher, BP356-100) in PBS) was added, and as the reaction occurred, the plate was read at 1-minute intervals for 10 minutes, recording absorbance at 340 nm using a BioTek Synergy H1 microplate reader (S/N: 22041503). By plotting a slope of the mean changes in absorbance over time, it is possible to compare levels extracellular LDH between treatments relative to a VSMC no-treatment control. This assay was performed at 3-, 6-, 18-, 24-, 48-, and 72-hours post-treatment.

3.3.2 SYTOX (NucGreen™) Assay

By using a SYTOX Green ("NucGreen™ Dead 488", propidium iodide; Invitrogen, R37109) dye that selectively permeates cells with compromised membranes to fluorescently label dead or dying nuclei against measures of total nuclei stained with NucBlue™ (Hoechst 33342; Invitrogen, R37605), it is possible to monitor cell death as a percent of total cells in response to treatment over time.

BMDMs were seeded in technical triplicate at a density of 50 000 cells per well in clear bottom, black polystyrene sterile 96-well microplates (Corning, 07-200-565), while VSMCs were seeded at a density of approximately 20 000 cells per well. To 300 µL of treatment solution (prepared according to the descriptions above), 1 drop of SYTOX Green and NucBlue dyes were added. From this solution, cells were treated in a volume of 100 µL per well. Readings were acquired using an Agilent BioTek Cytation 5 cell imaging multimode plate reader (S/N: 171115E) at 3-, 6-, 18-, 24-, 48-, and 72-hours post-treatment. Images were acquired with filter

sets for laser autofocus (LED PN: 1225010), brightfield (LED PN: 1223003), DAPI (Filter PN: 1225100, LED PN: 1225000), and GFP (Filter PN: 1225101, LED PN: 1225001). For longer experiments, where readings were taken every 6 hours, an Agilent BioTek BioSpa 8 incubator (S/N: 1711131D) was used to automatically feed plates into the reader. Images were quantified using BioTek Gen5 Image Prime v3.12.

3.3.3 CellEvent™ Red, Cleaved-Caspase-3/7 Assay

BMDMs were seeded in technical triplicate at a density of 50 000 cells per well in clear bottom, black polystyrene sterile 96-well microplates (Corning, CAT#07-200-565), while VSMCs were seeded at a density of approximately 20 000 cells per well. Cells were treated according to the descriptions above in a volume of 100 µL per well. To each well, 1 µL of CellEvent Red, Caspase-3/7 detection reagent (1:100; Invitrogen, CAT#C10430). Readings were taken every six hours using an Agilent BioTek BioSpa 8 incubator (S/N: 1711131D) to automatically feed plates into the reader, and images were acquired using an Agilent BioTek Cytation 5 cell imaging multimode plate reader (S/N: 171115E) with filter sets for laser autofocus (LED PN: 1225010), brightfield (LED PN: 1223003), DAPI (Filter PN: 1225100, LED PN: 1225000), and TexasRed (Filter PN: 1225102, LED PN: 1225002). Images were quantified using BioTek Gen5 Image Prime v3.12.

3.4 Lentiviral Transduction

3.4.1 Lentiviral Transduction of Primary Mouse BMDMs

BMDMs were infected with lentivirus at an MOI (multiplicity of infection) of 10 in media containing 10 µM cyclosporine A (CSA; Sigma, C3662), 10% L929 and 10% FBS in plain DMEM for a period of 24 hours. The cells were then released into fully supplemented growth media (10% FBS, 20% L929 in DMEM) to recover for another 24 hours before being infected

again at an MOI of 10 for 24 hours. After the second infection event, the cells are released back into fully supplemented growth media for 24 hours, and their media was changed every 48 hours until use. Percent-transduction was assessed 72 hours after release from the second infection event. This protocol was adapted from Pajarinen et al., 2015 and Noser et al., 2006[166,167].

3.4.2 Lentiviral Transduction of Primary VSMCs

VSMCs were infected with lentivirus at an MOI of 50 in media prepared with 6 μg/mL of polybrene (Sigma, CAT#H9268) and 2% FBS in plain DMEM for a period of 24 hours. The cells were then released into fully supplemented growth media to recover for 24 hours, and their media was changed every 48 hours until use. Percent-transduction was assessed 72 hours post-infection. This protocol was adapted from work by Sakoda et al., 2007, Lv et al., 2008, and Yang et al., 2010[168–170].

3.5 Protein Isolation and Western Blotting

The following protocol is adapted from work by Samson et al., 2020 and 2021[171,172]. Cells were lysed in ice-cold RIPA buffer made with 10 mM Tris-HCl, pH 8.0 (Fisher, BP153), 1 mM EGTA (Fisher, O2783), 2 mM $MgCl_2$ (Fisher, BP214), 0.5% v/v Triton X-100 (Fisher, BP151), 0.1% w/v sodium deoxycholate (ICN Biomedicals, 102906), 0.5% w/v SDS (Fisher, BP1311), and 90 mM NaCl (Fisher, BP358), supplemented with fresh 1x protease inhibitor cocktail (PIC; Roche, 04 693 132 001), 1x phosphatase inhibitor cocktail (PhIC; Roche, 04 906 837 001), 100 U/mL benzonase (Millipore, 70746-3), and 2 mM $MgCl_2$.

Total protein from whole cell lysates was quantified using BioRad Pierce 660 (PI-22660) and BCA (23228 and 23224) protein quantification kits. Standards were prepared using powdered BSA (Sigma, A7906) diluted in fresh RIPA buffer prepared during the protein isolation.

Samples were boiled at 75°C for 10 minutes in 1X loading dye (126 mM Tris-HCl pH 8.0, 20% v/v glycerol (Fisher, BP229), 4% w/v SDS, 0.02% w/v bromophenol blue (BioRad, 161-0404), 5% v/v ß-mercaptoethanol), and between 15-20 µg of protein was loaded per well of a Criterion TGX 8-16% gel (BioRad, 5671104). Samples were loaded along with an MLKL-/- whole cell lysate. Gels were run at 80-100 V until the desired separation was achieved. For blots where pMLKL/MLKL would be probed, gels were run past the 25 kDa mark to promote separation between true phospho-MLKL signal and non-specific bands. Samples were transferred onto 0.45 µm nitrocellulose membranes (BioRad, 1620115) at 100 V and 4°C for 30 minutes using a high-current power pack (BioRad, S/N: 1645052).

Membranes were blocked for 1-1.5 hours at room temperature (RT) in 5% w/v BSA, 0.1% v/v Tween-20 (Fisher, BP337-100) in TBS and incubated overnight at 4°C in primary antibodies diluted in 5% BSA TBS-Tween. Blots were probed using antibodies against RIPK1 (Rb, 1:1000; Cell Signaling, 3493S), pMLKL (Rb, 1:2000; Cell Signaling, 37333), MLKL (Rt, 1:2000; Millipore, MABC604MI), GSDMD (Rb, 1:1000; Abcam, ab219800), STAT3 (Rb, 1:2000; Cell Signaling, 12640S), STAT1 (Ms, 1:1000; Abcam, ab281999), and IRF1 (Rb, 1:1000; Cell Signaling, 8478S). Membranes were also probed for GAPDH (Rb, 1:5000; Millipore, ABS16) to use as a loading control. After being washed 3x 5-10 min in TBS-Tween, blots were incubated in the appropriate HRP-conjugated secondary antibody diluted in 5% BSA TBS-Tween for 1-1.5 hours at RT. The following HRP-conjugated secondary antibodies were used: anti-rabbit (Jackson ImmunoResearch Laboratories, 111-035-144), anti-mouse (Invitrogen, A16072), and anti-rat (AbD Serotec, STAR72) at a dilution of 1:5000.

Membranes were washed again 3x 5-10 min in TBS-Tween before being imaged on a ChemiDoc MP Imaging System (S/N: 734BR7783) using either Clarity or Clarity Max ECL

substates (BioRad, 1705061 and 1705062). Between probes for targets with similar molecular weights, membranes were incubated in stripping buffer (ThermoFisher, 21059) for 10-30 minutes at RT, before being re-blocked and probed with new primary antibody. Band intensity was quantified using Image Lab 6.1, and final values are normalized to GAPDH band intensity and reported as a fold-change compared to VSMC (10% L929) "no-treatment" control.

3.6 Immunofluorescence

3.6.1 Immunofluorescence of Fixed Cells

BMDMs and VSMCs were seeded at a density of 50 000 and 20 000 cells per well respectively in 18-well µ-chamber slides (Ibidi, 81816).

Sample Preparation: Methanol Fixation, pMLKL/MLKL Staining

The following protocol for immunofluorescence imaging of MLKL and pMLKL is adapted from work by Samson et al., 2020 and 2021[171,172]. Cells were chilled on ice for 3 minutes before being washed three times in ice-cold PBS. Samples were fixed in 100 µL per well of ice-cold methanol for 15 minutes, then washed three times in ice-cold PBS before blocking in cold 10% donkey serum (Sigma, D9663), 0.05% Triton X-100 (Fisher, BP151) in TBS for 1.5 hours. Cells were incubated overnight at 4°C in primary antibodies diluted in 10% donkey serum, TBS-Triton. Both BMDMs and VSMCs were incubated in primary antibodies against pMLKL (Rb, 1:200; Cell Signaling, 37333), MLKL (Rt, 1:50; Millipore, MABC604MI), while BMDMs were additionally probed for ß-actin (Ms, 1:750; Sigma, A5441) and VSMCs were probed for α-smooth muscle actin (α-SMA, 1:750; Ms, Novus, NBP2-33006). The following day, cells were washed two times in ice-cold TBS-Triton, and then incubated in anti-rabbit AF647 (Invitrogen, A21244), anti-rat AF568 (Invitrogen, A78946), and anti-mouse AF488 (Invitrogen, A11029) secondary antibodies diluted 1:1000 in 10% donkey serum TBS-Triton for three hours

at RT. Cells were washed two times in ice-cold TBS-Triton, and stained with Hoechst 33342 (1:2000 in PBS; Invitrogen, H3570) for 4 minutes at RT. Samples were washed 4 quick times in cold, plain PBS before being mounted in non-hardening mounting media (Ibidi, 50001).

Sample Preparation: PFA Fixation, Staining for Transcription Factors

Cells were washed twice in warm PBS, and then fixed in pre-warmed 4% PFA for 10 minutes at 37°C. Samples were washed three times for 5 minutes each in ice-cold PBS before incubating for 1 hour in ice-cold blocking and permeabilization buffer (10% donkey serum, 0.2% Triton X-100, 0.05% Tween-20, 1% BSA in PBS). Samples were stained overnight at 4°C in STAT1 (Ms, 1:25; Abcam, ab281999) and IRF1 (Rb, 1:200; Cell Signaling, 8478S) primary antibodies diluted in blocking and permeabilization buffer. Cells were washed three times in ice-cold PBS, then incubated in anti-mouse AF488 (Invitrogen, A11029) and anti-rabbit AF568 (Abcam, ab175470) secondary antibodies diluted 1:500 in 10% donkey serum in PBS. Samples were then washed three times in ice-cold PBS before incubating for 2 hours in primary-conjugated antibody against STAT3-AF647 (0.5 µg/mL; Cell Signaling, 14062S), using an AF647 Rb IgG control (0.5 µg/mL; Cell Signaling, 2985S) diluted in blocking and permeabilization buffer. Cells were washed three times in ice-cold PBS, before being stained for 10 minutes in DAPI. Samples were washed 4 quick times in cold, plain PBS before being mounted in non-hardening mounting media (Ibidi, 50001).

Airyscan Microscopy

Images were acquired using an inverted LSM880 microscope (Zeiss) with a Plan-Apochromat 20x/0.8 NA oil objective (Zeiss), along with 405-, 488-, 561-, and 633 nm laser lines using radially-stacked Airyscan GaASP detectors set to super-resolution (SR)-mode in Zen

Black. Filter method was set to an average of 2. Z-stacks were acquired with a step size of 0.16-0.18 µm. Image processing post-acquisition was performed in Zen Black v2.3 SP1 using the automated "2D AiryScan Processing" and maximum intensity projection functions on stacks of 5 slices. Mean fluorescence intensity (MFI) and positive pixel area were measured using FIJI v1.54.

3.6.2 Immunofluorescence of Fixed Tissue

Sample Preparation: Methanol Fixation, MLKL Staining

The following protocol for immunofluorescence imaging of MLKL in tissue is adapted from work by Samson et al., 2020 and 2021[171,172]. Frozen sections of aortic sinus were dried in a fumehood for 30 minutes at RT before being fixed for 30 minutes in ice-cold methanol at -20°C. Tissues were blocked overnight at 4°C in 10% donkey serum TBS-Triton. The following day, slides were incubated in MLKL (Rt, 1:50; Millipore, MABC604MI) and CD68 (Rb, 1:200; Proteintech, 28058-1-AP) primary antibodies diluted in 10% donkey serum in TBS-Triton at 4°C overnight. Tissues were washed three times in ice-cold TBS-Triton before incubating in anti-rat AF647 (Invitrogen, A21247) and anti-rabbit AF568 (Abcam, ab175470) secondary antibodies diluted 1:1000 in 10% donkey serum TBS-Triton overnight at 4°C. Samples were washed three times in TBS-Triton and then stained in primary-conjugated CD45-AF488 antibody (0.38 µg/mL; Cell Signaling, 59572S), using an AF488 Rb IgG control (0.38 µg/mL; Cell Signaling, 4340S), diluted in 10% donkey serum with TBS-Triton for 2 hours at RT. Slides were then washed two times with TBS-Triton and then stained with Hoechst 33342 diluted 1:2000 in PBS. Tissues were then washed four times in TBS-Triton, then dunked quickly twice in distilled water before being mounted with DAKO fluorescence mounting media (Agilent, S302380-2) and 1.5 NA coverslips (Fisher, 12544D).

Confocal Microscopy (Spinning Disk)

Images were acquired using a DMI6000B inverted spinning disk confocal microscope (Leica) equipped with an sCMOS camera (Photometrics Prime BSI) using a PlanApochromat 40x/1.3 NA oil objective, along with 405-, 490-, 561-, 639 nm laser lines and paired with 460/50-, 525/50-, 605/52-, 620/60 nm confocal filter sets in MetaMorph. Z-stacks were acquired with a step size of 0.5 µm. Image processing post-acquisition was performed in FIJI v1.54 using the maximum intensity project function on stacks of 21 slices. Mean fluorescence intensity (MFI) and positive pixel area were measured using FIJI v1.54.

3.7 ELISAs

Samples of BMDM conditioned media were obtained from cells that were treated for 24 hours under serum-reduced conditions (10% L929/DMEM) with oxLDL, LPS, or TNFα. A sample of conditioned media from WT and MLKL-/- BMDMs subjected to only serum-reduced conditions was used as an "untreated" control.

ELISAs were performed using DuoSet ELISA Ancillary Reagent Kit 2 (R&D Systems, CAT#DY0008) along with the following kits from R&D Systems: Mouse IL-1ß/IL-1F2 DuoSet (CAT#DY401), Mouse TNF-alpha DuoSet ELISA (CAT#DY410), Mouse IL-6 DuoSet ELISA (CAT#DY406).

Briefly, polystyrene 96-well microplates were coated with 100 µL/well of capture antibody diluted in PBS, and incubated overnight at room temperature. The following day, plates were washed in wash buffer (R&D Systems, CAT#WA126) before blocking for 1 hour at RT using reagent diluent (R&D Systems, CAT#DY995). Plates were then washed before incubating for 2 hours at RT in samples of conditioned media from WT and $MLKL^{-/-}$ BMDMs. After

washes, plates were incubated in detection antibody for 2 hours at RT. Plates were washed and incubated in diluted streptavidin-HRP for 20 minutes, protected from light. After being washed for the final time, plates incubated in TMB substrate for 20 minutes, protected from light, after which the reaction was stopped by adding STOP buffer. Optical density was measured at 450 nm and 540 nm using a BioTek Synergy H1 microplate reader (S/N: 22041503).

3.8 Statistical Analyses

Data is reported as a mean value +/- the standard error of the mean (SEM) or standard deviation (SD) of at least three independent experiments or biological replicates. Figures presenting preliminary data (where n = 1 or 2) are indicated in the figure legend. Statistical analysis was performed using GraphPad Prism 10.3.1 software. Comparisons between multiple experimental groups were performed using a two-way analysis of variance (ANOVA), where adjusted p-values for multiple comparisons were determined by Šidák or Dunnett's correction. Dunnett's correction is used to account for multiple comparisons that are made against a single control mean, while Šidák's correction is used to account for multiple comparisons that are made between multiple sets of means. Statistical significance is assessed according to the following p-value thresholds, where *$p<0.05$, **$p<0.01$, ***$p<0.001$, ****$p<0.0001$.

4.0 Results

4.1 BMDMs are more sensitive to cell death stimuli than VSMCs

By measuring extracellular levels of lactate dehydrogenase (LDH) in media collected from treated BMDMs and VSMCs and normalizing to a VSMC "no treatment" (NT) control, it may be possible to compare rates of cell death between these two cell types in response to treatment with pro-inflammatory and pro-atherogenic stimuli. Overall, VSMCs appear to release lower levels of LDH in response to treatment compared to BMDMs (Figure 2B-C, S1), even when treated with staurosporine (STS), a non-selective kinase inhibitor, and potent inductor of apoptosis[173]. While it is possible that lower levels of extracellular LDH could be attributed to lower rates of cell death in VSMCs as compared to BMDMs, it could be equally associated with reasons that are unrelated to cell death, including differences in metabolism and proliferation between these cell types[174,175]. In this sense, it may be difficult to use relative LDH release as an accurate measure to compare rates of cell death between BMDMs and VSMCs.

By using a propidium iodide-based stain (SYTOX Green) that selectively permeates cells with compromised plasma membranes to fluorescently label the nuclei of dead or dying cells, against measures of total nuclei stained with NucBlue (Hoechst), it is possible to monitor cell death as a percent of total cells in response to treatment over time (Figure 2, S1). In doing so, it appears that BMDMs are particularly sensitive not only to treatment with staurosporine (STS) and lipopolysaccharides (LPS), but also to serum-reduced conditions (Figure 2A-B, S1). When treated with STS or LPS + zVAD, BMDMs appear to undergo cell death as soon as 3- and 6-hours post-treatment, respectively (Figure 2B, S1). Under serum-reduced conditions alone ("NT"), BMDMs appear to die within 18 hours of treatment (Figure 2B, S1).

Conversely, it would seem that VSMCs are more tolerant to treatment than BMDMs, taking up to 18 hours to show signs of cell death by SYTOX assay when treated with STS or LPS (Figure 2A, C, S1). VSMCs would also seem to be generally more tolerant to serum-reduced conditions, taking up to 48 hours to begin to show increased rates of SYTOX positivity in samples that are subjected to serum-reduced conditions alone (Figure S1). While these observations are consistent with results from LDH assayed samples, it would seem that SYTOX Green is generally a more sensitive indicator of cell death in both BMDMs and VSMCs (Figure 2, S1).

When rates of cell death, measured by SYTOX positivity are directly compared at 6-hours post treatment between BMDMs and VSMCs, it would indeed seem that BMDMs undergo cell death in response to STS and LPS + zVAD treatment more readily than VSMCs (where $p = 0.0011$, $p < 0.0001$ respectively; Figure 1D). Interestingly, it would also seem that VSMCs are more tolerant to serum-reduced conditions in general when compared to BMDMs ($p < 0.0001$; Figure 1E).

To assess whether L929 conditioned media may account for differences seen in sensitivity to cell death stimulation between these cell types, VSMCs were equally treated in either 10% L929 or 2% FBS and subjected to LDH and SYTOX assays (Figure S1). However, VSMCs treated in 10% L929 appear to undergo cell death at rates comparable to VSMCs treated in 2% FBS, consistent between both SYTOX and LDH assayed samples (Figure S1).

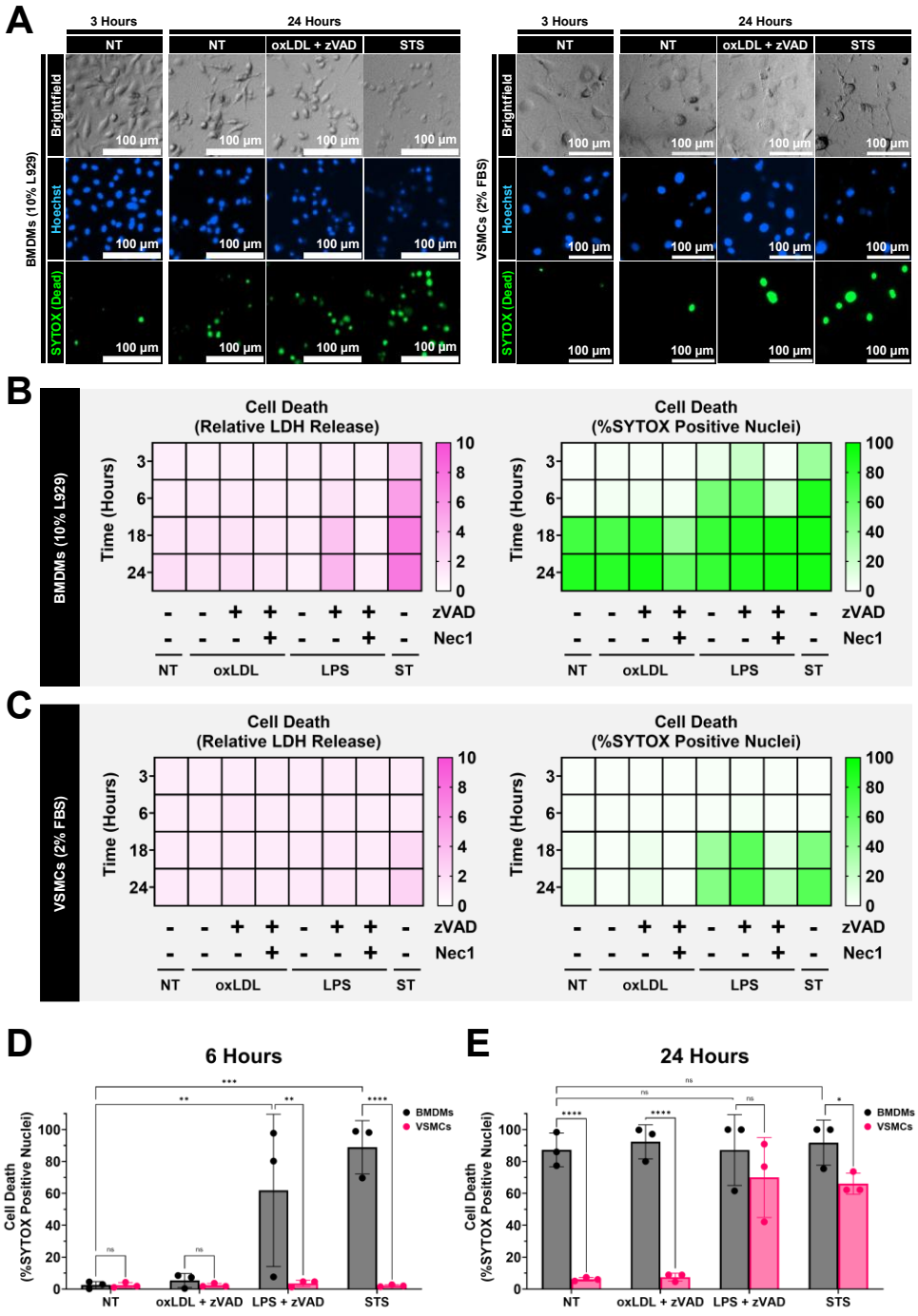

Figure 2. BMDMs appear to be more sensitive to cell death stimuli than VSMCs. A Brightfield and fluorescence widefield microscopy of BMDMs and VSMCs under serum-reduced conditions, treated with oxLDL + zVAD or staurosporine (STS). Shown in blue is total nuclei (stained with NucBlue), while the nuclei of dead or dying cells is shown in green (stained with SYTOX Green). **B-C** Heat maps showing rates of cell death in BMDMs and VSMCs as measured by LDH (magenta) and SYTOX (green) over time. **D-E** Comparison of rates of cell death as measured by SYTOX staining between BMDMs and VSMCs after 6 and 24 hours of treatment under serum-reduced conditions with oxLDL + zVAD, LPS + zVAD, or staurosporine. Data points shown represent the mean with SD from parallel LDH and SYTOX experiments (n = 3). Statistical significance was assessed using an ordinary two-way ANOVA with Šidák's multiple comparisons test, where *p<0.05, **p<0.01, ***p<0.001, ****p<0.0001.

4.2 BMDM conditioned media potentiates cell death in VSMCs

To determine whether conditioned media from BMDMs may be able to prime VSMCs to undergo cell death, VSMCs were treated in media from BMDMs conditioned for 24-hours with either, oxLDL, LPS , TNFα, or serum-reduced conditions alone ("NT"; Figure 3A-B, S2). When treated with conditioned media, particularly from BMDMs conditioned with oxLDL or TNFα, VSMCs seem to undergo overall higher rates of cell death, compared to VSMCs treated in the absence of BMDM conditioned media (Figure 3A-B, S2). Particularly of interest, it seems that VSMCs, which are otherwise not sensitive to oxLDL treatment, appear to show signs of increased SYTOX positivity when treated in the presence of conditioned media from BMDMs, even from BMDMs conditioned with serum-reduced media alone (Figure S2). When these samples are treated with Nec1, we see rates of SYTOX positive staining decline, which may suggest that the cell death being induced by these treatments is RIPK1-dependent (Figure 3B).

To assess whether residual oxLDL, TNFα, or LPS from the BMDM conditioned media may account for increases seen in cell death in these treatment groups, VSMCs were treated with increasing doses of these stimuli in the presence or absence of zVAD and stained with SYTOX Green (Figure 3C). Interestingly, it would appear that higher doses of oxLDL are not particularly cytotoxic to VSMCs. Indeed, even when treated with double the usual dose of oxLDL, VSMCs do not seem to undergo oxLDL-mediated cell death in the absence of BMDM conditioned media. Taken together, these results may suggest that VSMCs are not particularly sensitive to treatment with oxLDL, even at higher doses, and that BMDM conditioned media seems able to prime VSMCs to undergo oxLDL-mediated cell death. Curiously, VSMCs treated in BMDM conditioned media do appear to show some amount of increased sensitivity to STS as well, particularly when treated in media from BMDMs conditioned with TNFα (Figure 3A-B, D; S2).

To further understand the contribution of apoptosis to the SYTOX-positive staining observed, parallel sets of treated BMDMs and VSMCs were treated and stained with CellEvent Red, a dye that fluorescently labels the nuclei of cells with cleaved caspase-3/7 (Figure 3D, S3, S4). Interestingly, while the rate of percent-positive cleaved-caspase-3/7 nuclei between VSMCs treated with oxLDL + zVAD in 10% L929 or oxLDL BMDM conditioned media appears to be fairly similar (6 hours post-treatment, $p = 0.6953$; Figure 2D, S3, S4), the rate of SYTOX positive nuclei between these two groups is starkly different (6 hours post-treatment, $p = 0.0053$; Figure 2D, S3, S4), as VSMCs in oxLDL BMDM conditioned media show higher rates of SYTOX-positivity over cleaved-caspase-3/7 positivity, which may suggest that the cell death that is potentiated by BMDM conditioned media in VSMCs is likely not apoptosis.

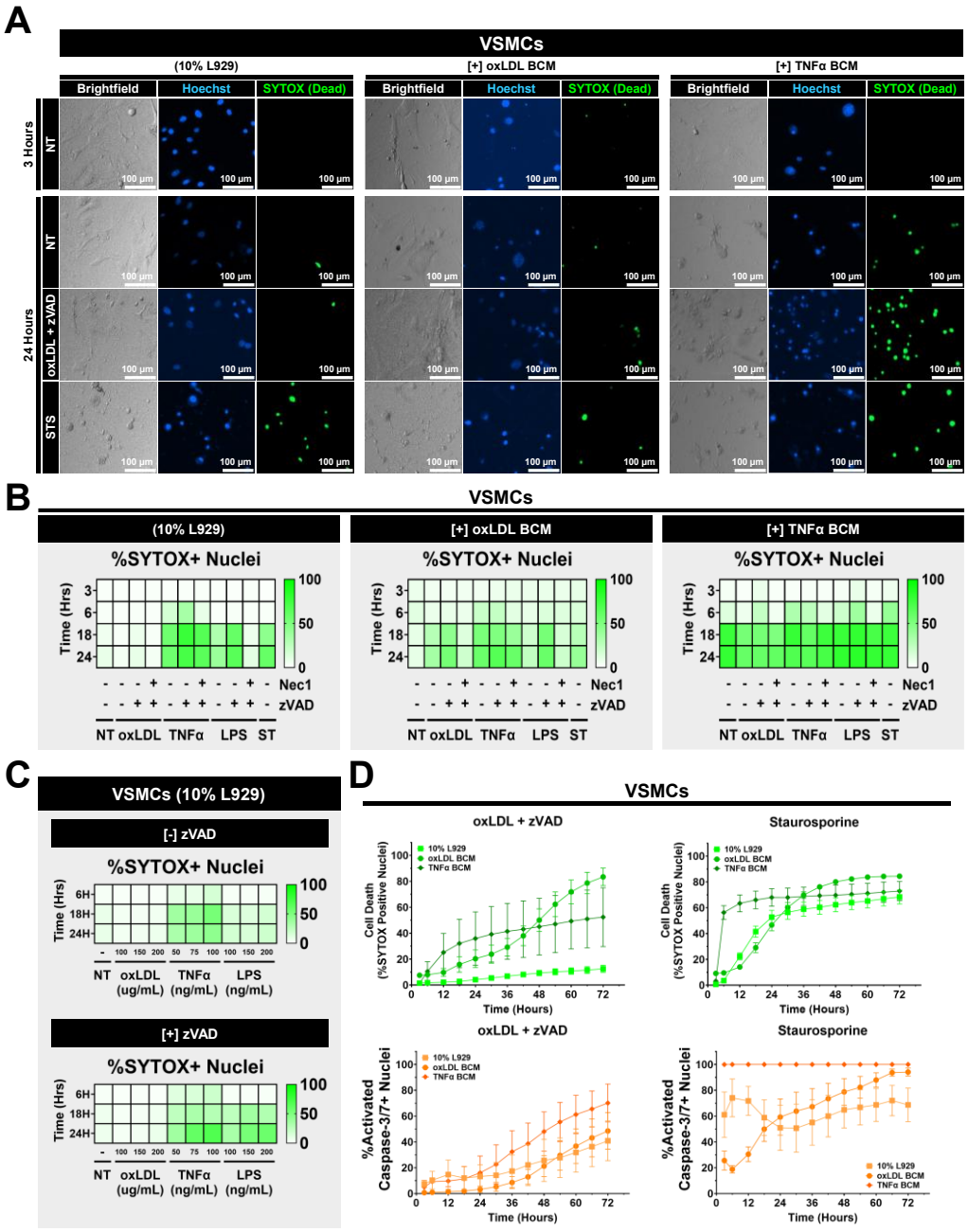

Figure 3. BMDM conditioned media potentiates cell death in VSMCs. A Brightfield and fluorescence widefield microscopy of VSMCs under serum-reduced conditions (10% L929) treated with oxLDL + zVAD or staurosporine (STS), in the presence or absence of BMDM conditioned media (BCM). Shown in blue is total nuclei (stained with NucBlue), while the nuclei of dead or dying cells is shown in green (stained with SYTOX Green). **B** Heat maps comparing rates of cell death in VSMCs treated in the presence or absence of BCM as measured by SYTOX staining (green) over time (mean +/- SD, n = 3). **C** Heat maps comparing rates of cell death in VSMCs treated under serum-reduced conditions (10% L929) with increasing concentrations of oxLDL, TNFα, and LPS as measured by SYTOX staining (green) over time (mean +/- SD, n = 3). **D** Line graphs comparing rates of cell death as measured by SYTOX (green) and activated caspase-3/7+ (orange) staining in response to treatment with oxLDL + zVAD or staurosporine (STS), in the presence or absence of BCM (mean +/- SEM, n = 5).

4.3 MLKL expression is upregulated in VSMCs treated with conditioned media

To understand the role of MLKL in the death of VSMCs treated with conditioned media, samples of VSMCs were treated for 18 hours with oxLDL +/- zVAD, Nec1 in the presence or absence of BMDM conditioned media, and stained for total and phosphorylated forms of MLKL. Equally, samples of BMDMs were treated for 18 hours with oxLDL +/- zVAD, Nec1 and also stained for total and pMLKL. When imaged using airyscan microscopy, BMDMs appear to be more densely packaged with MLKL than VSMCs (Figure 4A, S5). Interestingly, VSMCs appear to express higher levels of MLKL when treated with conditioned media from BMDMs, with correspondingly more pMLKL in these samples as well (Figure 4A, S5).

When total protein abundance is measured by Western blotting at 6- and 24-hours post-treatment, it appears that VSMCs treated with oxLDL in media from BMDMs conditioned with TNFα seem to express more MLKL than VSMCs treated without BMDM conditioned media, along with higher levels of relative phosphorylated MLKL (6 hours, $p = 0.0002$; 24 hours, $p = 0.0003$; Figure 4D-E, S6-8). When these cells are treated with Nec1, there is a loss of pMLKL signal, that corresponds with decreases in SYTOX-positivity (Figure 4D-E; Figure 3B, D). Interestingly, there also appears to be an increase in the abundance of GSDMD in VSMCs treated in media from BMDMs conditioned with TNFα (Figure 4D-E). Overall, these results seem to suggest that BMDM conditioned media may be able to upregulate MLKL in VSMCs, which may contribute to priming VSMCs to undergo cell death when treated with oxLDL. However, while VSMCs in conditioned media from BMDMs appear to express more MLKL, they do not seem to express CD68 (Figure S13).

In order to better understand the contribution of MLKL to SYTOX-positive staining observed in previous experiments, rates of cell death in wildtype and $MLKL^{-/-}$ BMDMs and

VSMCs were compared in samples treated with oxLDL +/- zVAD and Nec1 (Figure 4F, S10). In BMDMs and VSMCs treated under serum-reduced conditions, it seems that MLKL$^{-/-}$ cells are slightly less prone to cell death than their WT counterparts (Figure 4F). However, curiously, while MLKL$^{-/-}$ BMDMs treated with oxLDL + zVAD also appear to be somewhat more tolerant than their counterparts, MLKL$^{-/-}$ VSMCs treated in 10% L929 with oxLDL seem to be possibly more prone to cell death (Figure 4F, S10). Moreover, while MLKL$^{-/-}$ VSMCs in TNFα BCM seem generally less prone to cell death than their wildtype counterparts when treated with oxLDL + zVAD or under serum-reduced conditions alone, MLKL$^{-/-}$ VSMCs in oxLDL BCM appear to be somewhat more prone to cell death than their wildtype counterparts (Figure 4F, S10). While unexpected, these results may prompt the need for follow-up experiments to use a transient knockdown or knockout MLKL system, potentially with siRNA to account for whether transgenic MLKL$^{-/-}$ cells may have adapted to be overall less reliant on MLKL-mediated necroptosis.

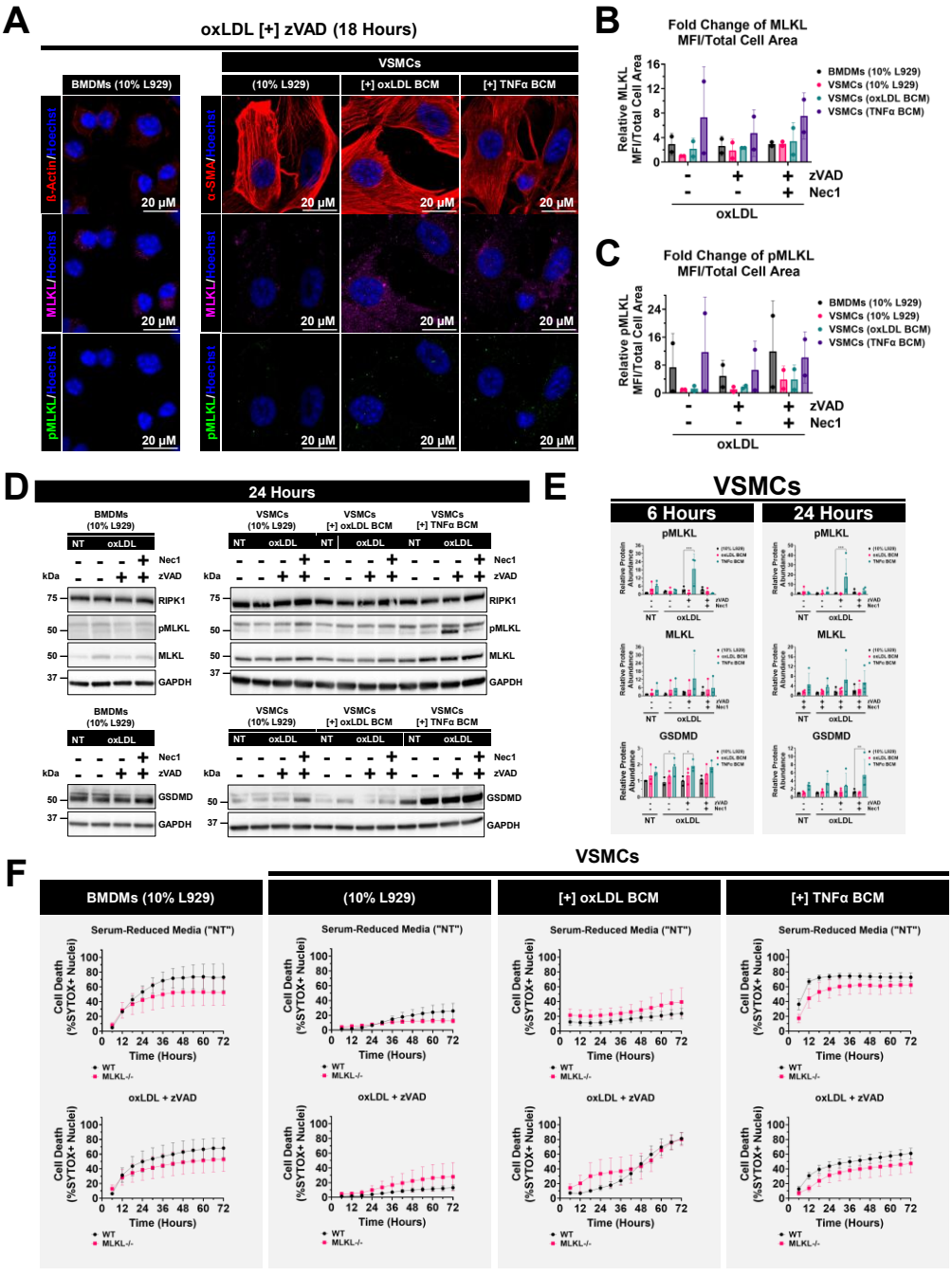

Figure 4. MLKL appears upregulated in VSMCs treated with conditioned media. A Airyscan confocal fluorescence microscopy of BMDMs and VSMCs 18 hours post-treatment with oxLDL + zVAD. VSMCs are shown treated in the presence or absence of BCM. **B-C** Fold change of MLKL and pMLKL MFI over total cell area, normalized to signal from a VSMC (10% L929) sample treated with oxLDL (mean +/- SD, n = 2). **D** Western blots of BMDMs and VSMCs 24 hours post-treatment with oxLDL +/- zVAD, Nec1. VSMCs are shown treated in the presence or absence of BCM. **E** Relative pMLKL, MLKL, and GSDMD expression in VSMCs treated in the presence or absence of BCM 6- and 24-hours post-treatment (mean +/- SD, n = 3-4). Statistical significance was assessed using an ordinary two-way ANOVA with Dunnett's multiple comparisons test, where *p<0.05, **p<0.01, ***p<0.001, ****p<0.0001. **F** Line graphs comparing rates of cell death as measured by SYTOX staining (green) over time in wildtype (WT) and MLKL-/- BMDMs and VSMCs (mean +/- SEM, n = 4).

4.4 TNFα signaling may contribute to MLKL upregulation in VSMCs

In order to better understand which secreted factors from BMDMs may influence potentiation of cell death and MLKL upregulation in VSMCs, ELISAs were performed on samples of media obtained from both wildtype and $MLKL^{-/-}$ BMDMs treated under serum-reduced conditions alone, or with oxLDL, LPS or TNFα (Figure 5A, S14). Although preliminary, it is interesting to note that while WT and $MLKL^{-/-}$ BMDMs treated in oxLDL both secrete some amount of TNFα or IL-16, only WT BMDMs seem to secrete IL-1ß (Figure 5A, S14).

Moreover, when VSMCs in 10% L929 are treated with TNFα, there appears to be an increase in both MLKL percent-positive area and MFI (Figure 5B, C, E; S12). However, when VSMCs in BMDM conditioned media are treated with TNFα, while there may be relatively similar levels MLKL between these groups, there appears to be somewhat less pMLKL in these samples, compared to VSMCs in 10% L929 that are treated with TNFα (Figure 5B, D, F; S12).

In order to better understand the potential contribution of TNFα signaling in BMDMs and VSMCs in the context of cell death, samples of cells were treated with a neutralizing inhibitor of TNFR1 along with TNFα or oxLDL +/- zVAD, Nec1 in the presence or absence of BMDM conditioned media (Figure 5G, S11). Remarkably, while treatment with TNFR1 inhibitor appears to somewhat decrease rates of cell death in VSMCs in 10% L929 treated with TNFα, the inhibitor seems to be cytotoxic to VSMCs under serum-reduced conditions, but only cytotoxic to VSMCs treated with oxLDL + zVAD when treated at a dose of 12 µg/mL, but not 18 µg/mL (Figure 5G, S11). Furthermore, upon addition of conditioned media to this treatment panel, cells seem to be even more sensitive to treatment with oxLDL + zVAD, and even serum reduction (Figure 5G, S11). Treatment with 18 µg/mL of TNFR1 inhibitor seems to kill between 20-40% of cells within the first three hours of treatment, but then levels of cell death seem to plateau at

this level and remain steady up to 72 hours post treatment (Figure 5G, S11). In this sense, at 72 hours post-treatment in VSMCs in oxLDL BCM, 18 μg/mL of TNFR1 inhibitor may seem to reduce rates of cell death in samples treated with TNFα or oxLDL + zVAD ($p < 0.0001$; Figure 5G), however, at 6 hours post-treatment, the inhibitor seems to stimulate a certain amount of cell death ($p = 0.0031$; Figure 5G). While these findings are generally surprising, what they may suggest is that TNFα signaling may be sufficient to lead to upregulation of MLKL, and that this upregulation may contribute to cell death in VSMCs.

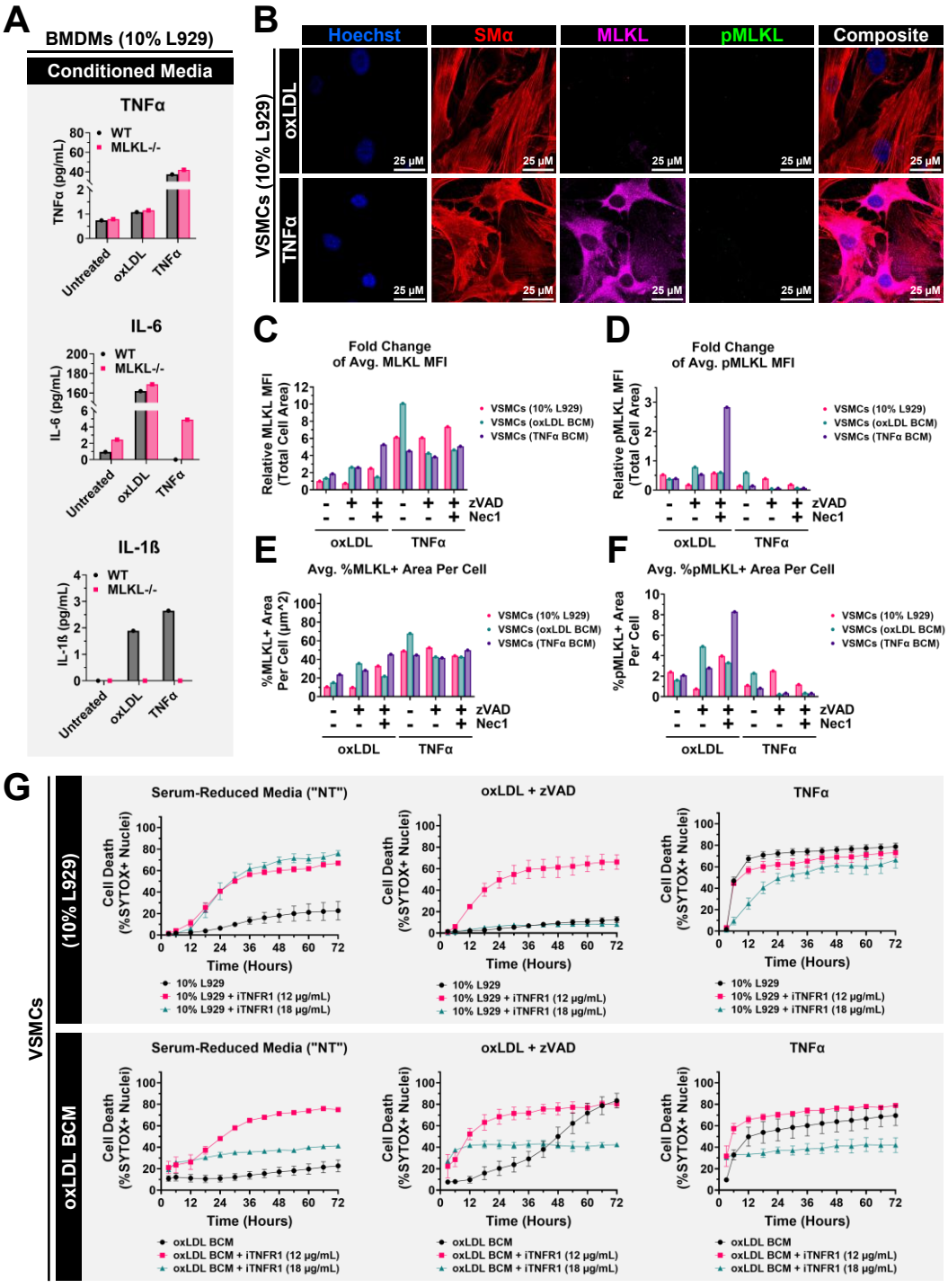

Figure 5. TNFα signaling may account for MLKL upregulation in VSMCs. A Preliminary data from ELISAs performed on conditioned media from wildtype (WT) and MLKL-/- BMDMs under serum reduced conditions ("NT") treated with oxLDL or TNFα. **B** Preliminary data from **a**iryscan confocal fluorescence microscopy of VSMCs under serum-reduced conditions (10% L929) 18 hours post-treatment with oxLDL or TNFα. **C-F** Relative MLKL and pMLKL positive area (μm^2) and MFI in VSMCs 18 hours post-treatment with oxLDL or TNFα +/- zVAD and Nec1, in the presence or absence of BCM. **G** Line graphs comparing rates of cell death as measured by SYTOX staining overtime in VSMCs treated under serum-reduced conditions with oxLDL + zVAD or TNFα with varying concentrations of TNFR1 inhibitor +/- BCM (mean +/- SEM, n = 2-5).

4.5 STAT1/IRF1 appear upregulated in VSMCs treated with conditioned media

In order to better understand how MLKL expression may be regulated in VSMCs, and how this might change in VSMCs treated in BMDM conditioned media, we started to explore the role of STAT1 and IRF1 signaling in these cells. *In vitro* studies have shown that combined STAT1 and IRF1 signaling can be used to upregulate expression of MLKL[176,177], and that upregulation of MLKL can prime cells to more readily undergo necroptosis[176–178]. In the context of atherosclerosis, what is curious about STAT1 signaling is that a balance of STAT1 against STAT3 signaling is associated with regulating VSMC phenotypic switching and trans-differentiation[179]. In this sense, we wondered whether BMDM conditioned media had an influence on this pendulum between STAT1 and STAT3 in VSMCs, and whether this could be related to MLKL upregulation.

To this end, VSMCs were treated with oxLDL in the presence or absence of BMDM conditioned media for STAT3, STAT1, and IRF1 and imaged these samples with airyscan confocal microscopy (Figure 6A-C, S15. In doing so, there seems to be an increase in both cytoplasmic and nuclear STAT1 MFI per positive area, while STAT3 appears to be somewhat consistent between VSMCs treated with and without BMDM conditioned media (Figure 6B-C).

When relative protein abundance is measured by Western blotting of VSMCs treated with oxLDL +/- zVAD, Nec1 in the presence or absence of BCM, there does appear to be upregulation of both STAT1 and IRF1 (Figure 6D-F, S9), particularly in the samples treated with media from BMDMs conditioned with TNFα. Interestingly, STAT3 may be upregulated in VSMCs treated with media from BMDMs conditioned in oxLDL (Figure 6F). While not conclusive, these results may suggest some involvement of STAT1 and possibly IRF1 in how VSMCs respond to

treatment with conditioned media from BMDMs, with possible implications for how this may affect their response to cell death stimuli, including oxLDL.

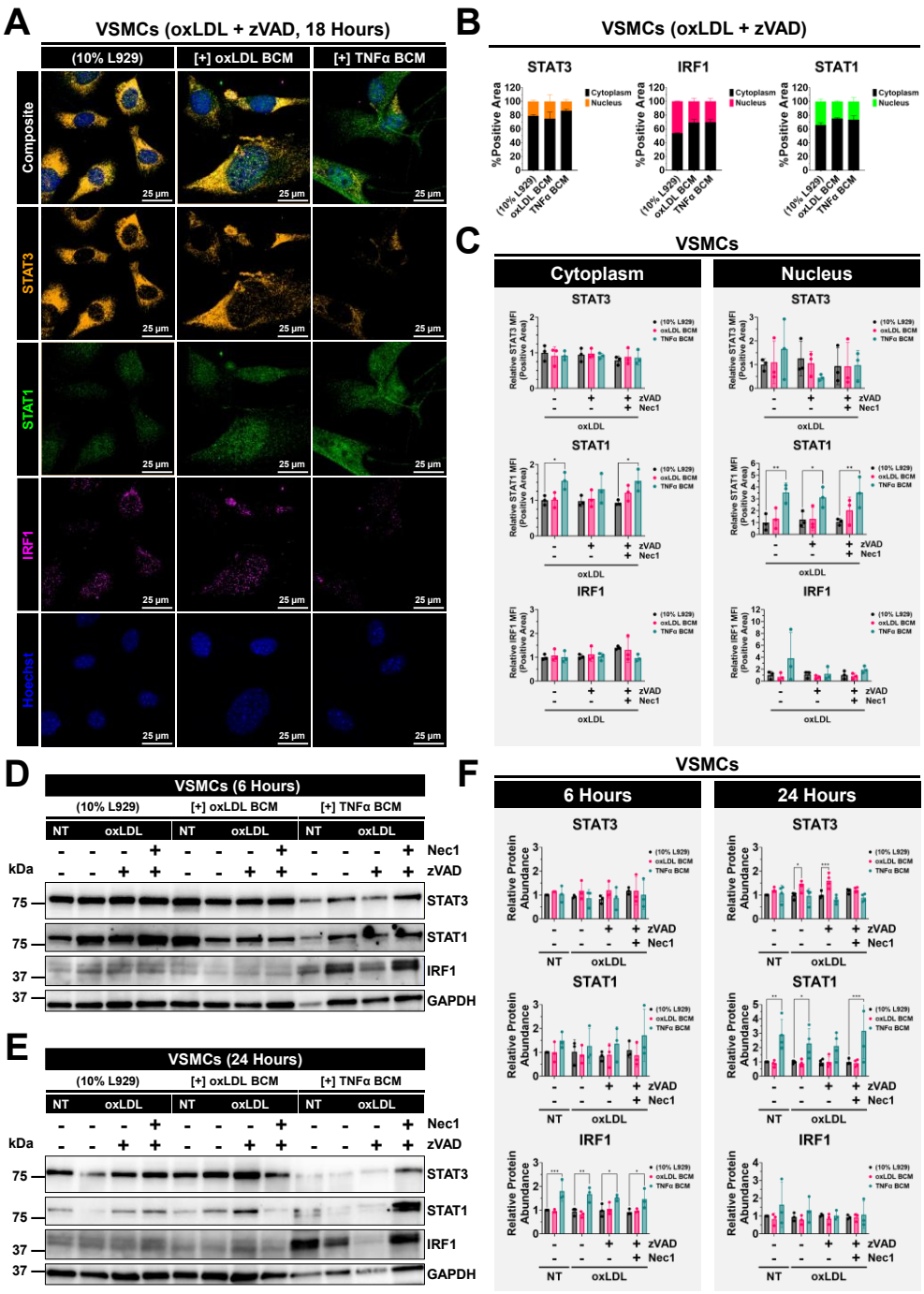

Figure 6. STAT1/IRF1 appear upregulated in VSMCs treated with conditioned media. A Airyscan confocal fluorescence microscopy of VSMCs 18 hours post-treatment with oxLDL + zVAD with and without BCM. **B** Stacked bar graphs describing the proportion of cytoplasmic v. nuclear positive area of STAT3, IRF1, and STAT1 in VSMCs treated with oxLDL + zVAD in the presence or absence of BCM (mean +/- SEM, n = 3). **C** Fold change of cytoplasmic and nuclear MFI over the corresponding positive area, normalized to signal from a VSMC (10% L929) sample treated with oxLDL (mean +/- SD, n = 3). **D-E** Western blots of VSMCs 6- and 24-hours post-treatment with oxLDL +/- zVAD, Nec1 with and without BCM. **F** Relative expression of STAT3, IRF1, and STAT1 in VSMCs 6- and 24-hours post-treatment with oxLDL +/- zVAD, Nec1, normalized to VSMC (10% L929) "no treatment" ("NT") control (mean +/- SD, n = 3-4). Statistical significance was assessed using an ordinary two-way ANOVA with Dunnett's multiple comparisons test, where *p<0.05, **p<0.01, ***p<0.001, ****p<0.0001.

4.6 MLKL seems to be more abundantly expressed in late atherosclerotic lesions

To better understand the role of MLKL *in vivo*, atherosclerotic lesions from the aortic sinus of ApoE$^{-/-}$ mice 4- and 16-weeks on Western diet were stained for CD68, CD45, and MLKL (Figure 7A-F). Within a lesion, CD45+/CD68+ area broadly describes plaque content from monocyte-derived macrophages, while CD68+/CD45- area would describe content from smooth-muscle cell derived macrophages. Infiltrating monocytes that have been newly recruited to the site of the lesion would be represented by CD45+ area, not yet expressing CD68.

From these early experiments, MLKL expression appears to be more abundant in late atherosclerotic lesions compared to early lesions (Figure 7D-F), and MLKL abundance seems to be mostly found within CD45+ or CD68+ plaque area (Figure 7A-C). Interestingly, while CD68- plaque area accounts for 15-30% of MLKL+ area, CD45- plaque area only accounts for 2-5% of MLKL+ area (Figure 7B-C), which may suggest that a large portion of MLKL content within an atherosclerotic lesion comes from monocytes and monocyte-derived macrophages.

Using PlaqView[180], an open-source tool for exploring single-cell genomics data from peer-reviewed articles, scRNA-seq data was pulled from studies using lineage tracing mouse models to map the trajectory of VSMCs throughout plaque progression and trans-differentation states[83,88]. From their work, the authors were able to project their findings onto scRNAseq data from plaque obtained from human carotid and coronary arteries. Between both studies, it would seem that human macrophages may express more MLKL, RIPK3, and IRF1 (Figure 7G). In particular, Pan et al., 2020[88] identified and characterized an "intermediary cell state" ("ICS") during smooth muscle cell phenotypic switching. When mapping relative mRNA abundance along the trajectory of an "SMC" to "ICS", it seems that relative MLKL mRNA may be higher in this intermediate SMC differentiation state, and possibly IRF1 mRNA as well (Figure 7G). While

preliminary, these findings open up an interesting avenue for continued research into the regulation of MLKL expression across VSMC trans-differentiation states throughout plaque growth and progression.

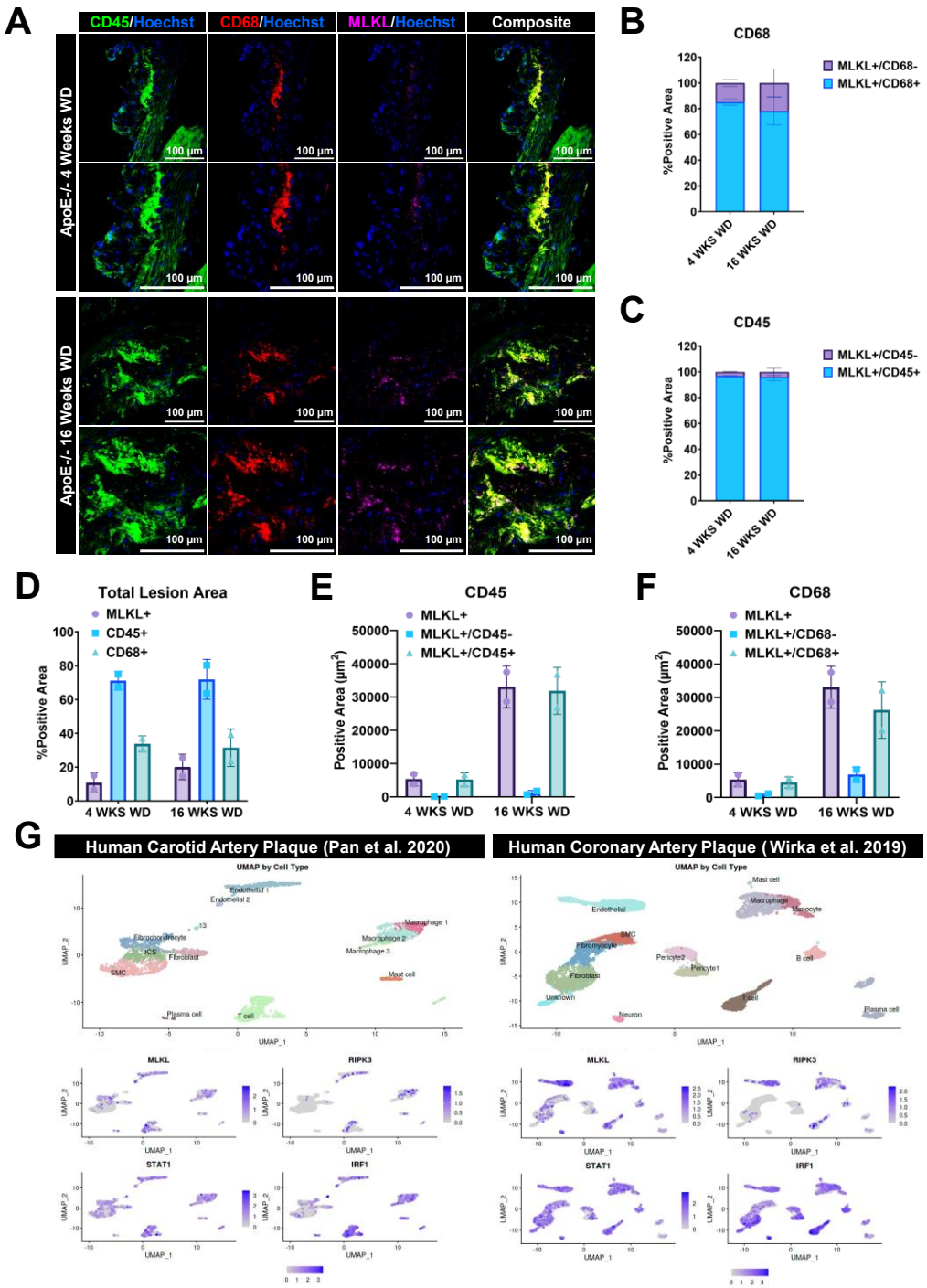

Figure 7. MLKL appears more abundantly expressed in late atherosclerotic lesions. A Images of atherosclerotic lesions from ApoE-/- mice 4- and 16-weeks on Western diet (WD), acquired using a spinning disk confocal microscope. **B-C** Stacked bar graphs comparing the distribution of MLKL+ area within CD68+/- and CD45+/- area (mean +/- SEM, n = 2). **D** Bar graphs describing positive MLKL, CD45, and CD68 area as a proportion of total lesion area (mean +/- SD, n = 2). **E-F** Bar graphs comparing the distribution of MLKL+ area within CD68+/-, CD45+/- area in early and late murine atherosclerotic lesions (mean +/- SD, n = 2). **G** UMAPs generated using PlaqView, describing relative expression of mRNA from work by Pan. et al., 2020 studying plaque obtained from patients undergoing carotid endarterectomy (3 patients, 8867 cells) and Wirka et al., 2019 studying plaque from patients undergoing coronary artery transplant (4 patients, 9 798 cells).

5.0 Discussion

Atherosclerosis is a chronic, progressive inflammatory disease whereby modified low-density lipoproteins accumulate along with immune cells within the intimal layer of the artery wall to form a plaque. A hallmark of advanced, rupture-prone atherosclerotic lesions is the presence of a necrotic core – a dense mass of pro-inflammatory and cellular debris. Our lab and others have previously demonstrated that a key driving force behind necrotic core formation and expansion is necroptosis, where the mixed lineage kinase domain like pseudokinase, MLKL is a key executioner of this process. Moreover, advances in single-cell sequencing technologies have revealed that vascular smooth muscle cells have the capacity to transdifferentiate into "macrophage-like" cells, accounting for almost half of the cell content in advanced plaques. While the contribution of necroptosis in macrophages and macrophage-derived foam cells to plaque growth and instability has been fairly-well studied, the role of necroptosis in vascular smooth muscle cells in this process remains unclear.

This work describes an inherent resistance of VSMCs to oxLDL-induced cell death, where necroptosis can be potentiated in these cells through secreted factors in conditioned media from BMDMs. Confocal microscopy along with Western blots reveal upregulation of MLKL and potentiation of necroptotic pMLKL signal in VSMCs treated with oxLDL in the presence of conditioned media from BMDMs. Moreover, these experiments have implicated STAT1 and IRF1 as possible transcriptional regulators of MLKL expression in VSMCs treated in BMDM conditioned media. Preliminary staining of murine atherosclerotic lesions and data pulled from a single-cell genomics database appears to suggest that MLKL abundance is more pronounced in macrophages, and upregulation of MLKL expression in VSMCs may be a precursory event to phenotypic switching *in vivo*.

5.1 Cell Death and Interactions between Macrophages and Vascular Smooth Muscle Cells

The capacity for macrophages to influence the behaviour of vascular smooth muscle cells in atherosclerotic lesions is not unprecedented. In particular, macrophages have been shown to promote VSMC proliferation, migration, and de-differentiation using both *in vivo* and *in vitro* models of atherosclerosis. Similarly, VSMCs have also been shown to direct monocyte-adhesion, recruitment, and survival within lesions[55,181].

Macrophage conditioned media is often used to promote lipid uptake in vascular smooth muscle cells and stimulate foam cell formation[93,182–188]. In particular, recent work from Dubland et al., 2021[96] demonstrated that secretion of lysosomal acid lipase (LAL) from macrophages leads to the release of cholesterol esters from lysosomes into the cytoplasm of vascular smooth muscle cells. This release of cholesterol esters ultimately promotes metabolism of these lipids. However, when VSMCs are treated with LAL along with pro-atherogenic lipoproteins (e.g. agLDL), which characteristically downregulate key cholesterol efflux transporters (e.g. ABCA1/G1), the release of these free cholesterol esters into the cytoplasm leads to an overwhelming accumulation of lipid-rich droplets within VSMCs. Accumulation of free cholesterol within the cytoplasm of VSMCs ultimately drives the development of a highly inflammatory, foam cell. In this sense, it may be interesting to determine whether exogeneous LAL activity contributes to priming oxLDL-induced necroptosis in VSMCs, or equally, whether it may be capable of stimulating MLKL upregulation. A role for LAL in MLKL upregulation in VSMCs would be particularly interesting because MLKL has previously been implicated in lipid trafficking and extracellular vesicle formation in macrophages[156,189].

With respect to potentiation of cell death in vascular smooth muscle cells by macrophages, existing studies have demonstrated that direct cell-to-cell contact between these

cell types is able to potentiate apoptosis through nitric oxide enhancement of Fas/FasL interactions[190–193]. In our work, we do see some potentiation of apoptotic cell death in VSMCs treated with staurosporine in the presence of BMDM conditioned media, without the need for direct co-culture. It is possible that direct co-culture of these two cell types might generate a more pronounced induction of cell death in VSMCs, likely through previously described NO-mediated Fas/FasL signaling[191,192]. However, the use of macrophage-conditioned media to prime necroptosis in vascular smooth muscle cells has not been previously shown.

Interestingly, recent work from Weindel et al., 2022[194] describes a novel mechanism in which GSDMD is shown to puncture mitochondria to release ROS, and essentially trigger a shift from pyroptosis to RIPK1/RIPK3/MLKL-dependent necroptosis. In their work, the authors were studying *Mycobacterium tuberculosis* infection in macrophages[194]; however, in the context of VSMCs, where we observe upregulation of GSDMD in cells treated with conditioned media (Figure 4, S8), it would be interesting to know if GSDMD activity facilitates necroptosis of these cells. Western blotting does appear to suggest that GSDMD upregulation seems to occur simultaneously with increased pMLKL signal. Assessing whether GSDMD is associated with mitochondria in these samples using confocal microscopy may help determine whether GSDMD could mediate necroptosis in VSMCs treated in BMDM conditioned media. More generally, it may be interesting to know if macrophages have the capacity to prime cell death in other cell types, including fibroblasts and endothelial cells. In the same vein, it could be interesting to determine whether other immune cells, like T-cells or neutrophils are able to potentiate necroptosis in vascular smooth muscle cells.

5.2 MLKL Regulation

In primary hepatocytes from patients with autoimmune hepatitis, combined STAT1 and IRF1 signaling has been shown to upregulate expression of MLKL[177]. Equally, work from Knuth et al., 2019[176] found that interferon-gamma (IFNγ) could induce MLKL upregulation through IRF1 and STAT1 signaling in human-derived epithelial and macrophage cell lines (EFM-192A, HeLa, MDA-MB 231, MV4-11). In both of these studies, upregulation of MLKL was described as having a "sensitizing" effect, associated with higher rates of necroptosis. More broadly, the role of IFNγ signaling and upregulation of MLKL to promote necroptosis has also been reported in lung epithelial cells and embryonic fibroblasts[178,195]. Interestingly, macrophage-secreted IL-1ß has been shown to stimulate adhesion, inflammation, and apoptosis of macrophage-like VSMCs through STAT3-signaling[196].

Experiments from Zhou et al., 2021[197] demonstrate that MLKL and calcium/calmodulin-dependent protein kinase II (CaMKII) mediate necroptosis in VSMCs. In particular, the authors show that siRNA KO of MLKL or CaMKII in VSMCs leads to a reduction in cell death, and that MLKL is necessary for activation of CaMKII[197]. In transgenic models of MLKL deletion, RIPK3 has been shown to trigger NLRP3-mediated inflammasome assembly in BMDMs[198] treated with LPS, leading to activation of caspase-1 and cleavage of pro-IL-1ß. While the authors did not assess activation of GSDMD, it would have been interesting to see if the cell death being induced was related to pyroptosis, possibly as a means of compensating for loss of MLKL-mediated necroptosis. In either case, this RIPK3-mediated form of cell death may explain the cell death observed in our $MLKL^{-/-}$ BMDMs and VSMCs (Figure 4F, S10).

Using ChIP-seq analysis performed in HeLa cells, Satoh et al., 2013[199] identified 1,441 STAT1 target genes, including IRF1, GSDMD, Bcl-3, and APOL1/3/4/6. Similarly, Wu et al.,

2022[200] performed ChIP-seq in primary human B-cells, activated with TLR9 agonist, CgP. In doing so, the authors identified 2,289 STAT3 target genes, including caspase-8, IL-6/7, and NOTCH2.

For vascular smooth muscle cells, STAT1 and STAT3 signaling are know regulators of phenotypic switching and trans-differentiation[179]. While VSMCs treated with oxLDL in BMDM conditioned media do not appear to express CD68 (Figure S13), increases in STAT1 signaling could be associated with some sort of intermediary state preceding, or leading up to, trans-differentiation in VSMCs. While our studies require more optimization, the role of STAT1 and IRF1 in regulating MLKL expression in VSMCs remains an interesting area of exploration for understanding cell death and atherosclerosis.

5.3 MLKL Expression in Atherosclerotic Lesions

To date, reported *in vivo* immunofluorescence staining for MLKL in vascular smooth muscle cells is limited. Work from Zhou et al., 2021[197] shows that total and phosphorylated forms of MLKL are dramatically upregulated in an induced model of murine abdominal aortic aneurysm (AAA), and that this signaling is RIPK3-dependent. Similarly, work from Bai et al., 2024[201] demonstrated that MLKL upregulation in α-SMA+ VSMCs was associated with advanced lesions from cigarette-tar stimulated ApoE$^{-/-}$ high-fat diet (HFD) mice, and that this upregulation was ER-dependent. *In vitro* stimulation of VSMCs with increasing doses of cigarette tar showed upregulation of RIPK1/3 and MLKL, with a corresponding increase in necroptotic pMLKL signal[201]. Taken together, it would seem that MLKL upregulation is possibly a phenotype of an acutely activated vascular smooth muscle cell.

5.4 Resilience of Vascular Smooth Muscle Cells to Cell Death

Over the years, VSMC resilience against apoptosis has been attributed to PI3K/Akt, ERK1/2, and NF-κB signaling to enhance activity and expression of anti-apoptotic proteins, Bcl-2 and Bcl-xL[202–209]. More broadly, autophagy and downregulation of cFLIP have also been associated with vascular smooth muscle cell resistance to oxidative stress[84,210,211]. Interestingly, the need for *in vitro* sensitization of VSMCs to apoptosis is often reported in cells treated in 25 mM, "high-glucose" cell culture media[205–207], although some have described potentiation of cell death by high-glucose media through generation of ROS[212].

In the context of atherosclerosis, priming of apoptotic cell death has been described in VSMCs co-treated with TNFα and 7-ketocholesterol[213] or free fatty acids[214]. Senescence and pro-inflammatory cytokines have also been shown to prime apoptosis in VSMCs[84,209,215]. Geng et al., 1996[215] reported human and rat VSMCs would not undergo cell death unless treated in a combination of TNFα, IFNγ, and IL-1ß[215], and that none of these stimuli alone could induce cell death. Their findings lead the authors to predict that the "production of immune cytokines by vascular cells and/or infiltrating leukocytes may regulate apoptotic death of SMCs during atherogenesis"[215].

Most reports describing resistance of VSMCs to cell death have done so in regards to apoptosis. There is limited discussion of VSMCs resistance to other forms of programmed cell death, including necroptosis or pyroptosis. Likewise, there is not much published data about priming of VSMCs to undergo necroptosis. In most cases, it is because these studies were published before pyroptosis or necroptosis had been discovered (2001-2005).

5.5 Future Directions and Implications of Studying MLKL in VSMCs and Atherosclerosis

Exploring the role of MLKL regulation and expression in vascular smooth muscle cells has broad implications for our understanding of atherosclerosis, particularly in relation to mechanisms of cell death, inflammation, and potentially lipid trafficking. In doing so, we not only advance our understanding of vascular disease, but also support the development of new, targeted therapies to improve patient outcomes.

In particular, identifying and comparing MLKL interacting partners between BMDMs and VSMCs under normal, lipid-loaded, or necroptotic conditions may provide further insight into the varying roles of MLKL in these cells. While still preliminary, lentiviral transduction of BMDMs and VSMCs has been optimized, and TurboID plasmids have been constructed for use in proximity labelling experiments to identify and compare potential interacting partners of MLKL (Figure S16). The overall design for this TurboID project, along with experiments optimizing biotin and streptavidin incubation time and concentrations are summarized in Figures S17-19.

5.6 Conclusions

To our knowledge, this work is the first to describe an inherent resistance of VSMCs to oxLDL-induced cell death. Our findings demonstrate that oxLDL-induced necroptosis of VSMCs can be potentiated through secreted factors from BMDM conditioned media (Figure 1). Confocal microscopy along with Western blots reveal upregulation of MLKL and potentiation of necroptotic pMLKL signal in VSMCs treated with oxLDL in the presence of conditioned media from BMDMs. Moreover, these experiments have implicated STAT1 and IRF1 as possible transcriptional regulators of MLKL expression in VSMCs treated in BMDM conditioned media. Preliminary staining of murine atherosclerotic lesions and data pulled from a single-cell

genomics database appears to suggest that MLKL abundance is more pronounced in macrophages, and upregulation of MLKL expression in VSMCs may be a precursory event to phenotypic switching *in vivo*.

We propose the following tentative hypothesis for a two-step mechanism to describe potentiation of cell death in vascular smooth muscle cells by macrophages (Figure 8). First, secreted factors from BMDM conditioned media (possibly TNFα, IFNγ, IL-6, and/or IL-1ß) prime VSMCs by triggering JAK/STAT signaling to phosphorylate STAT1. When phosphorylated, STAT1 phosphorylates and upregulates expression of IRF1. The combined action of pSTAT1 and pIRF1 leads to upregulation of MLKL expression in VSMCs. Second, upregulation of MLKL sensitizes VSMCs to oxLDL-mediated necroptosis through RIPK1/RIPK3/MLKL signaling. Alternatively, oxLDL-mediated necroptosis could be activated through GSDMD-mediated release of ROS from mitochondria to activate RIPK1/RIPK3/MLKL signaling.

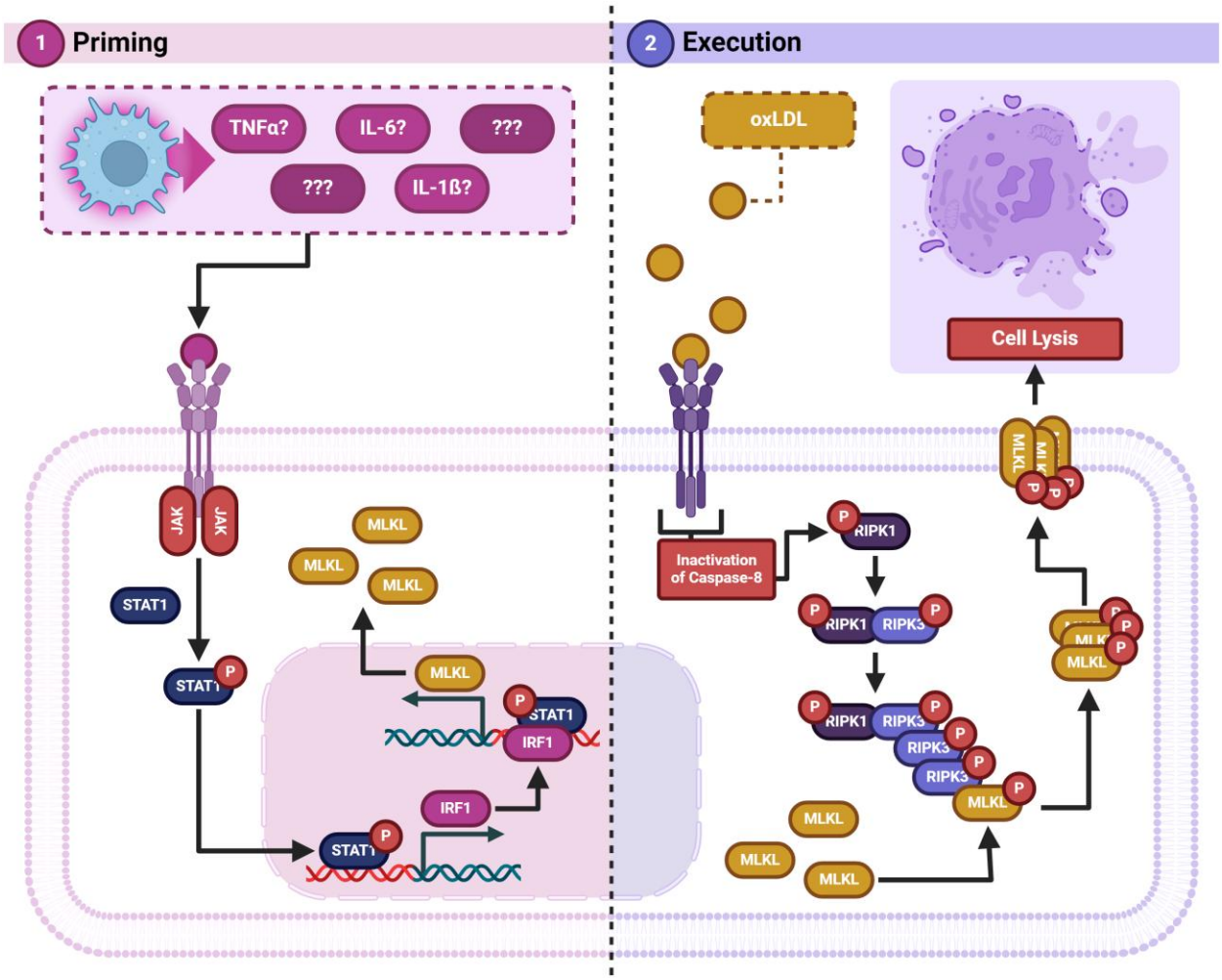

Figure 8. Working hypothesis for MLKL upregulation and potentiation of cell death in VSMCs by conditioned media. BMDM conditioned media likely potentiates cell death in VSMCs through a "two-step" process. (1) Secreted factors from BMDMs signal to VSMCs through some sort of receptor-mediated signaling mechanism, possibly JAK/STAT signaling, to promote expression of MLKL. (2) These VSMCs, once MLKL is upregulated, become more receptive to cell death signals received through oxLDL + zVAD treatment, potentiating necroptosis in these cells.

Supplementary Figures

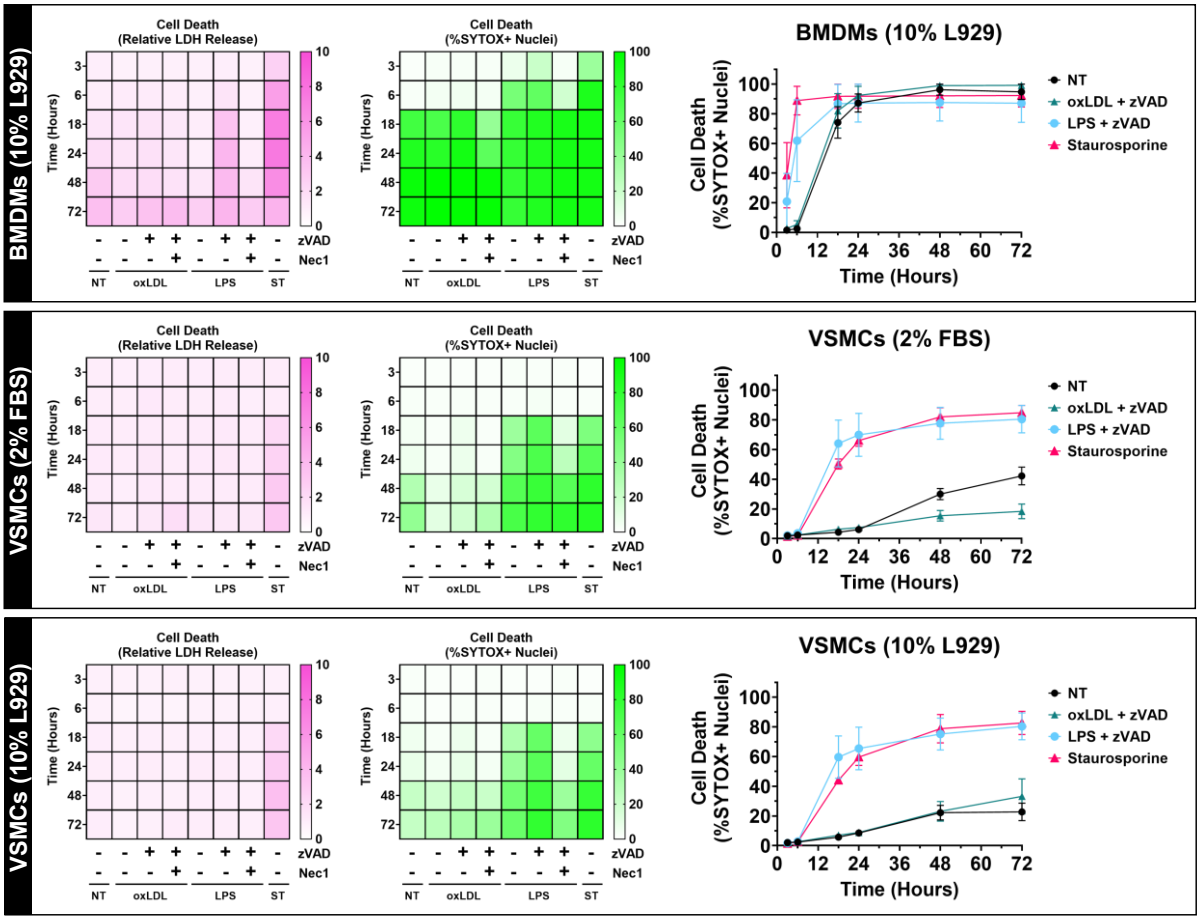

Figure S1. BMDMs undergo cell death at higher rates than VSMCs. Heat maps showing rates of cell death in BMDMs and VSMCs as measured by LDH (magenta) and SYTOX (green) assays over time. Data points shown represent the mean with SEM from parallel LDH and SYTOX experiments (n = 3).

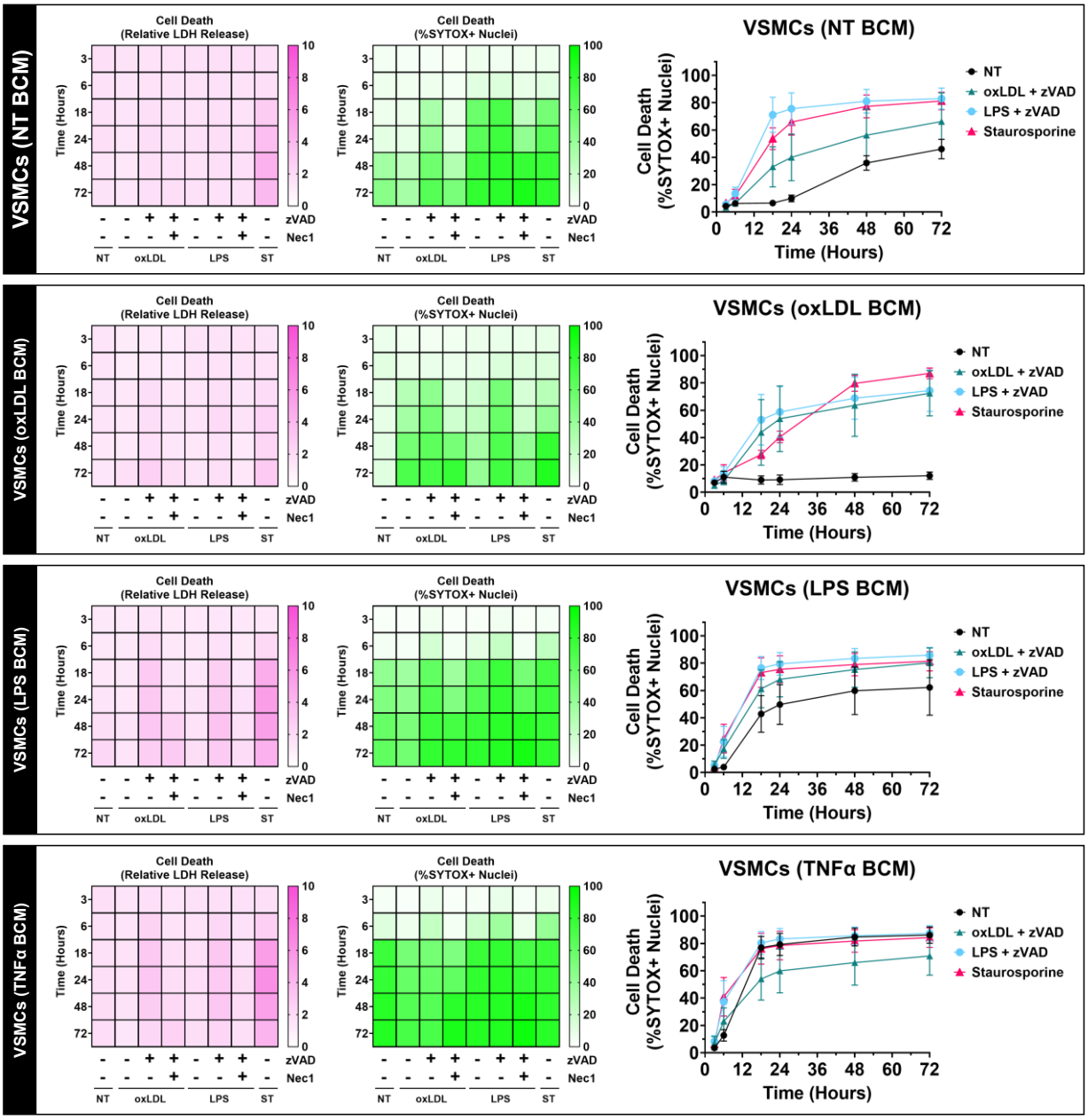

Figure S2. BMDM conditioned media appears to potentiate cell death in VSMCs. Heat maps comparing rates of cell death in VSMCs treated with and without BMDM conditioned media, as measured by LDH (magenta) and SYTOX (green) assays over time. Data points shown represent the mean with SEM from parallel LDH and SYTOX experiments (n = 3).

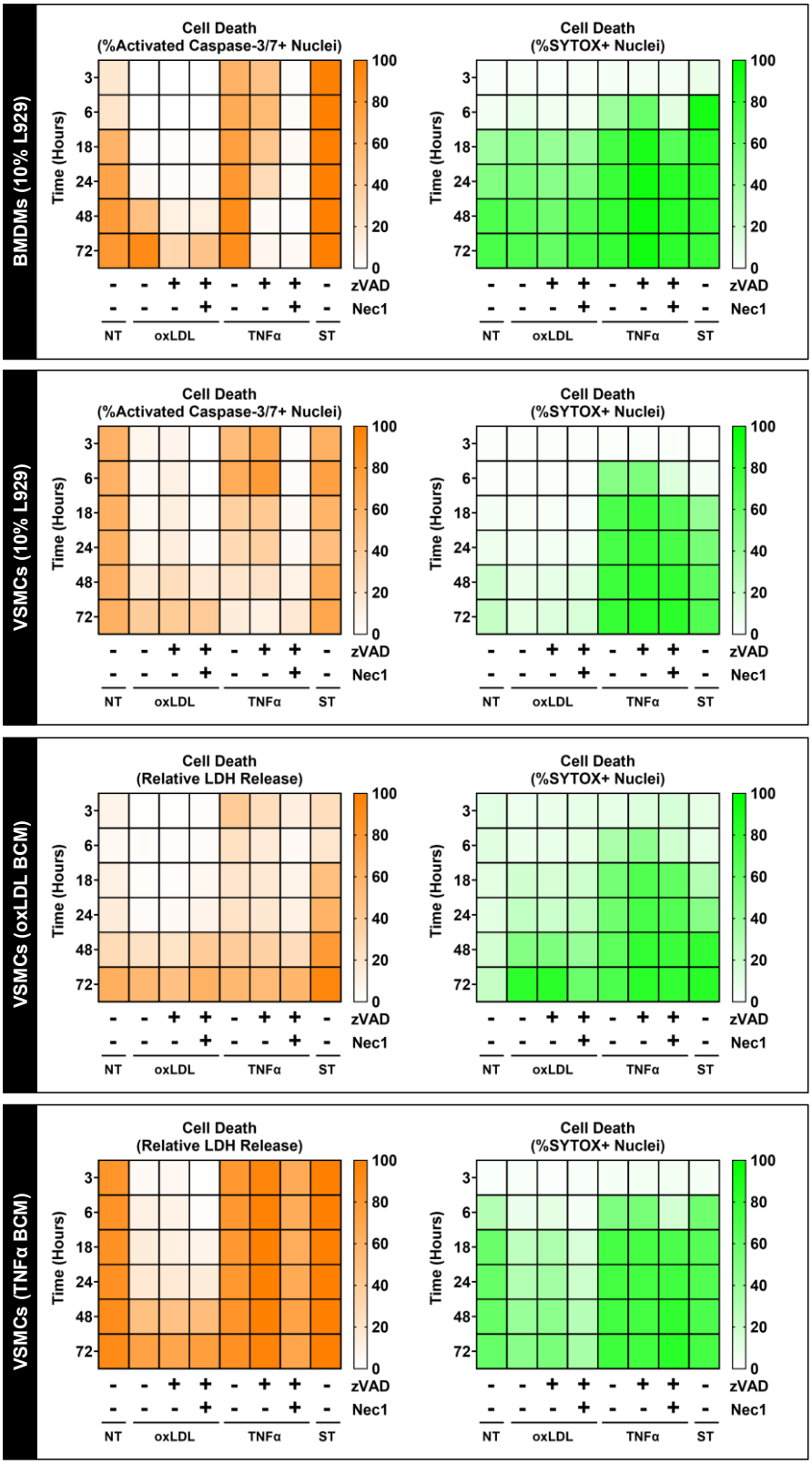

Figure S3. BMDM conditioned media potentiates cell death in VSMCs treated with oxLDL that is likely not apoptosis. Heat maps comparing rates of SYTOX+ cell death (green) against cleaved caspase-3/7+ nuclei (orange) in BMDMs and VSMCs over time (mean, n = 5).

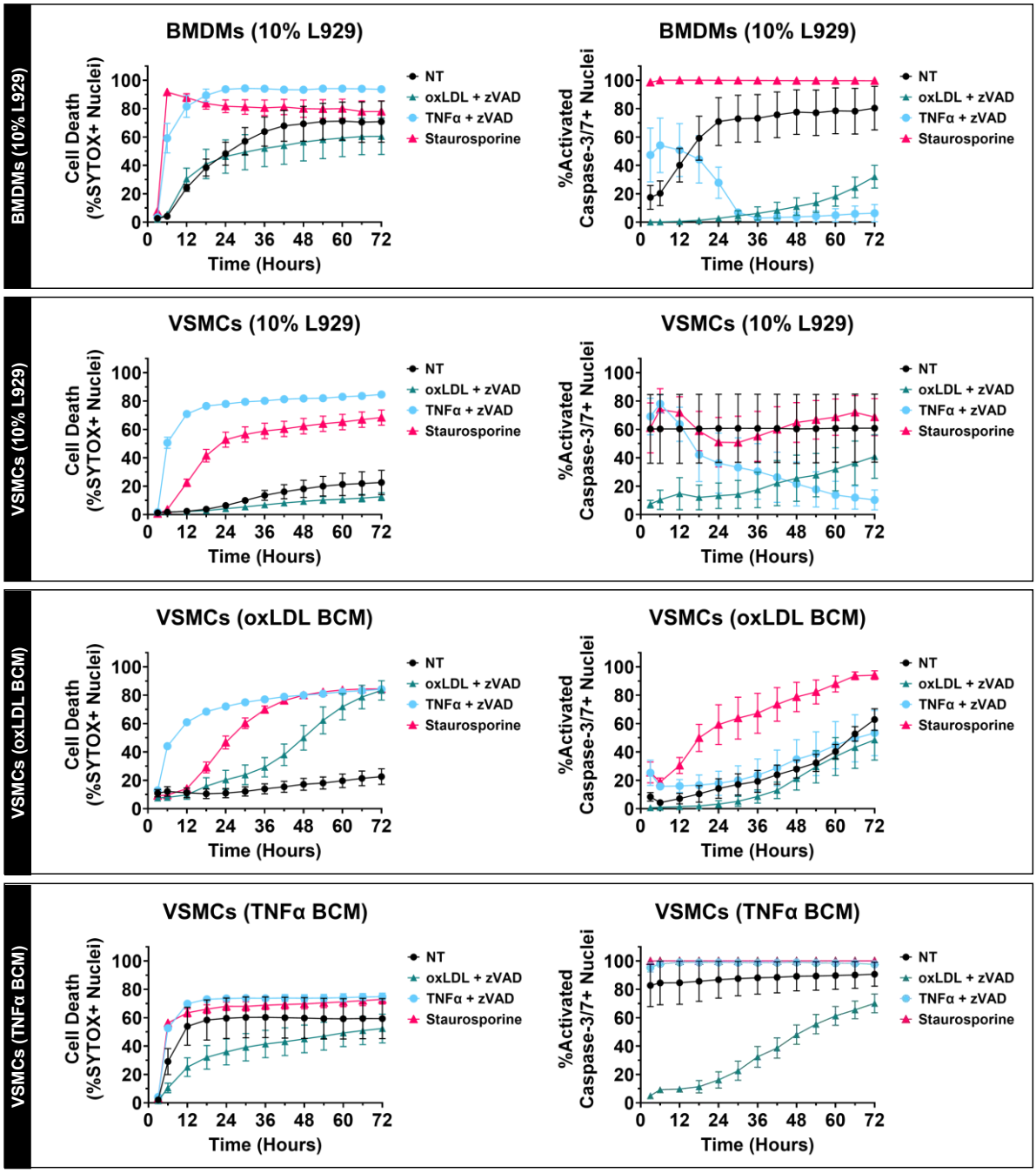

Figure S4. BMDM conditioned media potentiates cell death in VSMCs treated with oxLDL that is likely not apoptosis. Line graphs showing rates of SYTOX+ cell death (green) and cleaved caspase-3/7+ nuclei (orange) in BMDMs and VSMCs over time (mean +/- SEM, n = 5).

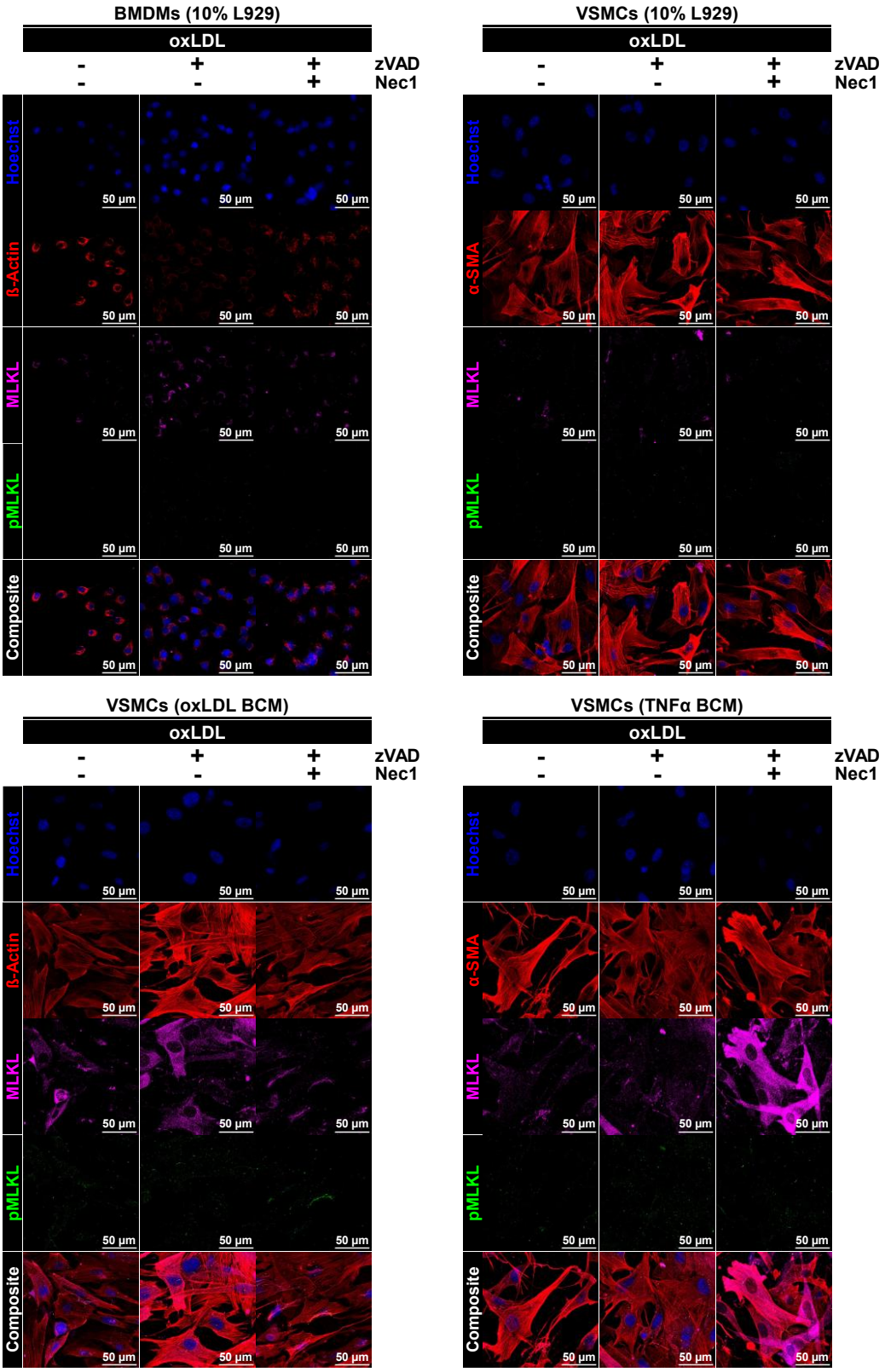

Figure S5. Airyscan confocal fluorescence microscopy of BMDMs and VSMCs under serum-reduced conditions, 18 hours post-treatment with oxLDL +/- zVAD, Nec1. VSMCs are shown treated in the presence or absence of BCM.

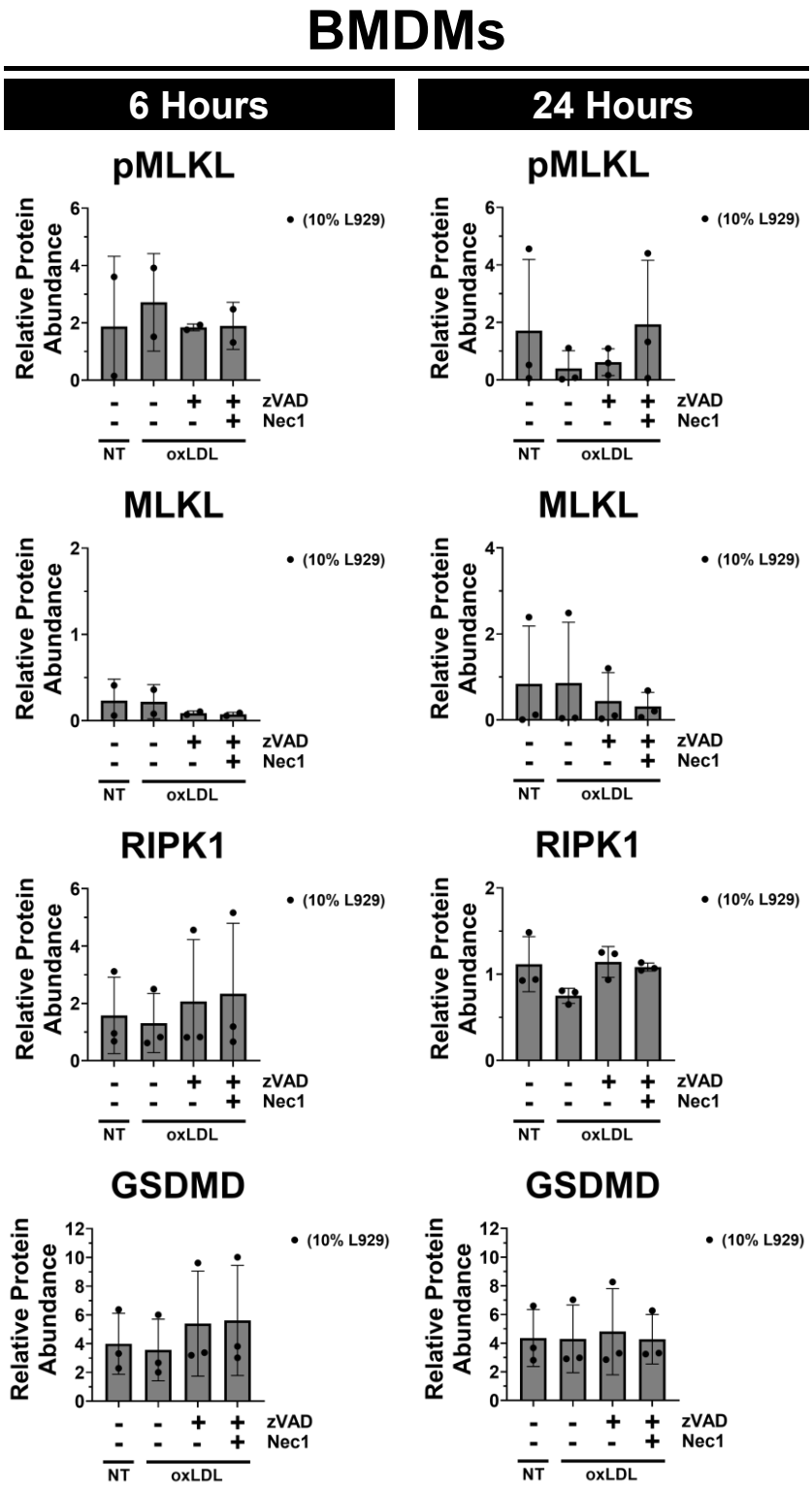

Figure S6. Relative protein abundance as measured by western blotting of samples from BMDMs treated under serum reduced conditions with oxLDL +/- zVAD, Nec1 (mean +/- SD, n = 3).

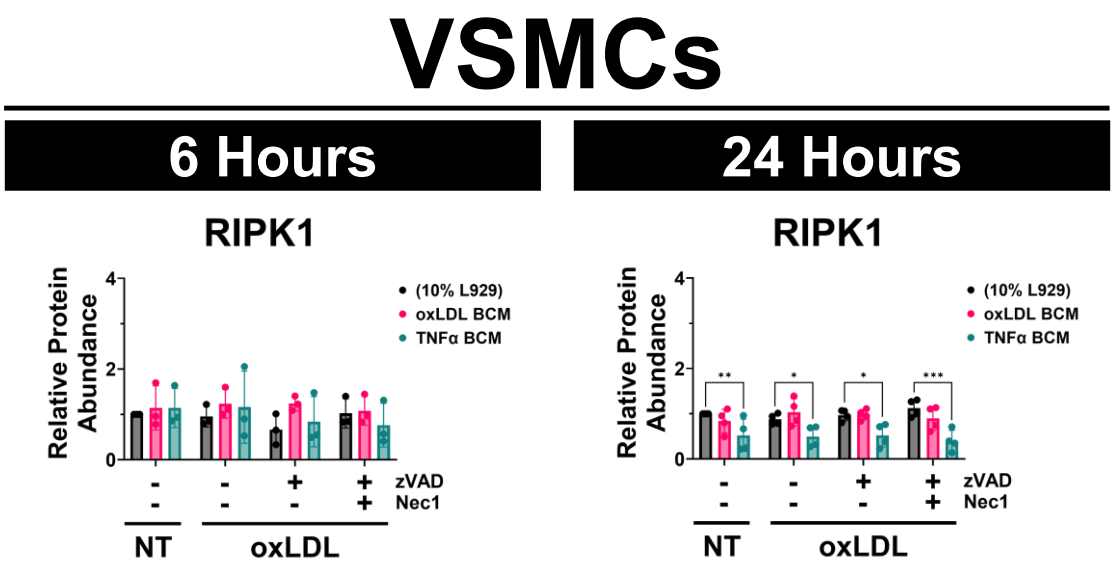

Figure S7. Relative protein abundance as measured by western blotting of samples from VSMCs treated under serum reduced conditions with oxLDL +/- zVAD, Nec1, with and without BMDM conditioned media (mean +/- SD, n = 3-4). Statistical significance was assessed using an ordinary two-way ANOVA with Dunnett's multiple comparisons test, where *p<0.05, **p<0.01, ***p<0.001, ****p<0.0001.

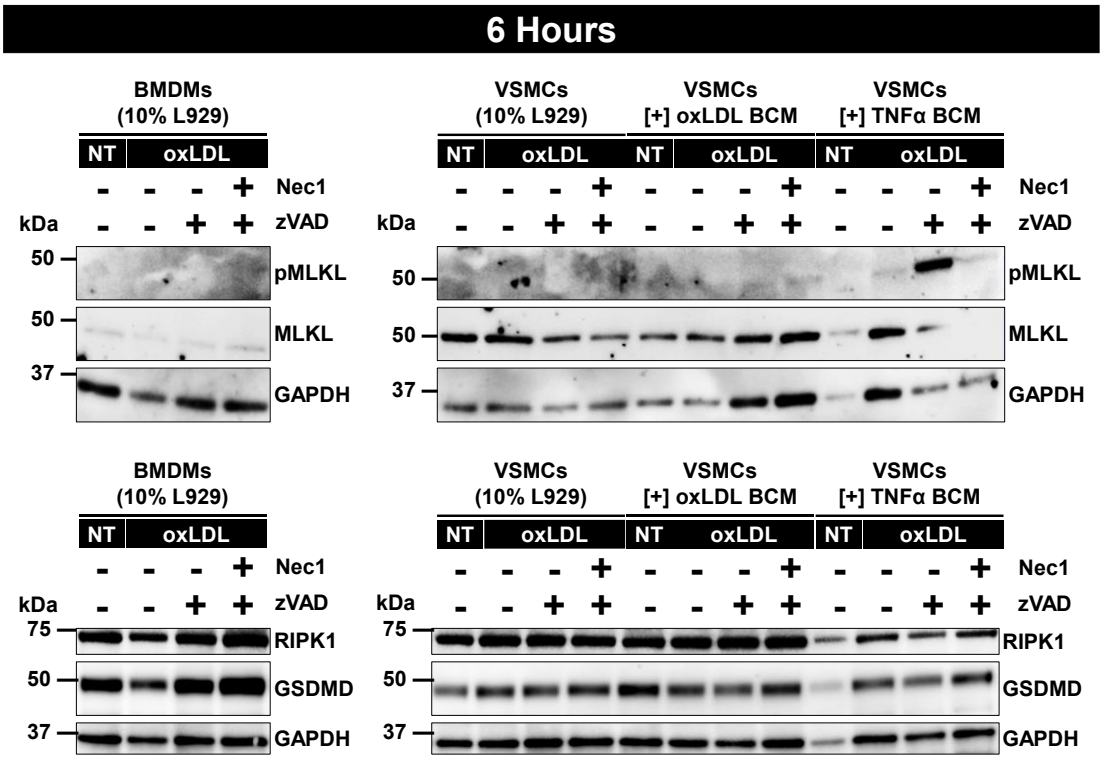

Figure S8. Western blots of BMDMs and VSMCs under serum-reduced conditions treated for 6 hours with oxLDL +/- zVAD, Nec1. VSMCs are shown treated in the presence or absence of BMDM conditioned media.

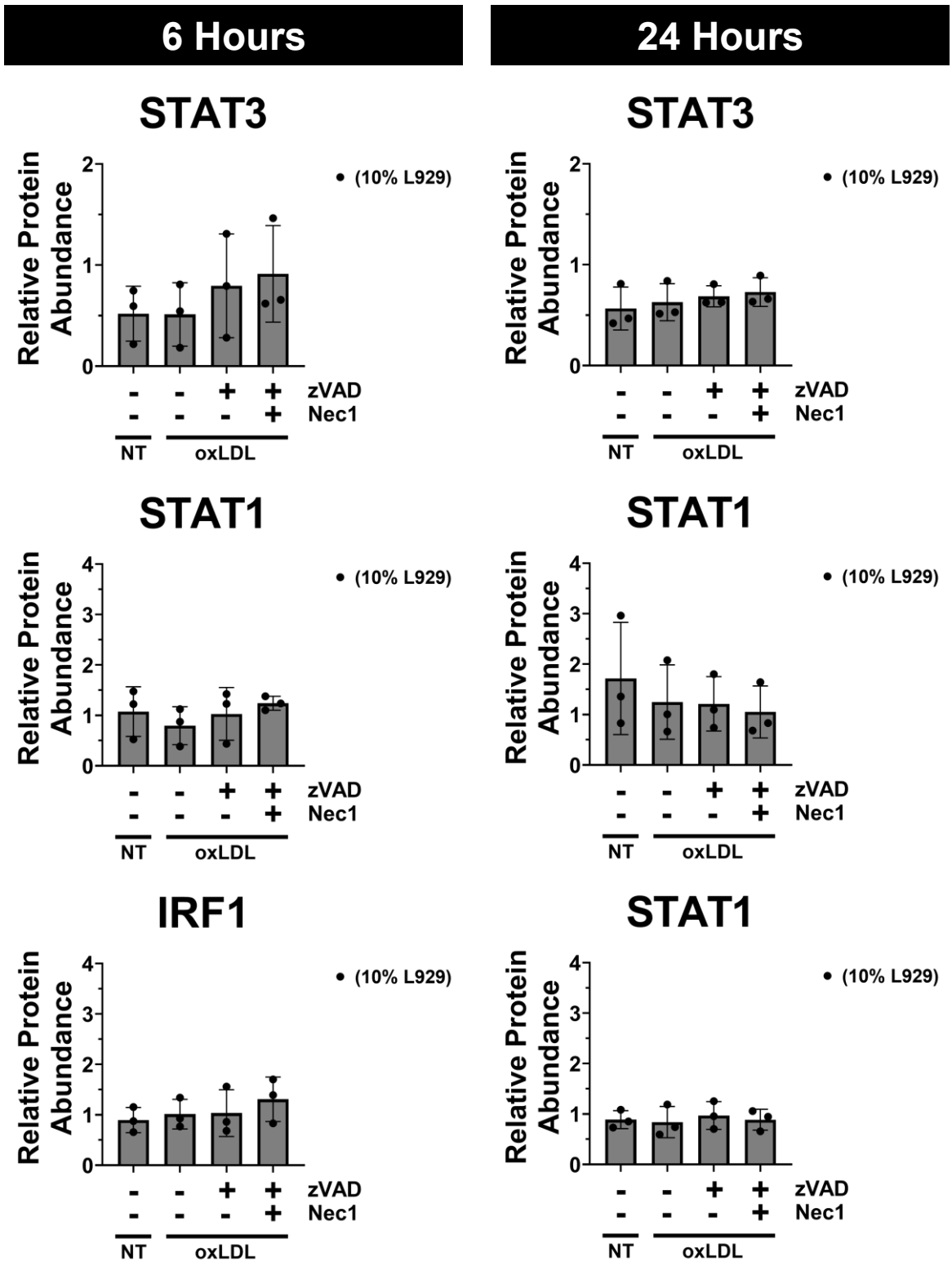

Figure S9. Relative protein abundance as measured by western blotting of samples from BMDMs treated under serum reduced conditions with oxLDL +/- zVAD, Nec1 (mean +/- SD, n = 3).

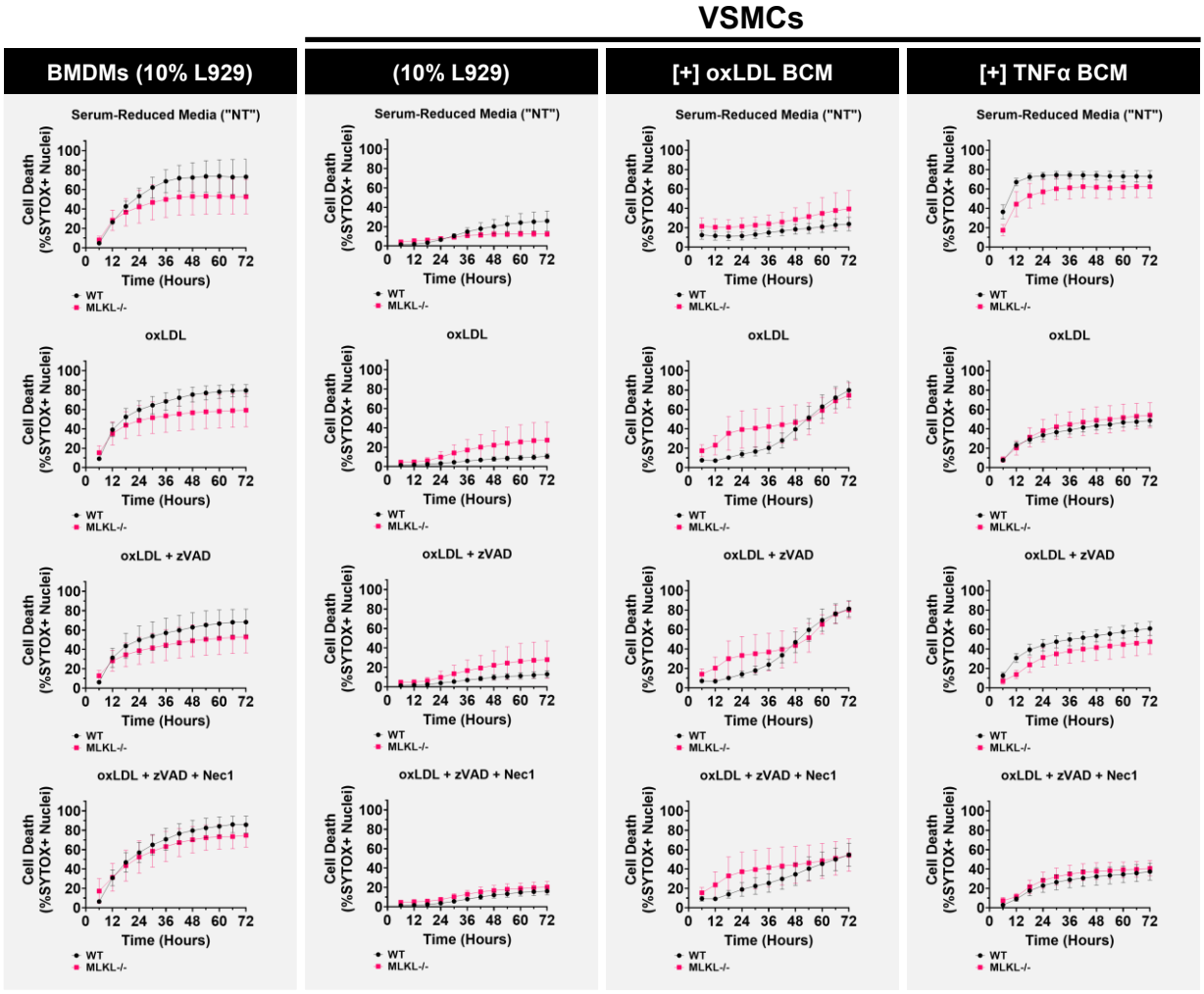

Figure S10. Line graphs comparing cell death over time, as measured by SYTOX assay of both WT and MLKL-/- BMDMs and VSMCs treated under serum reduced conditions with oxLDL +/- zVAD, Nec1. VSMCs are shown treated in the presence or absence of BMDM conditioned media (mean +/- SEM, n = 4).

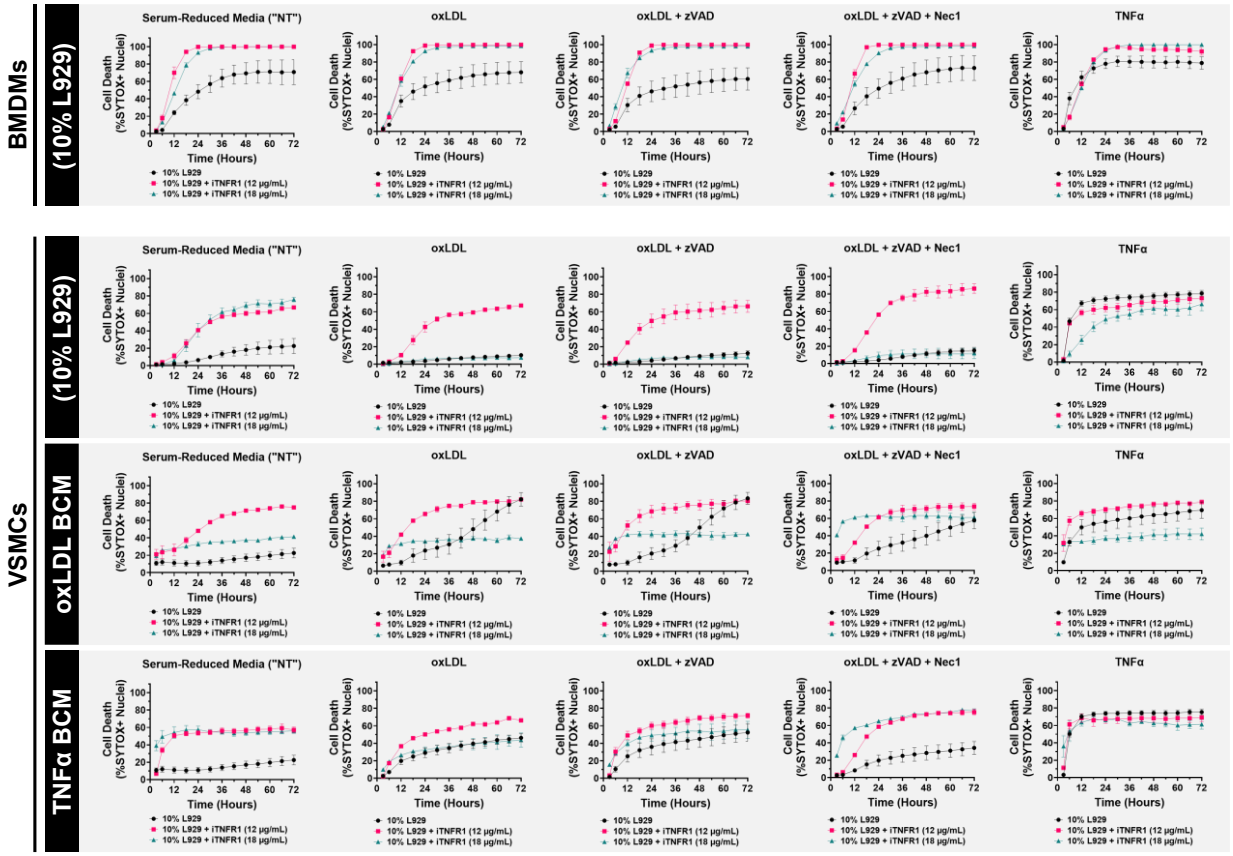

Figure S11. Line graphs comparing rates of cell death as measured by SYTOX staining overtime in VSMCs treated under serum-reduced conditions with oxLDL +/- zVAD, Nec1 or TNFα with varying concentrations of TNFR1 inhibitor +/- BMDM conditioned media (mean +/- SEM, n = 2-5).

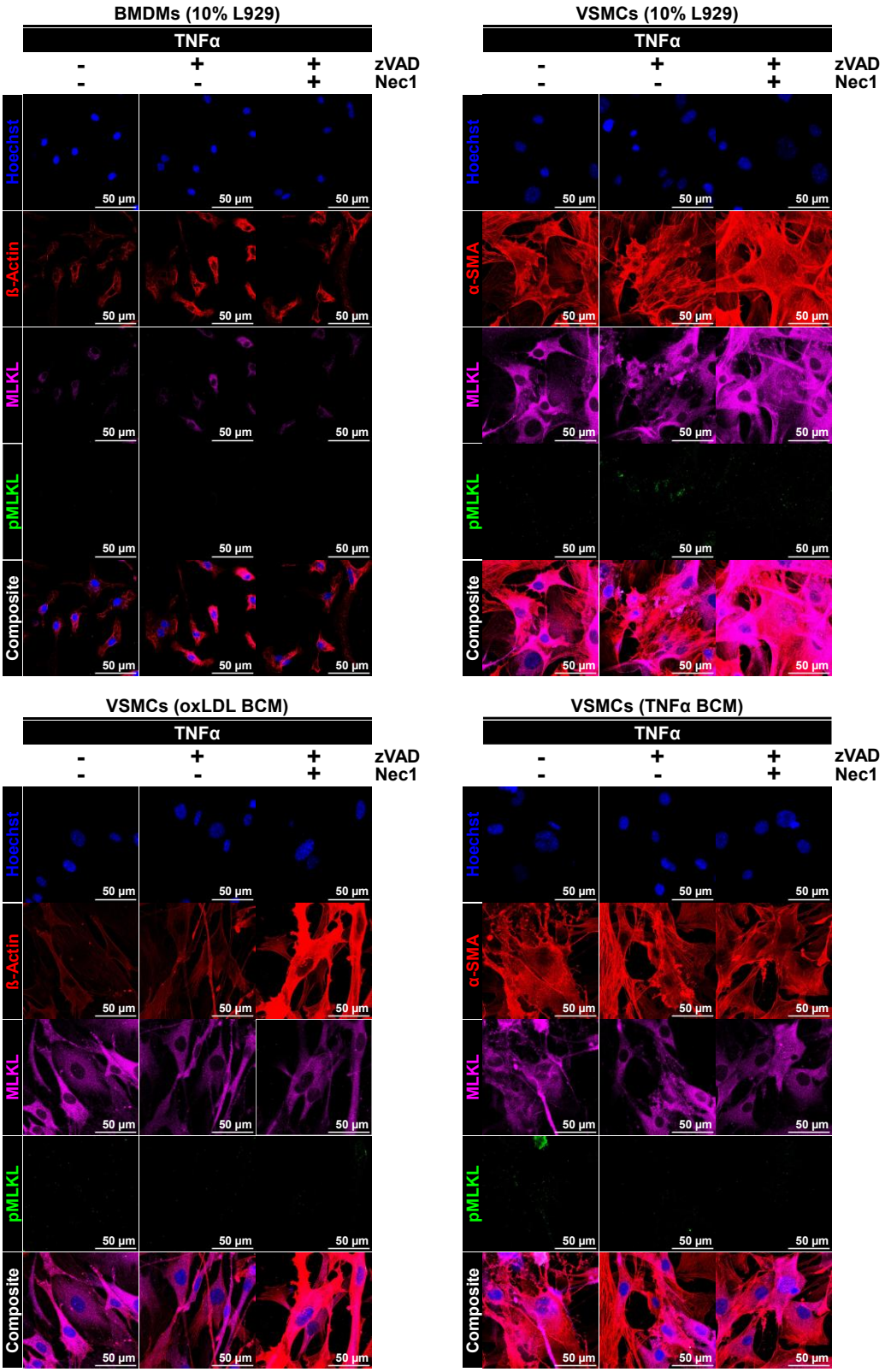

Figure S12. Preliminary data from airyscan confocal fluorescence microscopy of BMDMs and VSMCs under serum-reduced conditions 18 hours post-treatment with oxLDL or TNFα +/- zVAD, Nec1. VSMCs are shown treated in the presence or absence of BMDM conditioned media.

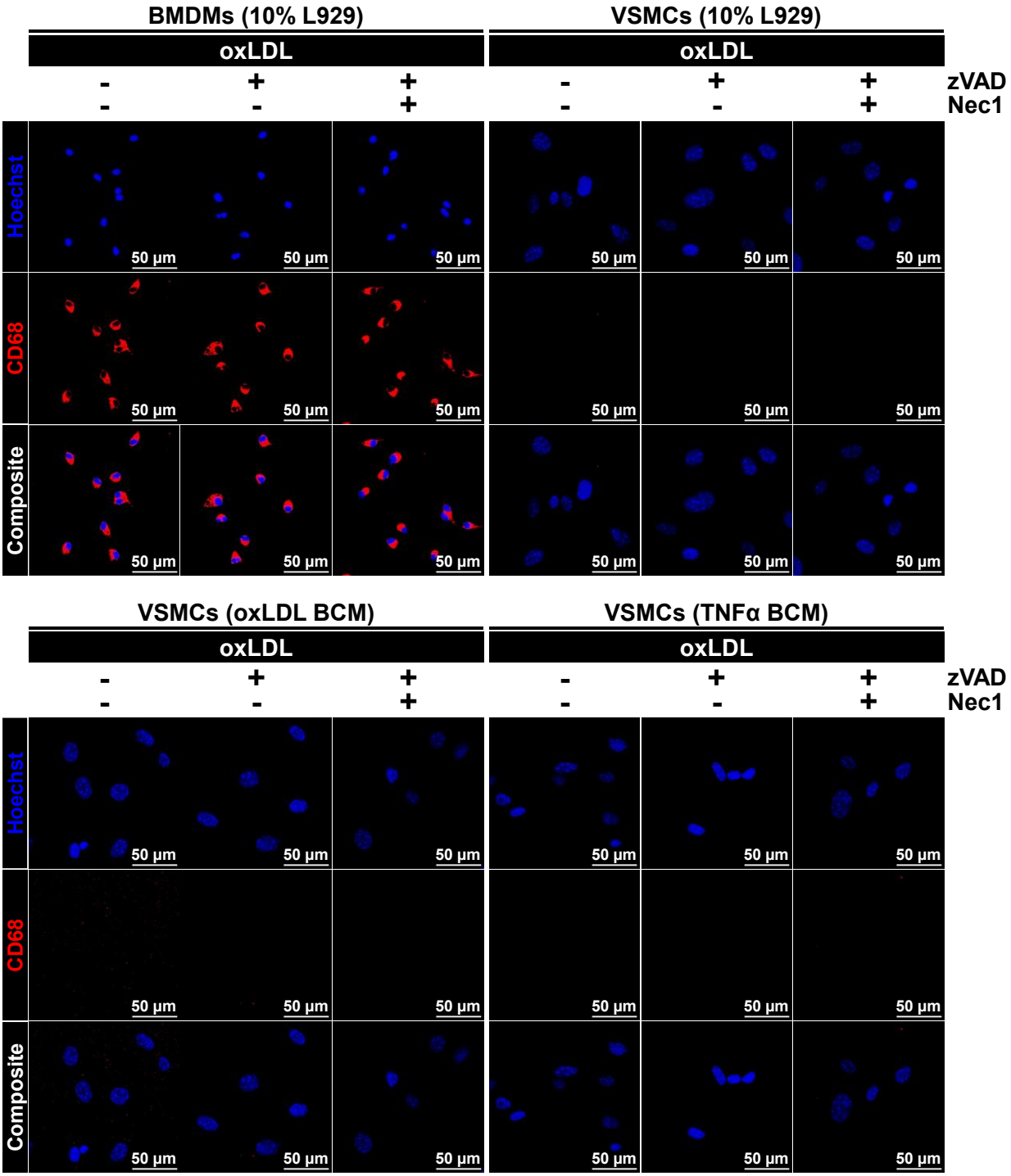

Figure S13. Preliminary data from confocal fluorescence microscopy of BMDMs and VSMCs under serum-reduced conditions, 18 hours post-treatment with oxLDL +/- zVAD, Nec1. VSMCs are shown treated in the presence or absence of BMDM conditioned media.

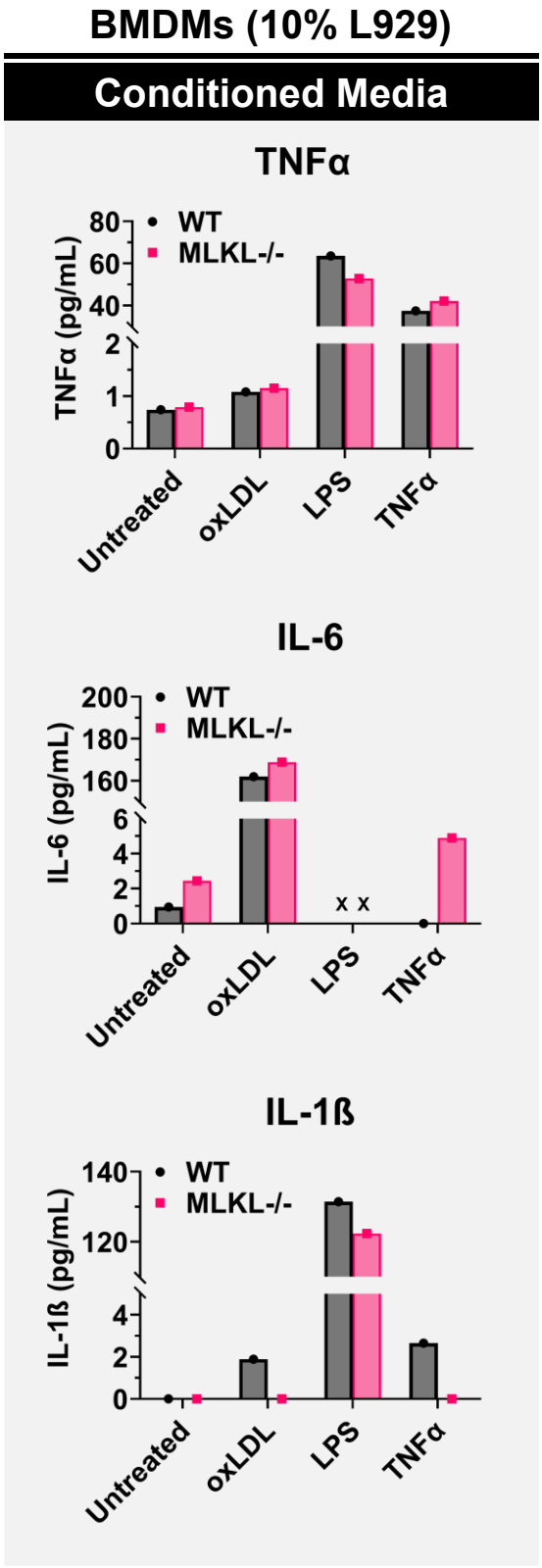

Figure S14. Preliminary data from ELISAs performed on conditioned media from wildtype (WT) and MLKL-/- BMDMs under serum reduced conditions treated with oxLDL, LPS, or TNFα. "X X" denotes samples where the signal was too high to meaningfully measure.

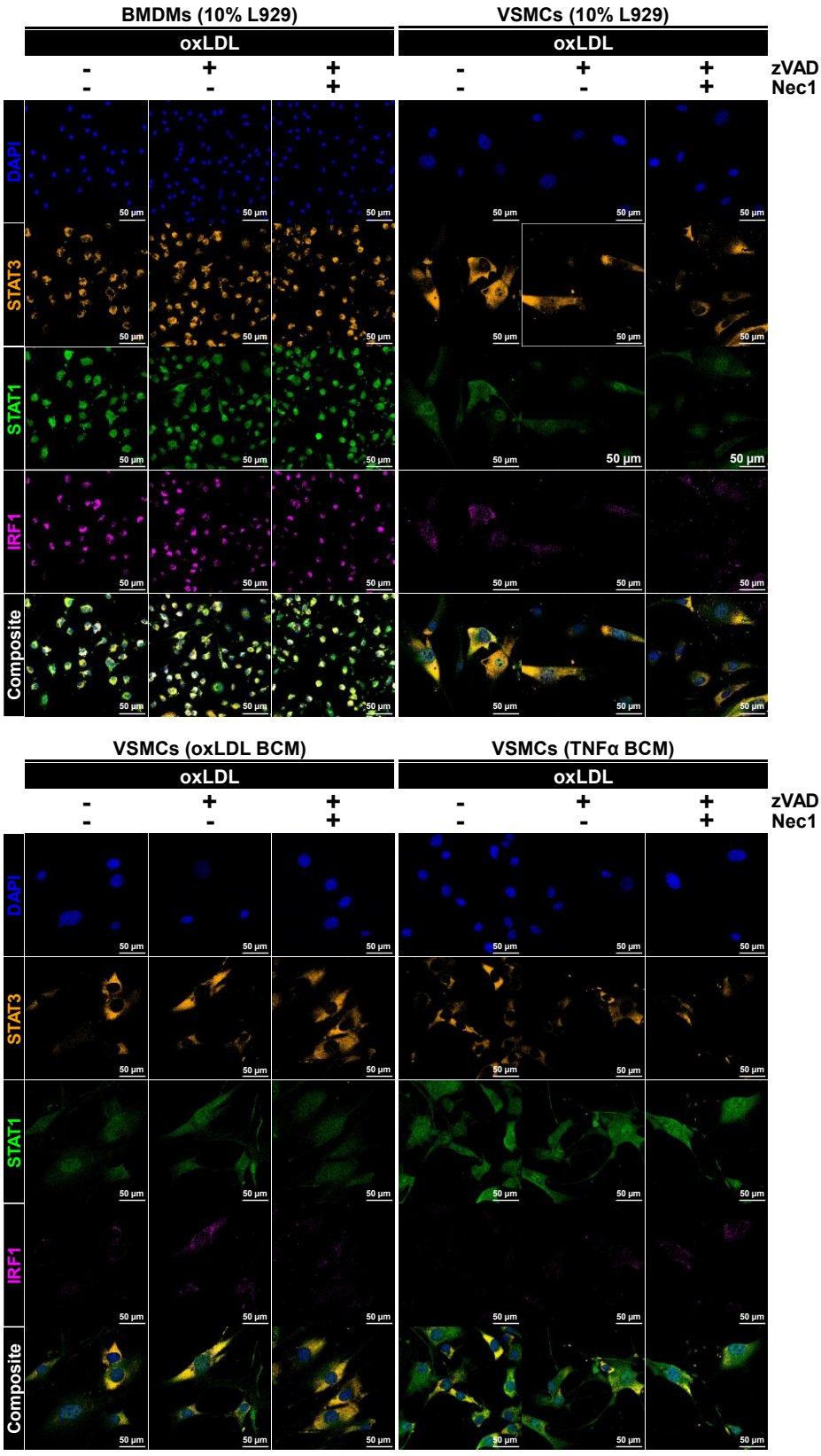

Figure S15. Airyscan confocal fluorescence microscopy of BMDMs and VSMCs 18 hours post-treatment with oxLDL +/- zVAD, Nec1. VSMCs are shown treated in the presence or absence of BMDM conditioned media.

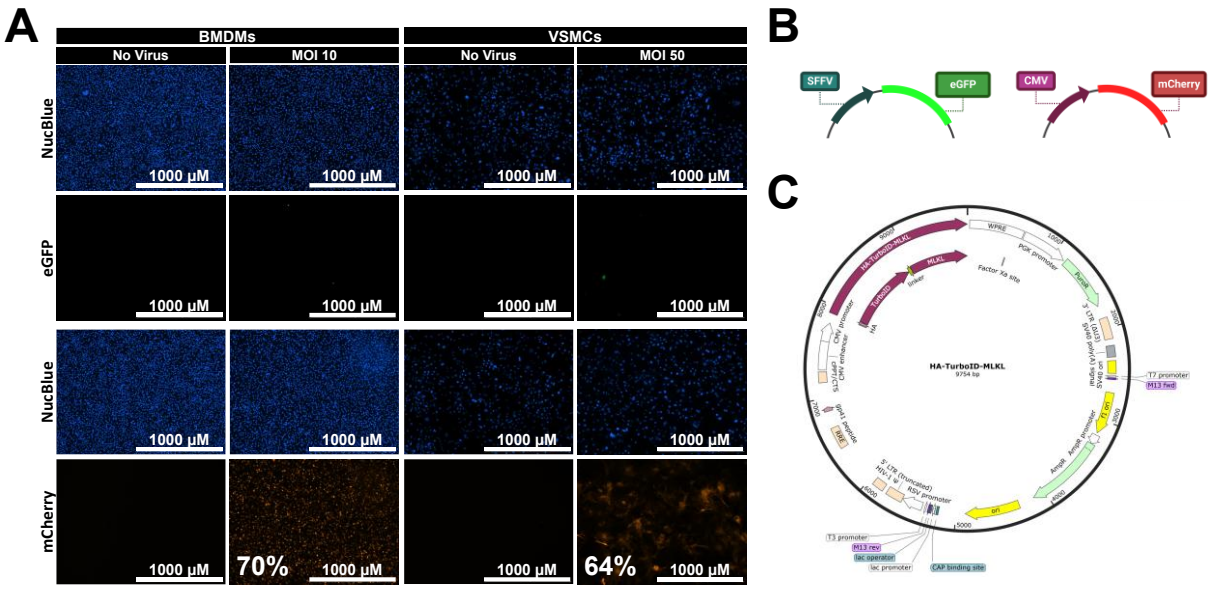

Figure S16. BMDMs and VSMCs preferentially express lentiviral vectors under an enhanced CMV promoter over and SFFV promoter. **A** Transduction efficiency of BMDMs and VSMCs 72 hours post-infection with LV-mCherry and LV-eGFP. BMDMs are subjected to two infection events with lentivirus mediated through an immunosuppressive transduction reagent, 10 µM of cyclosporine A (CSA). VSMCs are only infected once with lentivirus, using 6 µg/mL of polybrene as a transduction reagent. **B** Schematic describing the two lentivirus vectors assayed in this experiment. **C** Final plasmid map of the TurboID construct being prepared.

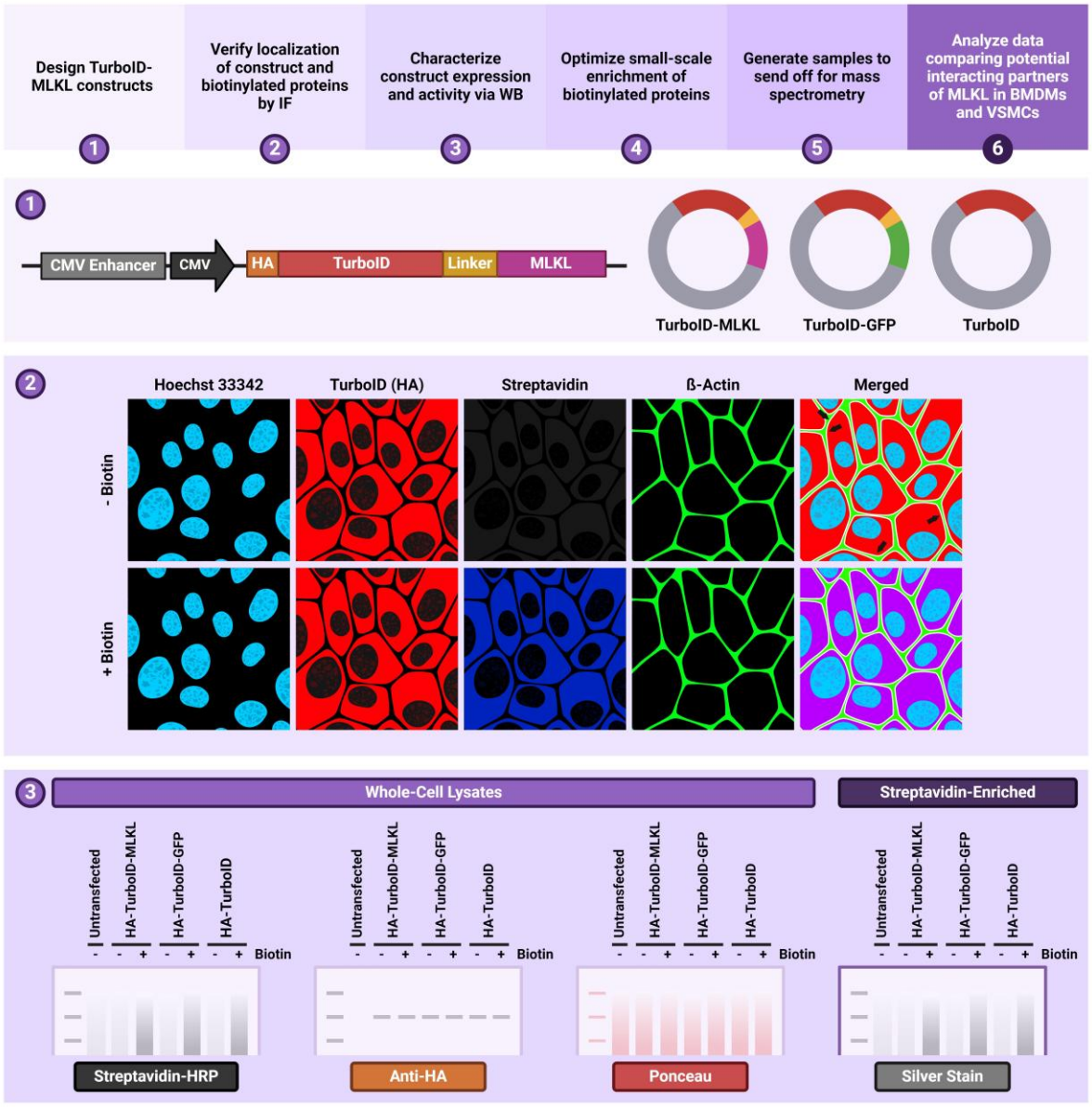

Figure S17. Schematic describing the overall stages of a proposed MLKL-interacting partners project, along with goals related to the first three stages of the pipeline, including a summary of the TurboID constructs that have been assembled by the uOttawa GEM Core.

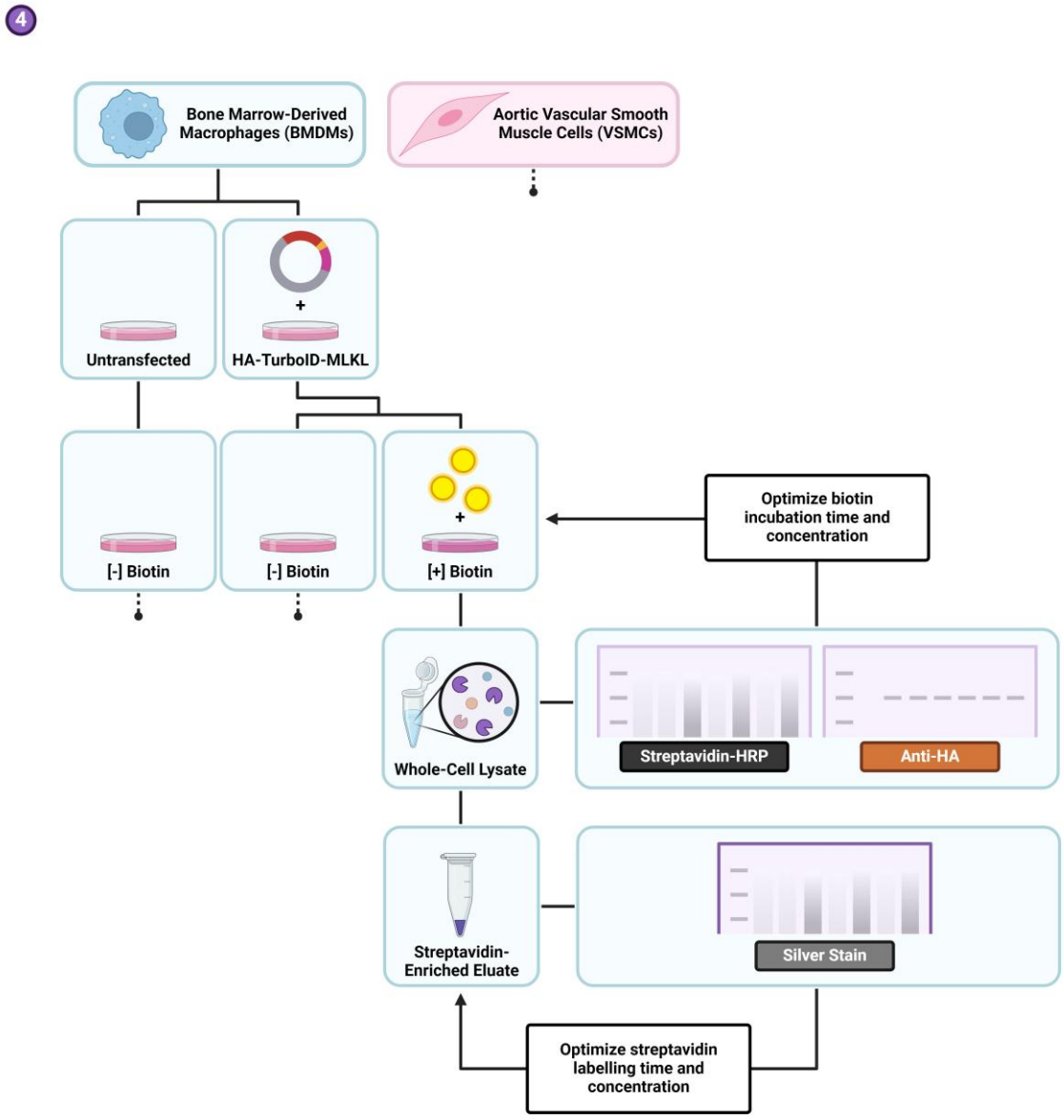

Figure S18. Schematic describing the overall process for optimizing small-scale enrichment of biotinylated proteins.

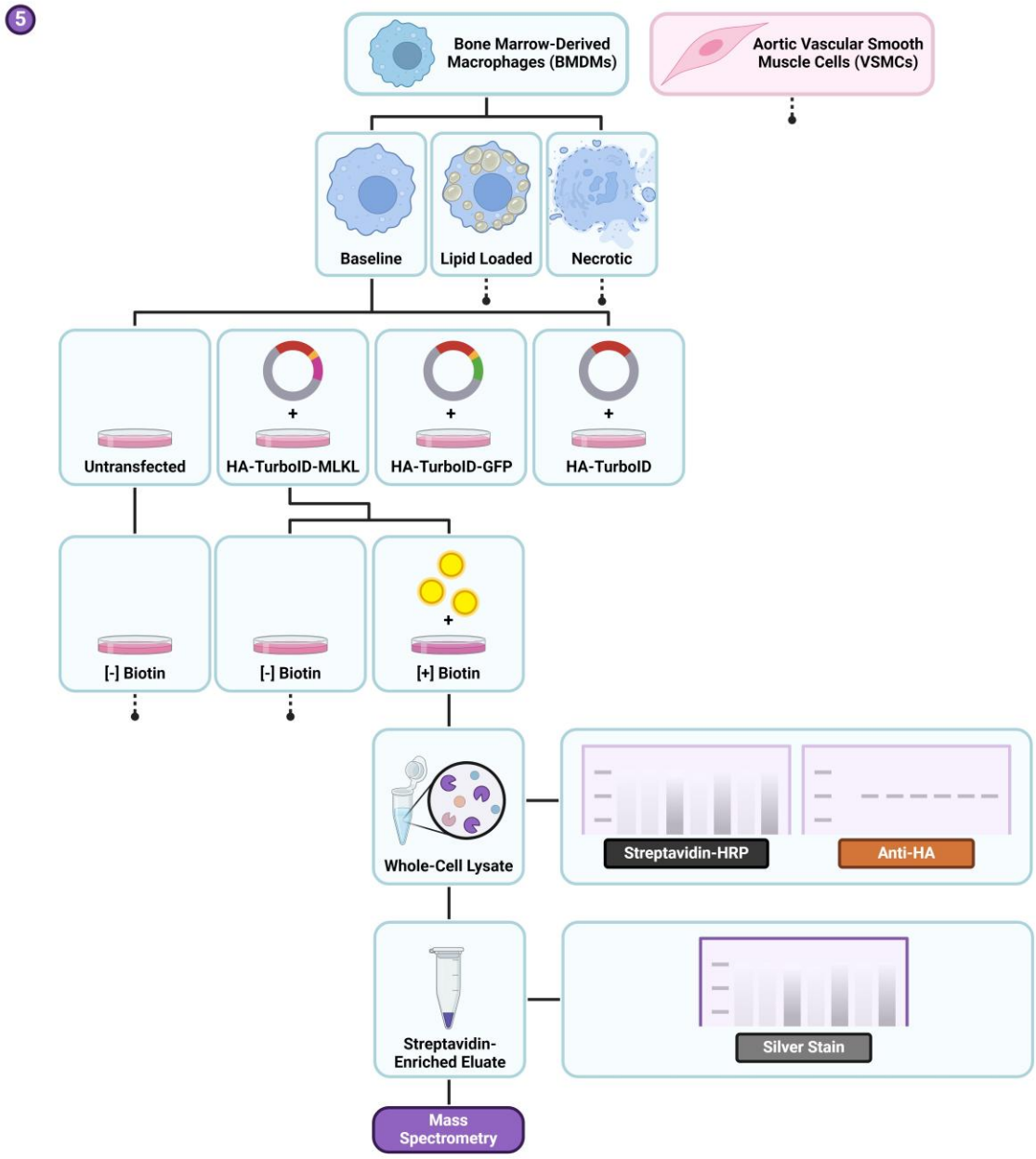

Figure S19. Schematic describing the overall process of preparing enriched biotinylated protein samples to send for analysis using mass spectrometry.

References

1. Libby, P. Inflammation in atherosclerosis. *Arterioscler Thromb Vasc Biol* **32**, 2045–2051 (2012).

2. Viola, J. & Soehnlein, O. Atherosclerosis – A matter of unresolved inflammation. *Semin Immunol* **27**, 184–193 (2015).

3. Libby, P. Inflammation during the life cycle of the atherosclerotic plaque. *Cardiovasc Res* **117**, 2525 (2021).

4. Soehnlein, O. & Libby, P. Targeting inflammation in atherosclerosis — from experimental insights to the clinic. *Nature Reviews Drug Discovery 2021 20:8* **20**, 589–610 (2021).

5. Raggi, P. *et al.* Role of inflammation in the pathogenesis of atherosclerosis and therapeutic interventions. *Atherosclerosis* **276**, 98–108 (2018).

6. Badimon, L. & Vilahur, G. Thrombosis formation on atherosclerotic lesions and plaque rupture. *J Intern Med* **276**, 618–632 (2014).

7. Chen, Y. C., Huang, A. L., Kyaw, T. S., Bobik, A. & Peter, K. Atherosclerotic Plaque Rupture. *Arterioscler Thromb Vasc Biol* **36**, e63–e72 (2016).

8. Bentzon, J. F., Otsuka, F., Virmani, R. & Falk, E. Mechanisms of plaque formation and rupture. *Circ Res* **114**, 1852–1866 (2014).

9. Tsao, C. W. *et al.* Heart Disease and Stroke Statistics-2022 Update: A Report from the American Heart Association. *Circulation* **145**, E153–E639 (2022).

10. Chan, F. K. M., Luz, N. F. & Moriwaki, K. Programmed Necrosis in the Cross Talk of Cell Death and Inflammation. *https://doi.org/10.1146/annurev-immunol-032414-112248* **33**, 79–106 (2015).

11. Puylaert, P., Zurek, M., Rayner, K. J., Meyer, G. R. Y. De & Martinet, W. Regulated Necrosis in Atherosclerosis. *Arterioscler Thromb Vasc Biol* **42**, 1283–1306 (2022).

12. Libby, P. The changing landscape of atherosclerosis. *Nature 2021 592:7855* **592**, 524–533 (2021).

13. Jebari-Benslaiman, S. *et al.* Pathophysiology of Atherosclerosis. *Int J Mol Sci* **23**, (2022).

14. Fan, J. & Watanabe, T. Atherosclerosis: Known and unknown. *Pathol Int* **72**, 151–160 (2022).

15. Wang, X., Shen, Y., Shang, M., Liu, X. & Munn, L. L. Endothelial mechanobiology in atherosclerosis. *Cardiovasc Res* **119**, 1656 (2023).

16. Zheng, D. *et al.* ROS-triggered endothelial cell death mechanisms: Focus on pyroptosis, parthanatos, and ferroptosis. *Front Immunol* **13**, (2022).

17. Zhu, H. *et al.* MiR-483-5p downregulation alleviates ox-LDL induced endothelial cell injury in atherosclerosis. *BMC Cardiovasc Disord* **23**, (2023).

18. Howe, K. L., Cybulsky, M. & Fish, J. E. The Endothelium as a Hub for Cellular Communication in Atherogenesis: Is There Directionality to the Message? *Front Cardiovasc Med* **9**, 888390 (2022).

19. Ghaffari, S. *et al.* Endothelial HMGB1 Is a Critical Regulator of LDL Transcytosis via an SREBP2-SR-BI Axis. *Arterioscler Thromb Vasc Biol* **41**, 200–216 (2021).

20. Huang, L. *et al.* SR-B1 drives endothelial cell LDL transcytosis via DOCK4 to promote atherosclerosis. *Nature* **569**, 565–569 (2019).

21. Armstrong, S. M. *et al.* A novel assay uncovers an unexpected role for SR-BI in LDL transcytosis. *Cardiovasc Res* **108**, 268–277 (2015).

22. Chang, G. J. *et al.* Oxidation of LDL to a biologically active form by derivatives of nitric oxide and nitrite in the absence of superoxide. Dependence on pH and oxygen. *Arterioscler Thromb* **14**, 1808–1814 (1994).

23. Malekmohammad, K., Bezsonov, E. E. & Rafieian-Kopaei, M. Role of Lipid Accumulation and Inflammation in Atherosclerosis: Focus on Molecular and Cellular Mechanisms. *Front Cardiovasc Med* **8**, (2021).

24. Hoff, H. F., Whitaker, T. E. & O'Neil, J. Oxidation of low density lipoprotein leads to particle aggregation and altered macrophage recognition. *J Biol Chem* **267**, 602–9 (1992).

25. Hoff, H. F., Zyromski, N., Armstrong, D. & O'Neil, J. Aggregation as well as chemical modification of LDL during oxidation is responsible for poor processing in macrophages. *J Lipid Res* **34**, 1919–29 (1993).

26. Panasenko, O. M. *et al.* Oxidation-induced aggregation of LDL increases their uptake by smooth muscle cells from human aorta. *Bull Exp Biol Med* **143**, 200–203 (2007).

27. Rayner, K. J. Cell death in the vessel wall: The good, the bad, the ugly. *Arterioscler Thromb Vasc Biol* **37**, e75 (2017).

28. Doran, A. C. Inflammation Resolution: Implications for Atherosclerosis. *Circ Res* **130**, 130–148 (2022).

29. Chistiakov, D. A., Melnichenko, A. A., Myasoedova, V. A., Grechko, A. V. & Orekhov, A. N. Mechanisms of foam cell formation in atherosclerosis. *Journal of Molecular Medicine 2017 95:11* **95**, 1153–1165 (2017).

30. Yan, J. & Horng, T. Lipid Metabolism in Regulation of Macrophage Functions. *Trends Cell Biol* **30**, 979–989 (2020).

31. Gui, Y., Zheng, H. & Cao, R. Y. Foam Cells in Atherosclerosis: Novel Insights Into Its Origins, Consequences, and Molecular Mechanisms. *Front Cardiovasc Med* **9**, (2022).

32. Goldstein, J. L. & Brown, M. S. The low-density lipoprotein pathway and its relation to atherosclerosis. *Annu Rev Biochem* **46**, 897–930 (1977).

33. Goldstein, J. L., Anderson, R. G. W., Buja, L. M., Basu, S. K. & Brown, M. S. Overloading human aortic smooth muscle cells with low density lipoprotein-cholesteryl esters reproduces features of atherosclerosis in vitro. *Journal of Clinical Investigation* **59**, 1196 (1977).

34. Brown, M. S. & Goldstein, J. L. Lipoprotein metabolism in the macrophage: Implications for cholesterol deposition in atherosclerosis. *Annu Rev Biochem* **Vol. 52**, 223–261 (1983).

35. Goldstein, J. L. & Brown, M. S. The LDL receptor. *Arterioscler Thromb Vasc Biol* **29**, 431–438 (2009).

36. Brown, M. S. & Goldstein, J. L. A proteolytic pathway that controls the cholesterol content of membranes, cells, and blood. *Proc Natl Acad Sci U S A* **96**, 11041–11048 (1999).

37. Xiang, P., Blanchard, V. & Francis, G. A. Smooth Muscle Cell—Macrophage Interactions Leading to Foam Cell Formation in Atherosclerosis: Location, Location, Location. *Front Physiol* **13**, 921597 (2022).

38. Bories, G. F. P. & Leitinger, N. Macrophage metabolism in atherosclerosis. *FEBS Lett* **591**, 3042–3060 (2017).

39. Moore, K. J., Sheedy, F. J. & Fisher, E. A. Macrophages in atherosclerosis: a dynamic balance. *Nature Reviews Immunology 2013 13:10* **13**, 709–721 (2013).

40. Choi, H. Y., Ruel, I., Choi, S. & Genest, J. New Strategies to Promote Macrophage Cholesterol Efflux. *Front Cardiovasc Med* **0**, 1991 (2021).

41. Ozcan, L. & Tabas, I. Role of endoplasmic reticulum stress in metabolic disease and other disorders. *Annu Rev Med* **63**, 317–328 (2012).

42. An, Y. *et al.* Endoplasmic reticulum stress-mediated cell death in cardiovascular disease. *Cell Stress Chaperones* **29**, 158–174 (2024).

43. Kojima, Y., Weissman, I. L. & Leeper, N. J. The Role of Efferocytosis in Atherosclerosis. *Circulation* **135**, 476 (2017).

44. Van Vré, E. A., Ait-Oufella, H., Tedgui, A. & Mallat, Z. Apoptotic cell death and efferocytosis in atherosclerosis. *Arterioscler Thromb Vasc Biol* **32**, 887–893 (2012).

45. Thorp, E. & Tabas, I. Mechanisms and consequences of efferocytosis in advanced atherosclerosis. *J Leukoc Biol* **86**, 1089–1095 (2009).

46. Sluimer, J. C. RAC-king up Efferocytosis in Atherosclerotic Plaques With Aldehyde Dehydrogenase 2 Deficiency. *Arterioscler Thromb Vasc Biol* **42**, 717–718 (2022).

47. Thorp, E. *et al.* Shedding of the Mer Tyrosine Kinase Receptor Is Mediated by ADAM17 Protein through a Pathway Involving Reactive Oxygen Species, Protein Kinase Cδ, and p38 Mitogen-activated Protein Kinase (MAPK). *J Biol Chem* **286**, 33335 (2011).

48. Bäck, M., Yurdagul, A., Tabas, I., Öörni, K. & Kovanen, P. T. Inflammation and its resolution in atherosclerosis: mediators and therapeutic opportunities. *Nature Reviews Cardiology 2019 16:7* **16**, 389–406 (2019).

49. Cai, B. *et al.* MerTK receptor cleavage promotes plaque necrosis and defective resolution in atherosclerosis. *J Clin Invest* **127**, 564–568 (2017).

50. Mai, F. Y. *et al.* Caspase-3-mediated GSDME activation contributes to cisplatin- and doxorubicin-induced secondary necrosis in mouse macrophages. *Cell Prolif* **52**, (2019).

51. Wen, S., Wang, Z. H., Zhang, C. X., Yang, Y. & Fan, Q. L. Caspase-3 Promotes Diabetic Kidney Disease Through Gasdermin E-Mediated Progression to Secondary Necrosis During Apoptosis. *Diabetes Metab Syndr Obes* **13**, 313–323 (2020).

52. De Schutter, E. *et al.* Plasma membrane perforation by GSDME during apoptosis-driven secondary necrosis. *Cell Mol Life Sci* **79**, (2021).

53. Vandenabeele, P., Riquet, F. & Cappe, B. Necroptosis: (Last) Message in a Bubble. *Immunity* **47**, 1–3 (2017).

54. Choi, M. E., Price, D. R., Ryter, S. W. & Choi, A. M. K. Necroptosis: a crucial pathogenic mediator of human disease. *JCI Insight* **4**, (2019).

55. Doran, A. C., Meller, N. & McNamara, C. A. Role of Smooth Muscle Cells in the Initiation and Early Progression of Atherosclerosis. *Arterioscler Thromb Vasc Biol* **28**, 812–819 (2008).

56. Leonetti, S. *et al.* Soluble CD40 receptor is a biomarker of the burden of carotid artery atherosclerosis in subjects at high cardiovascular risk. *Atherosclerosis* **343**, 1–9 (2022).

57. Newby, A. C. Metalloproteinases and Vulnerable Atherosclerotic Plaques[image]. *Trends Cardiovasc Med* **17**, 253 (2007).

58. Sarén, P., Welgus, H. G. & Kovanen, P. T. TNF-alpha and IL-1beta selectively induce expression of 92-kDa gelatinase by human macrophages. *J Immunol* **157**, 4159–65 (1996).

59. Grover, S. P. & Mackman, N. Tissue Factor: An Essential Mediator of Hemostasis and Trigger of Thrombosis. *Arterioscler Thromb Vasc Biol* **38**, 709–725 (2018).

60. Kleinegris, M. C., Ten Cate-Hoek, A. J. & Ten Cate, H. Coagulation and the vessel wall in thrombosis and atherosclerosis. *Pol Arch Med Wewn* **122**, 557–566 (2012).

61. Weisel, J. W. Fibrinogen and fibrin. *Adv Protein Chem* **70**, 247–299 (2005).

62. Wolberg, A. S. Fibrinogen and fibrin: synthesis, structure, and function in health and disease. *J Thromb Haemost* **21**, 3005–3015 (2023).

63. Ząbczyk, M., Ariëns, R. A. S. & Undas, A. Fibrin clot properties in cardiovascular disease: from basic mechanisms to clinical practice. *Cardiovasc Res* **119**, 94–111 (2023).

64. Fahed, A. C. & Jang, I. K. Plaque erosion and acute coronary syndromes: phenotype, molecular characteristics and future directions. *Nature Reviews Cardiology 2021 18:10* **18**, 724–734 (2021).

65. Rajavashisth, T. B. *et al.* Inflammatory cytokines and oxidized low density lipoproteins increase endothelial cell expression of membrane type 1-matrix metalloproteinase. *J Biol Chem* **274**, 11924–11929 (1999).

66. Quillard, T. *et al.* TLR2 and neutrophils potentiate endothelial stress, apoptosis and detachment: implications for superficial erosion. *Eur Heart J* **36**, 1394–1404 (2015).

67. Franck, G. *et al.* Flow Perturbation Mediates Neutrophil Recruitment and Potentiates Endothelial Injury via TLR2 in Mice: Implications for Superficial Erosion. *Circ Res* **121**, 31–42 (2017).

68. Mullick, A. E. *et al.* Increased endothelial expression of Toll-like receptor 2 at sites of disturbed blood flow exacerbates early atherogenic events. *J Exp Med* **205**, 373–383 (2008).

69. Mullick, A. E., Tobias, P. S. & Curtiss, L. K. Modulation of atherosclerosis in mice by Toll-like receptor 2. *J Clin Invest* **115**, 3149–3156 (2005).

70. Botts, S. R., Fish, J. E. & Howe, K. L. Dysfunctional Vascular Endothelium as a Driver of Atherosclerosis: Emerging Insights Into Pathogenesis and Treatment. *Front Pharmacol* **12**, (2021).

71. Mundi, S. *et al.* Endothelial permeability, LDL deposition, and cardiovascular risk factors—a review. *Cardiovasc Res* **114**, 35 (2018).

72. Bu, L. L. *et al.* New Dawn for Atherosclerosis: Vascular Endothelial Cell Senescence and Death. *International Journal of Molecular Sciences 2023, Vol. 24, Page 15160* **24**, 15160 (2023).

73. Deanfield, J. E., Halcox, J. P. & Rabelink, T. J. Endothelial function and dysfunction: Testing and clinical relevance. *Circulation* **115**, 1285–1295 (2007).

74. Liu, Y. *et al.* Dissonant response of M0/M2 and M1 bone-marrow-derived macrophages to RhoA pathway interference. *Cell Tissue Res* **366**, 707–720 (2016).

75. Hickman, E. *et al.* Expanded characterization of in vitro polarized M0, M1, and M2 human monocyte-derived macrophages: Bioenergetic and secreted mediator profiles. *PLoS One* **18**, (2023).

76. Susser, L. I. & Rayner, K. J. Through the layers: how macrophages drive atherosclerosis across the vessel wall. *J Clin Invest* **132**, (2022).

77. Locati, M., Curtale, G. & Mantovani, A. Diversity, Mechanisms, and Significance of Macrophage Plasticity. *Annu Rev Pathol* **15**, 123–147 (2020).

78. Shapouri-Moghaddam, A. *et al.* Macrophage plasticity, polarization, and function in health and disease. *J Cell Physiol* **233**, 6425–6440 (2018).

79. Gianopoulos, I. & Daskalopoulou, S. S. Macrophage profiling in atherosclerosis: understanding the unstable plaque. *Basic Res Cardiol* **119**, 35–56 (2024).

80. Zernecke, A. *et al.* Meta-Analysis of Leukocyte Diversity in Atherosclerotic Mouse Aortas. *Circ Res* **127**, 402–426 (2020).

81. Basatemur, G. L., Jørgensen, H. F., Clarke, M. C. H., Bennett, M. R. & Mallat, Z. Vascular smooth muscle cells in atherosclerosis. *Nat Rev Cardiol* **16**, 727–744 (2019).

82. Bennett, M. R., Sinha, S. & Owens, G. K. Vascular Smooth Muscle Cells in Atherosclerosis. *Circ Res* **118**, 692–702 (2016).

83. Wirka, R. C. *et al.* Atheroprotective roles of smooth muscle cell phenotypic modulation and the TCF21 disease gene as revealed by single-cell analysis. *Nat Med* **25**, 1280 (2019).

84. Grootaert, M. O. J. *et al.* Vascular smooth muscle cell death, autophagy and senescence in atherosclerosis. *Cardiovasc Res* **114**, 622–634 (2018).

85. Chen, R., McVey, D. G., Shen, D., Huang, X. & Ye, S. Phenotypic Switching of Vascular Smooth Muscle Cells in Atherosclerosis. *J Am Heart Assoc* **12**, 31121 (2023).

86. Spin, J. M., Maegdefessel, L. & Tsao, P. S. Vascular smooth muscle cell phenotypic plasticity: focus on chromatin remodelling. *Cardiovasc Res* **95**, 147 (2012).

87. Shankman, L. S. *et al.* KLF4 Dependent Phenotypic Modulation of SMCs Plays a Key Role in Atherosclerotic Plaque Pathogenesis. *Nat Med* **21**, 628 (2015).

88. Pan, H. *et al.* Single-Cell Genomics Reveals a Novel Cell State During Smooth Muscle Cell Phenotypic Switching and Potential Therapeutic Targets for Atherosclerosis in Mouse and Human. *Circulation* **142**, 2060–2075 (2020).

89. Pan, H. *et al.* Atherosclerosis Is a Smooth Muscle Cell–Driven Tumor-Like Disease. *Circulation* **149**, 1885–1898 (2024).

90. Grootaert, M. O. J. & Bennett, M. R. Vascular smooth muscle cells in atherosclerosis: time for a re-assessment. *Cardiovasc Res* **117**, 2326–2339 (2021).

91. Liu, M. & Gomez, D. Smooth Muscle Cell Phenotypic Diversity. *Arterioscler Thromb Vasc Biol* **39**, 1715–1723 (2019).

92. Gomez, D., Swiatlowska, P. & Owens, G. K. Epigenetic Control of Smooth Muscle Cell Identity and Lineage Memory. *Arterioscler Thromb Vasc Biol* **35**, 2508–2516 (2015).

93. Wang, Y. *et al.* Smooth Muscle Cells Contribute the Majority of Foam Cells in ApoE (Apolipoprotein E)-Deficient Mouse Atherosclerosis. *Arterioscler Thromb Vasc Biol* **39**, 876–887 (2019).

94. Miller, C. L. & Zhang, H. Clarifying the Distinct Roles of Smooth Muscle Cell-Derived Versus Macrophage Foam Cells and the Implications in Atherosclerosis. *Arterioscler Thromb Vasc Biol* **41**, 2035–2037 (2021).

95. Vengrenyuk, Y. *et al.* Cholesterol loading reprograms the microRNA-143/145-myocardin axis to convert aortic smooth muscle cells to a dysfunctional macrophage-like phenotype. *Arterioscler Thromb Vasc Biol* **35**, 535–546 (2015).

96. Dubland, J. A. *et al.* Low LAL (Lysosomal Acid Lipase) Expression by Smooth Muscle Cells Relative to Macrophages as a Mechanism for Arterial Foam Cell Formation. *Arterioscler Thromb Vasc Biol* **41**, E354–E368 (2021).

97. Nagata, S., Suzuki, J., Segawa, K. & Fujii, T. Exposure of phosphatidylserine on the cell surface. *Cell Death Differ* **23**, 952 (2016).

98. Li, K., van Delft, M. F. & Dewson, G. Too much death can kill you: inhibiting intrinsic apoptosis to treat disease. *EMBO J* **40**, (2021).

99. Xu, X., Lai, Y. & Hua, Z. C. Apoptosis and apoptotic body: disease message and therapeutic target potentials. *Biosci Rep* **39**, (2019).

100. Bertheloot, D., Latz, E. & Franklin, B. S. Necroptosis, pyroptosis and apoptosis: an intricate game of cell death. *Cell Mol Immunol* **18**, 1106 (2021).

101. McArthur, K. *et al.* BAK/BAX macropores facilitate mitochondrial herniation and mtDNA efflux during apoptosis. *Science (1979)* **359**, (2018).

102. Yuanming, H., Benedict, M. A., Ding, L. & Núñez, G. Role of cytochrome c and dATP/ATP hydrolysis in Apaf-1-mediated caspase-9 activation and apoptosis. *EMBO J* **18**, 3586–3595 (1999).

103. Purring-Koch, C. & McLendon, G. Cytochrome c binding to Apaf-1: the effects of dATP and ionic strength. *Proc Natl Acad Sci U S A* **97**, 11928–11931 (2000).

104. Elmore, S. Apoptosis: a review of programmed cell death. *Toxicol Pathol* **35**, 495–516 (2007).

105. Stoneman, V. E. A. & Bennett, M. R. Role of apoptosis in atherosclerosis and its therapeutic implications. *Clin Sci* **107**, 343–354 (2004).

106. Robinson, N. *et al.* Programmed necrotic cell death of macrophages: Focus on pyroptosis, necroptosis, and parthanatos. *Redox Biol* **26**, (2019).

107. Yu, P. *et al.* Pyroptosis: mechanisms and diseases. *Signal Transduction and Targeted Therapy 2021 6:1* **6**, 1–21 (2021).

108. Wang, Q. *et al.* Pyroptosis: A pro-inflammatory type of cell death in cardiovascular disease. *Clin Chim Acta* **510**, 62–72 (2020).

109. Jia, C. *et al.* Role of pyroptosis in cardiovascular diseases. *Int Immunopharmacol* **67**, 311–318 (2019).

110. Amarante-Mendes, G. P. *et al.* Pattern Recognition Receptors and the Host Cell Death Molecular Machinery. *Front Immunol* **9**, (2018).

111. Platnich, J. M. & Muruve, D. A. NOD-like receptors and inflammasomes: A review of their canonical and non-canonical signaling pathways. *Arch Biochem Biophys* **670**, 4–14 (2019).

112. Ball, D. P. *et al.* Caspase-1 interdomain linker cleavage is required for pyroptosis. *Life Sci Alliance* **3**, (2020).

113. Xu, J. & Núñez, G. The NLRP3 inflammasome: activation and regulation. *Trends Biochem Sci* **48**, 331–344 (2023).

114. Burdette, B. E., Esparza, A. N., Zhu, H. & Wang, S. Gasdermin D in pyroptosis. *Acta Pharm Sin B* **11**, 2768–2782 (2021).

115. Shi, J. *et al.* Cleavage of GSDMD by inflammatory caspases determines pyroptotic cell death. *Nature* **526**, 660–665 (2015).

116. Devant, P. & Kagan, J. C. Molecular mechanisms of gasdermin D pore-forming activity. *Nat Immunol* **24**, 1064–1075 (2023).

117. Scheffer, L. L. *et al.* Mechanism of Ca^{2+}-triggered ESCRT assembly and regulation of cell membrane repair. *Nat Commun* **5**, 5646 (2014).

118. Gong, Y. N. *et al.* ESCRT-III Acts Downstream of MLKL to Regulate Necroptotic Cell Death and Its Consequences. *Cell* **169**, 286-300.e16 (2017).

119. Rühl, S. *et al.* ESCRT-dependent membrane repair negatively regulates pyroptosis downstream of GSDMD activation. *Science (1979)* **362**, 956–960 (2018).

120. Wang, W. *et al.* Sensing plasma membrane pore formation induces chemokine production in survivors of regulated necrosis. *Dev Cell* **57**, 228-245.e6 (2022).

121. Dai, Z. *et al.* Gasdermin D-mediated pyroptosis: mechanisms, diseases, and inhibitors. *Front Immunol* **14**, 1178662 (2023).

122. Taabazuing, C. Y., Okondo, M. C. & Bachovchin, D. A. Pyroptosis and apoptosis pathways engage in bidirectional crosstalk in monocytes and macrophages. *Cell Chem Biol* **24**, 507 (2017).

123. Henry, T. & Monack, D. M. Activation of the inflammasome upon Francisella tularensis infection: interplay of innate immune pathways and virulence factors. *Cell Microbiol* **9**, 2543–2551 (2007).

124. Suzuki, T. *et al.* Differential Regulation of Caspase-1 Activation, Pyroptosis, and Autophagy via Ipaf and ASC in Shigella-Infected Macrophages. *PLoS Pathog* **3**, e111 (2007).

125. Fink, S. L. & Cookson, B. T. Caspase-1-dependent pore formation during pyroptosis leads to osmotic lysis of infected host macrophages. *Cell Microbiol* **8**, 1812–1825 (2006).

126. Fink, S. L. & Cookson, B. T. Pyroptosis and host cell death responses during Salmonella infection. *Cell Microbiol* **9**, 2562–2570 (2007).

127. Brennan, M. A. & Cookson, B. T. Salmonella induces macrophage death by caspase-1-dependent necrosis. *Mol Microbiol* **38**, 31–40 (2000).

128. Cookson, B. T. & Brennan, M. A. Pro-inflammatory programmed cell death. *Trends Microbiol* **9**, 113–114 (2001).

129. Demarco, B. *et al.* Caspase-8-dependent gasdermin D cleavage promotes antimicrobial defense but confers susceptibility to TNF-induced lethality. *Sci Adv* **6**, (2020).

130. Jiang, M., Qi, L., Li, L. & Li, Y. The caspase-3/GSDME signal pathway as a switch between apoptosis and pyroptosis in cancer. *Cell Death Discovery 2020 6:1* **6**, 1–11 (2020).

131. Hu, Y. *et al.* The multifaceted roles of GSDME-mediated pyroptosis in cancer: therapeutic strategies and persisting obstacles. *Cell Death & Disease 2023 14:12* **14**, 1–17 (2023).

132. Seo, J., Nam, Y. W., Kim, S., Oh, D. B. & Song, J. Necroptosis molecular mechanisms: Recent findings regarding novel necroptosis regulators. *Experimental & Molecular Medicine 2021 53:6* **53**, 1007–1017 (2021).

133. Zhang, X., Ren, Z., Xu, W. & Jiang, Z. Necroptosis in atherosclerosis. *Clinica Chimica Acta* **534**, 22–28 (2022).

134. Weinlich, R., Oberst, A., Beere, H. M. & Green, D. R. Necroptosis in development, inflammation and disease. *Nature Reviews Molecular Cell Biology 2016 18:2* **18**, 127–136 (2016).

135. Newton, K. *et al.* Caspase cleavage of RIPK3 after Asp333 is dispensable for mouse embryogenesis. *Cell Death Differ* **31**, 254–262 (2024).

136. Tran, H. T. *et al.* RIPK3 cleavage is dispensable for necroptosis inhibition but restricts NLRP3 inflammasome activation. *Cell Death Differ* **31**, 662–671 (2024).

137. Newton, K. *et al.* Cleavage of RIPK1 by caspase-8 is crucial for limiting apoptosis and necroptosis. *Nature* **574**, 428–431 (2019).

138. Feltham, R., Vince, J. E. & Lawlor, K. E. Caspase-8: not so silently deadly. *Clin Transl Immunology* **6**, (2017).

139. Chen, Y. S. *et al.* Pan-Caspase Inhibitor zVAD Induces Necroptotic and Autophagic Cell Death in TLR3/4-Stimulated Macrophages. *Mol Cells* **45**, 257–272 (2022).

140. Negroni, A. *et al.* RIP3 AND pMLKL promote necroptosis-induced inflammation and alter membrane permeability in intestinal epithelial cells. *Digestive and Liver Disease* **49**, 1201–1210 (2017).

141. Davies, K. A. *et al.* The brace helices of MLKL mediate interdomain communication and oligomerisation to regulate cell death by necroptosis. *Cell Death Differ* **25**, 1567–1580 (2018).

142. Hildebrand, J. M. *et al.* Activation of the pseudokinase MLKL unleashes the four-helix bundle domain to induce membrane localization and necroptotic cell death. *Proc Natl Acad Sci U S A* **111**, 15072–15077 (2014).

143. Pasparakis, M. & Vandenabeele, P. Necroptosis and its role in inflammation. *Nature* **517**, 311–320 (2015).

144. Kamari, Y. *et al.* Characterisation of atherosclerotic lesions with scanning electron microscopy (SEM) of wet tissue. *Diab Vasc Dis Res* **5**, 44–47 (2008).

145. HEGYI, L., SKEPPER, J. N., CARY, N. R. B. & MITCHINSON, M. J. FOAM CELL APOPTOSIS AND THE DEVELOPMENT OF THE LIPID CORE OF HUMAN ATHEROSCLEROSIS. *J Pathol* **180**, 423–429 (1996).

146. Guyton, J. R., Klemp, K. F., Black, B. L. & Bocan, T. M. A. Extracellular lipid deposition in atherosclerosis. *Eur Heart J* **11**, 20–28 (1990).

147. Guyton, J. R. & Klemp, K. F. Transitional features in human atherosclerosis. Intimal thickening, cholesterol clefts, and cell loss in human aortic fatty streaks. *Am J Pathol* **143**, 1444 (1993).

148. Corrado, D. *et al.* Sudden death in the young. Is acute coronary thrombosis the major precipitating factor? *Circulation* **90**, 2315–2323 (1994).

149. Bocan, T. M. A., Schifani, T. A. & Guyton, J. R. Ultrastructure of the human aortic fibrolipid lesion. Formation of the atherosclerotic lipid-rich core. *Am J Pathol* **123**, 413 (1986).

150. Hadian, K. & Stockwell, B. R. The therapeutic potential of targeting regulated non-apoptotic cell death. *Nature Reviews Drug Discovery 2023* 1–20 (2023) doi:10.1038/s41573-023-00749-8.

151. Yahagi, K. *et al.* Pathophysiology of native coronary, vein graft, and in-stent atherosclerosis. *Nature Reviews Cardiology 2015 13:2* **13**, 79–98 (2015).

152. Karunakaran, D. *et al.* Targeting macrophage necroptosis for therapeutic and diagnostic interventions in atherosclerosis. *Sci Adv* **2**, (2016).

153. Lin, J. *et al.* A role of RIP3-mediated macrophage necrosis in atherosclerosis development. *Cell Rep* **3**, 200–210 (2013).

154. Hosseini, Z. *et al.* Resolvin D1 Enhances Necroptotic Cell Clearance Through Promoting Macrophage Fatty Acid Oxidation and Oxidative Phosphorylation. *Arterioscler Thromb Vasc Biol* **41**, 1062–1075 (2021).

155. Jia, Y. *et al.* miR-223-3p Prevents Necroptotic Macrophage Death by Targeting Ripk3 in a Negative Feedback Loop and Consequently Ameliorates Advanced Atherosclerosis. *Arterioscler Thromb Vasc Biol* **44**, 218–237 (2024).

156. Rasheed, A. *et al.* Loss of MLKL (Mixed Lineage Kinase Domain-Like Protein) Decreases Necrotic Core but Increases Macrophage Lipid Accumulation in Atherosclerosis. *Arterioscler Thromb Vasc Biol* **40**, 1155–1167 (2020).

157. Karunakaran, D. *et al.* RIPK1 Expression Associates With Inflammation in Early Atherosclerosis in Humans and Can Be Therapeutically Silenced to Reduce NF-κB Activation and Atherogenesis in Mice. *Circulation* **143**, 163–177 (2021).

158. Leng, Y. *et al.* Receptor Interacting Protein Kinases 1/3: The Potential Therapeutic Target for Cardiovascular Inflammatory Diseases. *Front Pharmacol* **12**, 762334 (2021).

159. Leeper, N. J. The Role of Necroptosis in Atherosclerotic Disease. *JACC Basic Transl Sci* **1**, 548 (2016).

160. Zhe-Wei, S., Li-Sha, G. & Yue-Chun, L. The Role of Necroptosis in Cardiovascular Disease. *Front Pharmacol* **9**, (2018).

161. Canham, L. *et al.* EVA1A (Eva-1 Homolog A) Promotes Endothelial Apoptosis and Inflammatory Activation Under Disturbed Flow Via Regulation of Autophagy. *Arterioscler Thromb Vasc Biol* **43**, 547–561 (2023).

162. Linton, M. F. *et al.* The Role of Lipids and Lipoproteins in Atherosclerosis. *Science (1979)* **111**, 166–186 (2019).

163. Yu, B. *et al.* The role of hypoxia-inducible factors in cardiovascular diseases. *Pharmacol Ther* **238**, 108186 (2022).

164. Sergin, I. & Razani, B. Self-eating in the plaque: What macrophage autophagy reveals about atherosclerosis. *Trends in Endocrinology and Metabolism* **25**, 225–234 (2014).

165. Martinet, W. & De Meyer, G. R. Y. Autophagy in atherosclerosis: A cell survival and death phenomenon with therapeutic potential. *Circ Res* **104**, 304–317 (2009).

166. Pajarinen, J. *et al.* Establishment of Green Fluorescent Protein and Firefly Luciferase Expressing Mouse Primary Macrophages for In Vivo Bioluminescence Imaging. *PLoS One* **10**, (2015).

167. Noser, J. A. *et al.* Cyclosporine Increases Human Immunodeficiency Virus Type 1 Vector Transduction of Primary Mouse Cells. *J Virol* **80**, 7769–7774 (2006).

168. Sakoda, T., Kasahara, N., Kedes, L. & Ohyanagi, M. Calcium phosphate coprecipitation greatly enhances transduction of cardiac myocytes and vascular smooth muscle cells by lentivirus vectors. *Exp Clin Cardiol* **12**, (2007).

169. Lv, L. *et al.* Lentivirus-mediated RNA Interference Targeting STAT4 Inhibits the Proliferation of Vascular Smooth Muscle Cells. *Arch Med Res* **39**, 582–589 (2008).

170. Yang, J. *et al.* CBP knockdown inhibits angiotensin II-induced vascular smooth muscle cells proliferation through downregulating NF-kB transcriptional activity. *Mol Cell Biochem* **340**, 55–62 (2010).

171. Samson, A. L. *et al.* A toolbox for imaging RIPK1, RIPK3, and MLKL in mouse and human cells. *Cell Death & Differentiation 2021 28:7* **28**, 2126–2144 (2021).

172. Samson, A. L. *et al.* MLKL trafficking and accumulation at the plasma membrane control the kinetics and threshold for necroptosis. *Nature Communications 2020 11:1* **11**, 1–17 (2020).

173. Belmokhtar, C. A., Hillion, J. & Ségal-Bendirdjian, E. Staurosporine induces apoptosis through both caspase-dependent and caspase-independent mechanisms. *Oncogene 2001 20:26* **20**, 3354–3362 (2001).

174. DiPeso, L., Ji, D. X., Vance, R. E. & Price, J. V. Cell death and cell lysis are separable events during pyroptosis. *Cell Death Discovery 2017 3:1* **3**, 1–10 (2017).

175. Kabakov, A. E. & Gabai, V. L. Cell Death and Survival Assays. *Methods in Molecular Biology* **1709**, 107–127 (2018).

176. Knuth, A. K. *et al.* Interferons Transcriptionally Up-Regulate MLKL Expression in Cancer Cells. *Neoplasia* **21**, 74–81 (2019).

177. Günther, C. *et al.* The pseudokinase MLKL mediates programmed hepatocellular necrosis independently of RIPK3 during hepatitis. *J Clin Invest* **126**, 4346–4360 (2016).

178. Hao, Q., Shetty, S., Tucker, T. A., Idell, S. & Tang, H. Interferon-γ Preferentially Promotes Necroptosis of Lung Epithelial Cells by Upregulating MLKL. *Cells* **11**, (2022).

179. Kirchmer, M. N. *et al.* Modulation of vascular smooth muscle cell phenotype by STAT-1 and STAT-3. *Atherosclerosis* **234**, 169–175 (2014).

180. Ma, W. F. *et al.* Enhanced single-cell RNA-seq workflow reveals coronary artery disease cellular cross-talk and candidate drug targets. *Atherosclerosis* **340**, 12–22 (2022).

181. Beck-Joseph, J. & Lehoux, S. Molecular Interactions Between Vascular Smooth Muscle Cells and Macrophages in Atherosclerosis. *Front Cardiovasc Med* **8**, 737934 (2021).

182. Stein, O., Halperin, G. & Stein, Y. Enhancement of cholesterol esterification in aortic smooth muscle cells by medium of macrophages conditioned with acetylated LDL. *FEBS Lett* **123**, 303–306 (1981).

183. Wolfbauer, G., Glick, J. M., Minor, L. K. & Rothblat, G. H. Development of the smooth muscle foam cell: uptake of macrophage lipid inclusions. *Proceedings of the National Academy of Sciences* **83**, 7760–7764 (1986).

184. Stein, O., Dabach, Y., Ben-Naim, M., Hollander, G. & Stein, Y. Macrophage-conditioned medium and beta-VLDLs enhance cholesterol esterification in SMCs and HSFs by LDL receptor-mediated and other pathways. *Arterioscler Thromb* **13**, 1350–1358 (1993).

185. Stein, O., Ben-naim, M., Dabach, Y., Hollander, G. & Steina, Y. Murine macrophages secrete factors that enhance uptake of non-lipoprotein [3H]cholesteryl ester by aortic smooth muscle cells. *Biochimica et Biophysica Acta (BBA) - Lipids and Lipid Metabolism* **1212**, 305–310 (1994).

186. Mietus-Snyder, M., Gowri, M. S. & Pitas, R. E. Class A scavenger receptor up-regulation in smooth muscle cells by oxidized low density lipoprotein. Enhancement by calcium flux and concurrent cyclooxygenase-2 up-regulation. *Journal of Biological Chemistry* **275**, 17661–17670 (2000).

187. He, C. *et al.* Macrophages release plasma membrane-derived particles rich in accessible cholesterol. *Proc Natl Acad Sci U S A* **115**, E8499–E8508 (2018).

188. Hu, X. *et al.* Release of cholesterol-rich particles from the macrophage plasma membrane during movement of filopodia and lamellipodia. *Elife* **8**, (2019).

189. Yoon, S., Kovalenko, A., Bogdanov, K. & Wallach, D. MLKL, the Protein that Mediates Necroptosis, Also Regulates Endosomal Trafficking and Extracellular Vesicle Generation. *Immunity* **47**, 51-65.e7 (2017).

190. Boyle, J. J., Bowyer, D. E., Weissberg, P. L. & Bennett, M. R. Human blood-derived macrophages induce apoptosis in human plaque-derived vascular smooth muscle cells by Fas-ligand/Fas interactions. *Arterioscler Thromb Vasc Biol* **21**, 1402–1407 (2001).

191. Imanishi, T. *et al.* Apoptosis of vascular smooth muscle cells is induced by Fas ligand derived from monocytes/macrophage. *Atherosclerosis* **161**, 143–151 (2002).

192. Boyle, J. J., Weissberg, P. L. & Bennett, M. R. Human macrophage-induced vascular smooth muscle cell apoptosis requires NO enhancement of Fas/Fas-L interactions. *Arterioscler Thromb Vasc Biol* **22**, 1624–1630 (2002).

193. Lv, P. *et al.* SM22α Loss Contributes to Apoptosis of Vascular Smooth Muscle Cells via Macrophage-Derived circRasGEF1B. *Oxid Med Cell Longev* **2021**, 5564884 (2021).

194. Weindel, C. G. *et al.* Mitochondrial ROS promotes susceptibility to infection via gasdermin D-mediated necroptosis. *Cell* **185**, 3214-3231.e23 (2022).

195. Chen, J., Kuroki, S., Someda, M. & Yonehara, S. Interferon-γ induces the cell surface exposure of phosphatidylserine by activating the protein MLKL in the absence of caspase-8 activity. *J Biol Chem* **294**, 11994–12006 (2019).

196. Xue, Y. *et al.* Macrophages regulate vascular smooth muscle cell function during atherosclerosis progression through IL-1β/STAT3 signaling. *Communications Biology 2022 5:1* **5**, 1–16 (2022).

197. Zhou, T. *et al.* Mlkl and camkii are involved in ripk3-mediated smooth muscle cell necroptosis. *Cells* **10**, (2021).

198. Lawlor, K. E. *et al.* RIPK3 promotes cell death and NLRP3 inflammasome activation in the absence of MLKL. *Nature Communications 2015 6:1* **6**, 1–19 (2015).

199. Satoh, J. I. & Tabunoki, H. A Comprehensive Profile of ChIP-Seq-Based STAT1 Target Genes Suggests the Complexity of STAT1-Mediated Gene Regulatory Mechanisms. *Gene Regul Syst Bio* **7**, 41 (2013).

200. Wu, J. *et al.* Genome-Wide ChIP-seq and RNA-seq Analyses of STAT3 Target Genes in TLRs Activated Human Peripheral Blood B Cells. *Front Immunol* **13**, 821457 (2022).

201. Bai, X. *et al.* Cigarette tar accelerates atherosclerosis progression via RIPK3-dependent necroptosis mediated by endoplasmic reticulum stress in vascular smooth muscle cells. *Cell Commun Signal* **22**, (2024).

202. Giordano, A. *et al.* Rapamycin antagonizes NF-kappaB nuclear translocation activated by TNF-alpha in primary vascular smooth muscle cells and enhances apoptosis. *Am J Physiol Heart Circ Physiol* **290**, (2006).

203. Redondo, S. *et al.* Overproduction of cyclo-oxygenase-2 (COX-2) is involved in the resistance to apoptosis in vascular smooth muscle cells from diabetic patients: a link between inflammation and apoptosis. *Diabetologia* **54**, 190–199 (2011).

204. Ruiz, E. *et al.* Human vascular smooth muscle cells from diabetic patients are resistant to induced apoptosis due to high Bcl-2 expression. *Diabetes* **55**, 1243–1251 (2006).

205. Li, H., Télémaque, S., Miller, R. E. & Marsh, J. D. High glucose inhibits apoptosis induced by serum deprivation in vascular smooth muscle cells via upregulation of Bcl-2 and Bcl-xl. *Diabetes* **54**, 540–545 (2005).

206. Sakuma, H. *et al.* High glucose inhibits apoptosis in human coronary artery smooth muscle cells by increasing bcl-xL and bfl-1/A1. *Am J Physiol Cell Physiol* **283**, (2002).

207. Shi, L. *et al.* Liraglutide attenuates high glucose-induced abnormal cell migration, proliferation, and apoptosis of vascular smooth muscle cells by activating the GLP-1 receptor, and inhibiting ERK1/2 and PI3K/Akt signaling pathways. *Cardiovasc Diabetol* **14**, (2015).

208. Ponnusamy, A. *et al.* FTI-277 inhibits smooth muscle cell calcification by up-regulating PI3K/Akt signaling and inhibiting apoptosis. *PLoS One* **13**, (2018).

209. Rosner, D. *et al.* Interferon-gamma induces Fas trafficking and sensitization to apoptosis in vascular smooth muscle cells via a PI3K- and Akt-dependent mechanism. *Am J Pathol* **168**, 2054–2063 (2006).

210. Salabei, J. K. *et al.* PDGF-mediated autophagy regulates vascular smooth muscle cell phenotype and resistance to oxidative stress. *Biochem J* **451**, 375–388 (2013).

211. Imanishi, T. *et al.* Transition of apoptotic resistant vascular smooth muscle cells to troptotic sensitive state is correlated with downregulation of c-FLIP. *J Vasc Res* **37**, 523–531 (2000).

212. Guo, R. *et al.* Resveratrol protects vascular smooth muscle cells against high glucose-induced oxidative stress and cell proliferation in vitro. *Med Sci Monit Basic Res* **20**, 82 (2014).

213. Hyun, S. L. *et al.* TNF-α activates death pathway in human aorta smooth muscle cell in the presence of 7-ketocholesterol. *Biochem Biophys Res Commun* **333**, 1093–1099 (2005).

214. Rho, M. C. *et al.* Sensitization of vascular smooth muscle cell to TNF-α-mediated death in the presence of palmitate. *Toxicol Appl Pharmacol* **220**, 311–319 (2007).

215. Geng, Y. J., Wu, Q., Muszynski, M., Hansson, G. K. & Libby, P. Apoptosis of vascular smooth muscle cells induced by in vitro stimulation with interferon-γ, tumor necrosis factor-α, and interleukin-1β. *Arterioscler Thromb Vasc Biol* **16**, 19–27 (1996).